Title
Insights into the regulation of leading edge actin networks in vivo

Author
Iwasa, Janet Haru

Publication Date
2006

Peer reviewed|Thesis/dissertation

Insights into the Regulation of Leading Edge Actin Networks in vivo

by

Janet Haru Iwasa

DISSERTATION

Submitted in partial satisfaction of the requirements for the degree of

DOCTOR OF PHILOSOPHY

in

Biochemistry

in the

GRADUATE DIVISION

of the

UNIVERSITY OF CALIFORNIA, SAN FRANCISCO

Acknowledgements

This work was made possible through the support I have had the good fortune to receive from many individuals during my years in graduate school. However, this work would have been completely impossible without the support of my parents, who nurtured my interest in science from a young age and provided me with constant encouragement throughout graduate school.

Dyche Mullins has been an inspiration, both for his thoughtful dedication and infectious enthusiasm for science, as well as his remarkable aesthetic and artistic sense. I have often turned to him for guidance, first for my experiments, and later for my art, and was always met with a patient ear and encouraging words. He provided unwavering support, both for my scientific research and personal goals, as well as the freedom to explore and choose my own path. For these things, I will always be grateful.

The Mullins lab has been an incredible place to work, due entirely to the talent, kindness and generosity of its members. I have grown both personally and professionally from my interactions with labmates, and I consider each of its members, past and present, a valuable friend. In chronological order, I thank Jonathan Zalevsky, Leah Lempert, Mark Dayel, Alex Kelly, Heather Kranitz, Beth Holleran Mullins, Ethan Garner, Orkun Akin, Margot Quinlan, Lawrence LeClaire, Chris Campbell, Brad Zuchero, and Chris Rivera. I also thank Phoebe Grigg for her cheerful and kind assistance throughout my time at UCSF.

I am grateful for the thoughtful advice of my thesis committee members, Ron Vale and Dave Morgan, and my rotation advisors Anita Sil and Pat O'Farrell. Ron and members of the Vale lab, particularly Steve Rogers, Nico Stuurman, Samara Reck-Peterson, Kevin Slep, Antonina Roll-Mecak and Eric Griffis, have been great sources for advice and friendship.

I thank my friends, especially my housemates Sunshine Wu, Dmitri Nusinow and Sonia Salas, who have always provided me with companionship, excellent advice and a warm and welcoming home.

Finally, I thank Adam Douglass, whose love and support has carried me through graduate school.

Insights into the Regulation of Leading Edge Actin Networks *in vivo*

by

Janet Haru Iwasa

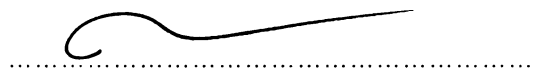

R. Dyche Mullins, Ph.D.

Thesis Advisor & Committee Chairman

Abstract

Cell migration is an essential process for life; in the human body, cell motility appears in many forms, from the directed movement of neuronal growth cones, to the amoeboid crawling of an immune cell. Networks of actin filaments at the front of the cell, or the leading edge, power this motility. According to the dendritic nucleation model, cell motility is driven by a sequence of biochemical events at the leading edge. First, actin filaments are nucleated off of pre-existing "mother" filaments by activated Arp2/3 complexes. The nascent filaments elongate until they are capped by capping protein. The cumulative force of actin filament elongation is thought to provide the energy required to drive the membrane forward during cell crawling. As actin filaments age, they are taken apart by cofilin and recycled back to the cell edge.

We have used fluorescent speckle microscopy techniques to study the localization and activity of actin regulatory proteins in *Drosophila melanogaster* S2 cells. In the cell-edge proximal compartment, called the lamellipod, the Arp2/3 complex and capping protein undergo retrograde motion at the same rate as lamellipodial actin, but dissociate from the lamellipodial actin network at different times. Capping protein dissociates first, after traversing only 1/3 of the lamellipod, while Arp2/3 traverses approximately 2/3 of the lamellipod before dissociating. Cytoskeletal

tropomyosin associates primarily with the cell body proximal lamellar actin network. Depletion of capping protein from S2 cells results in loss of lamellipodial actin dynamics and mislocalization of the Arp2/3 complex, while depletion of actin disassembly factors, including cofilin and twinfilin, result in the expansion of the lamellipod at the expense of the lamellum. These results suggest that actin filament capping and disassembly play opposing roles in the establishment and maintenance of actin networks at the leading edge.

In a separate project, we examine the regulation of the Arp2/3 complex by 14-3-3 proteins. We find that 14-3-3 proteins bind to the Arp2/3 complex directly and are able to competitively inhibit Arp2/3 binding to nucleation promotion factors. This interaction appears dependent on Arp2/3 phosphorylation, and preliminary evidence suggests that this interaction may occur in vivo.

Contributions

Jonathan Zalevsky performed the affinity chromatography of Arp2/3-binding proteins using Acanthamoeba extract (shown in Figure 3-1a) and identified the species bound. He named the p30 species, which he identified as a member of the 14-3-3 protein family, Squiggy.

Dyche Mullins performed analytical ultracentrifugation on the yeast 14-3-3 protein BMH2 and interpreted the results. These findings are discussed in Chapter 3. In addition, he created the leading edge übermodel shown in Figure 1-1.

Brad "Acan do it" Zuchero collaborated in the preparation of Carmil constructs that are discussed in the Appendix, and also created the original version of Figure A-1. Antonina Roll-Mecak (Vale lab) constructed multiple GFP Rab-expressing cell lines that were used to test for colocalization with Carmil in S2 cells shown in Figure A-4. These Rab constructs were originally created by Jim Wilhelm.

With these exceptions, I performed all experiments and created all figures in this thesis dissertation under the supervision and guidance of R. Dyche Mullins.

Table of Contents

List of Tables

Chapter Two

Chapter Three

Appendix

List of Figures

Chapter One

Chapter Two

Chapter Three

Appendix

Chapter One

Introduction

Actin networks at the leading edge of motile cells

The ability of cells to undergo directed motility is necessary for the normal growth and development of multicellular organisms. If we peel away the plasma membrane at the front of a typical crawling cell and look underneath, we find an intricate network of actin and actin regulatory proteins that work together to power the cell forward (Svitkina and Borisy, 1999). This dense array of short, branched, actin filaments at the very leading edge, is continuously being built at the cell edge and disassembled as the network flows rearward, in a process termed actin treadmilling. Towards the cell body, the filaments become longer, more sparse and bundled. Numerous proteins are involved in maintaining and regulating actin architecture at the leading edge. Our understanding of the biochemical and cell biological roles of these proteins have given rise to the dendritic nucleation model, illustrated in Figure 1-1 (Pollard et al., 2000). Briefly, this model postulates that actin is nucleated from mother filaments at the cell edge, creating a dense branched network that elongates and provides the energy required to push the plasma membrane forward. Filament capping occurs soon after nucleation, which ensures the maintenance of short filaments and a more mechanically rigid network. As filaments age, they fragment and depolymerize, and actin monomers are recycled back to the front of the cell. Each step of the dendritic nucleation model depends upon the activity of many actin regulatory proteins. Several of the key players are discussed in detail below.

1. Actin

Actin is a highly conserved and abundant ATPase that exists in monomeric and filamentous forms in cells. In vitro, ATP-actin polymerizes spontaneously into helical filaments when above the critical concentration and grows asymmetrically, with a fast growing "barbed" end and a slow growing "pointed" end. In vitro experiments have shown that the critical concentration for actin polymerization is typically around 0.1 μM for the barbed end and 0.6 μM for the pointed end (Pollard et al., 2000). In motile cells, however, the cellular concentration of monomeric ATP-actin

is typically 10-fold or greater than the critical concentration required for actin polymerization (Pollard et al., 2000). Cells manage to maintain a large pool of monomeric ATP actin through the action of proteins such as thymosinβ_4, which bind to actin monomers and inhibit them from polymerizing and/or exchanging nucleotide (Goldschmidt-Clermont et al., 1992; Safer et al., 1990). This pool of polymerization-ready actin monomers is necessary to enable cells to form cytoskeletal structures quickly and dynamically in response to their environment. It is critical that actin network assembly be coupled and in equilibrium with actin network disassembly in order to maintain this monomeric actin pool in vivo. Indeed, the primary role of many essential actin-binding proteins is to aid in the recycling of actin.

In motile cells, the barbed ends of actin filaments are typically oriented towards the direction of cell movement and their pointed ends towards the cell body. The summed force created by the elongation of actin filament barbed ends at the cell edge is proposed to be what drives membrane protrusion (Tilney et al., 1981). Filament growth in cells is generally limited to fast barbed end growth due to monomeric actin binding by the abundant, small globular protein profilin. Profilin binds to the barbed end of actin monomers with sub-micromolar affinity, sterically hindering them from binding to the pointed end of filaments or other monomers. An important product of this activity is that profilin effectively inhibits the *de novo* formation of actin filaments by blocking the formation of an actin trimer, the minimum nucleus for stable actin filament growth. Additionally, profilin acts both to increase the rate of ATP exchange and to decrease the intrinsic ATPase activity of actin (Mockrin and Korn, 1980; Nishida, 1985; Tobacman and Korn, 1982).

The ATPase activity of actin plays an important role in its regulation; many known actin regulatory proteins bind selectively to either ATP- or ADP-bound forms. In vitro, actin hydrolyzes its ATP soon after it is incorporated into an actin filament, with a $t_{1/2}$ of around 10 seconds. However, gamma phosphate release occurs slowly, with a $t_{1/2}$ of over 8 minutes (Blanchoin et al., 2000; Carlier, 1991). Since most polymerization-ready monomeric actin in the cell is bound to profilin and ATP, filaments at the cell edge are primarily composed of ATP actin while older, more cell-

body proximal filaments tend to be composed of ADP-Pi or ADP actin. The correlation of actin filament age and proximity to the cell edge appears to play an important role in the localization and activity of actin binding proteins. Proteins whose functions are involved in actin network breakdown, such as cofilin, tend to bind specifically to filamentous ADP actin distal from the cell edge (Carlier et al., 1997), while proteins involved in actin network building, such as the Arp2/3 complex and profilin, bind preferentially to filamentous ATP actin proximal to the cell edge (Blanchoin et al., 2000; Carlier et al., 1999). Several actin-binding proteins, including cofilin, have been shown to enhance the rate of ATP hydrolysis or phosphate release by actin; this activity is believed to result in the faster observed rate of phosphate release and nucleotide exchange observed in vivo than that observed in vitro (Carlier, 1991).

2. The Arp2/3 Complex

The ordered, branched actin structures seen in motile cells, the inhibition of de novo actin nucleation in vivo and the abundance of barbed end capping all pointed to the existence of a factor in cells that both crosslinks and nucleates new actin filaments at the leading edge. This factor was discovered to be the Arp2/3 complex, a seven-subunit complex composed of actin related proteins (Arps) 2 and 3, and five novel proteins, named ArpC1-ArpC5 (Mullins et al., 1998; Mullins and Pollard, 1999). Arp2/3 has been found in all eukaryotic cells to date, and is particularly abundant in constitutively motile cell types such as *Acanthamoeba castellani*, the organism from which it was first purified (Machesky et al., 1994).

In vitro, the Arp2/3 complex binds to the sides and pointed ends of actin filaments, forming a Y-shaped branch that appears similar to actin structures seen at the leading edge of motile cells by electron microscopy (Mullins et al., 1998; Svitkina and Borisy, 1999). The nucleation activity of Arp2/3 is regulated by binding to nucleation promotion factors (NPFs) of the WASp/Scar family (Machesky et al., 1999) and requires filamentous actin side-binding (Dayel and Mullins, 2004). Arp2/3 is thought to undergo a conformational change upon activation, in which the Arps are

brought close together to form a pseudo-actin dimer. A nucleus is formed upon the addition of an actin monomer, and fast barbed end elongation ensues (Mullins and Pollard, 1999; Rodal et al., 2005). In support of this hypothesis, the Arp2/3 crystal structure was solved revealing a bi-lobed horseshoe-shaped complex, with the two Arps on either lobe within close proximity of one another (Robinson et al., 2001). However, the Arps do not appear as an actin pseudo-dimer, and the conformation solved in the crystal structure is believed to represent the inactive state of the complex. While there have been some suggestive electron microscopy and 3D reconstruction studies of the Arp2/3 complex in branched networks, a crystal structure of the active complex has not yet been achieved (Egile et al., 2005; Volkmann et al., 2001).

As with actin, the nucleotide state of the Arps appears to play a role in their regulation. Dayel and Mullins showed that the hydrolysis of ATP by Arp2 coincides with the activation of the Arp2/3 complex, and that hydrolysis requires the presence of filamentous actin, NPF, and the binding of a single actin monomer. They propose that the combined energy of binding monomeric and filamentous actin allows for the conformational change in Arp2/3, subsequent nucleus formation and barbed end growth (Dayel and Mullins, 2004).

In vivo, the Arp2/3 complex localizes to the leading edge of motile cells at actin network branchpoints (Svitkina and Borisy, 1999). Correct localization of Arp2/3 is likely to dependent in part on its transient association with membrane-associated NPFs (Sirotkin et al., 2005) and its preference for ATP actin filaments (Blanchoin et al., 2000). Several studies have implicated cytoskeletal tropomyosin as another important factor in limiting Arp2/3 activity to the lamellipod, a narrow cell edge-proximal region of motile cells. Biochemical studies have shown that tropomyosin decoration of actin filaments inhibits filament side binding by Arp2/3 as well as cofilin-mediated filament severing (Blanchoin et al., 2001). By immunostaining, DesMarais et al. found that tropomyosin is excluded from areas of dense filamentous actin and Arp2/3 localization (DesMarais et al., 2002). Gupton et al. have demonstrated that microinjection of skeletal muscle tropomyosin inhibits the formation of the lamellipod in PtK1 cells, exemplified by the depletion of

Arp2/3 and cofilin from the leading edge and a marked loss of signature lamellipodial actin kinetics (Gupton et al., 2005).

The activity of the Arp2/3 complex also appears to be regulated by post-translational modifications. Several studies have shown that Arp2/3 subunits appear to be phosphorylated in vivo (Singh et al., 2003b). LeClaire et al. has recently found that phosphorylation of subunits including Arp2 appear to negatively regulate Arp2/3 activity; they postulate that phosphorylation inhibits the conformational change that allows Arp2/3 to bind to the pointed end of new actin filaments (Lawrence LeClaire, personal communication).

Two other classes of actin nucleators, the formin and Spire families, have recently been identified. Formins have been shown to bind to the barbed end of actin filaments, and have both barbed end capping and nucleation activities in vitro (Pruyne et al., 2002; Zigmond et al., 2003). Several groups have shown that formins are processive actin filament cappers that are able to remain bound to the barbed end without inhibiting filament growth (Kozlov and Bershadsky, 2004; Romero et al., 2004). A crystal structure of the FH2 domain of Bni1, a yeast formin, reveals a homodimeric complex that forms a donut-like structure (Xu et al., 2004). The FH2 donut is thought to bind to the end of an actin filament and move with step-like motions as actin adds to the fast-growing barbed end (Kovar, 2006). Arp2/3 independent actin nucleation by formins appears to favor the formation of long, bundled actin networks, such as the actin network in the yeast cytokinetic ring and actin cables of fission yeast (Pelham and Chang, 2002; Severson et al., 2002).

Spire is a large, multi-domain protein that includes four WH2 domains that are each able to bind to actin monomers. Spire appears to nucleate filaments by a novel mechanism involving a linker sequence between the most C-terminal WH2 domains that may help in orienting the actin monomers to form a pseudo actin dimer (Quinlan et al., 2005). Preliminary results from J. Brad

Zuchero and R. Dyche Mullins suggest that this mechanism of actin nucleation may also occur in other WH2-containing protein families (personal communication).

3. Nucleation Promotion Factors

In vitro, the Arp2/3 complex exhibits a very low intrinsic nucleation rate when mixed with actin monomers. In the presence of a nucleation promotion factor (NPF), however, the rates of actin assembly are increased by 50 fold (Machesky et al., 1999; Welch et al., 1998a).

Three regions comprise the Arp2/3-activating module, often referred to as the VCA domain, which is typically found at the extreme C-terminus of a NPF: (1) one or more WASP homology 2 (WH2) or verprolin homology (V) domains, which bind to actin monomers, (2) a central (C) region, also known as the cofilin homology sequence, which binds to Arp2/3 and actin, and (3) an acidic (A) region which binds and activates the Arp2/3 complex. Each of these regions is necessary for the efficient activation of the Arp2/3 complex and appears to play a distinct role in the creation of an actin nucleus (Skoble et al., 2000). Binding of the A domain, in addition to filamentous and monomeric actin, is thought to induce the active, closed conformation of Arp2/3, and is necessary for efficient activation of Arp2/3 (Dayel and Mullins, 2004; Goley et al., 2004). Actin monomers are brought into close proximity to Arp2/3 by the WH2 domain, allowing for the stabilization of the nascent actin nucleus. The C domain is able to bind to both the Arp2/3 complex and an actin monomer, but these interactions are mutually exclusive. Kelly et al. hypothesize that the C domain plays an active and dynamic role in the activation of Arp2/3 by first stabilizing the active Arp2/3 conformation, then rapidly guiding an actin monomer towards the Arps to form an Arp2/3-actin nucleus (Kelly et al., 2006).

Because the VCA region is such a potent activator of Arp2/3, cells have evolved diverse mechanisms by which to regulate how and when VCA may bind and activate Arp2/3 in vivo. NPFs of the Wiscott-Aldrich syndrome protein (WASP) family use an intra-molecular

autoinhibitory mechanism to regulate Arp2/3 activity, while NPFs of the WAVE/SCAR family employ a trans-molecular regulatory strategy. The WASP family is characterized as having a GTPase binding domain (GBD) in their central region that binds to small GTPases of the Rho family with high specificity for Cdc42 (Aspenstrom et al., 1996). Next to the GBD is a basic region, which binds to phosphatidylinositol (4,5)-bisphosphate (PIP2) (Prehoda et al., 2000). In the absence of either of these factors, WASP proteins are in a 'closed' autoinhibited state and are unable to activate Arp2/3, but addition of both Cdc42 and PIP2 allows for WASP to 'open' and for the VCA domain to efficiently activate Arp2/3 (Prehoda et al., 2000). In the cell, a dual-input regulatory mechanism ensures that Arp2/3 is activated in response to the correct signal (active, GTP-bound Cdc42) and in the correct location (at PIP2-enriched patches of membranes).

Recent studies have shown, however, that there are additional factors that regulate WASP activation in vivo. Another family of proteins, called WASP interacting proteins (WIPs), forms a stable complex with N-WASP, a ubiquitously found member of the WASP family; the N-WASP-WIP complex is thought to represent the predominant form of N-WASP in cells (Ho et al., 2001). WIP appears to stabilize the inactive N-WASP complex in cells, and this inhibition is relieved by the binding of a novel protein, Toca-1 (Ho et al., 2004). Interestingly, Ho et al. found that Toca-1 binds to Cdc42 directly, and that this binding is required for relief of WIP-induced inhibition of N-WASP activity. It appears that some combination of Cdc42, PIP2 and Toca-1 is likely to be required for WASP activation of the Arp2/3 complex in vivo, but mechanistic details are still lacking.

In vivo regulation of WAVE/SCAR proteins is not nearly as well understood as that of WASP family proteins. Like WASP, WAVE proteins act downstream of a Rho family GTPase, Rac, but as WAVE lacks a GBD, it appears that this interaction must be indirect (Miki et al., 1998). Full-length WAVE also appears completely active in vitro and is able to activate Arp2/3 as effectively as the WAVE VCA region alone, indicating that, unlike WASP, WAVE is not autoinhibited

(Machesky et al., 1999). This suggests that there must be factors in the cell that bind to and inactivate WAVE in trans.

The WAVE complex has now been identified and confirmed both in vitro and in vivo. A huge species, the WAVE complex appears to be composed of four proteins: PIR121/p140SRA-1, Nap1, Abi, and HSPC300, in addition to WAVE (Eden et al., 2002; Gautreau et al., 2004). One of these proteins, PIR121/p140SRA-1, is a member of a family known to bind Rac, and may be the elusive missing link between WAVE and Rho family GTPases. The role of the complex, however, has been controversial. Eden et al. reported that the pentameric WAVE complex is inactive, and that the addition of Rac causes dissociation of the complex and release of an active WAVE/HSPC300 species (Eden et al., 2002). Other groups have found that the pentameric WAVE complex is active in vivo and in vitro, and addition of Rac does not cause the dissociation of the complex; rather, they argue that the integrity of the complex is critical for localization and stability of WAVE rather than its activation (Innocenti et al., 2005; Steffen et al., 2004). Further studies are needed to resolve these conflicting models.

4. Capping Protein

Capping protein is an abundant, obligate heterodimer that binds to actin barbed ends with high affinity (Kd = 0.1 nM) and has been found in all eukaryotes examined thus far (Schafer et al., 1996; Wear and Cooper, 2004). Filament binding by capping protein inhibits both polymerization and depolymerization from the barbed end, and inhibits actin end-to-end annealing in vitro (Cooper et al., 1984; Isenberg et al., 1980). The crystal structure of the capping protein heterodimer reveals a mushroom-like structure with C-terminal flexible arms ('tentacles') extending from the mushroom cap that are thought to bind to each barbed end actin monomer (Yamashita et al., 2003).

Capping protein localizes to sites of active actin assembly in vivo, including actin patches in *Saccharomyces cerevisiae* and in the lamellum of fibroblast cells (Schafer et al., 1998; Waddle et al., 1996). In motile cells, capping protein is thought to play a critical role in the regulation of the dendritic actin networks at the leading edge. Without barbed end capping, actin filaments are theoretically free to undergo uncontrolled growth and will quickly deplete the cell of free actin monomers. Capping protein plays not only an important biochemical role in regulating the monomeric pool of actin, but also is a key player in determining the architecture of lamellipodial actin networks. Maintenance of a short, branched network is important for its mechanical properties. An actin network of long, sparsely branched filaments would likely be less mechanically rigid and thus less force-producing, and would likely collapse against the load of the leading edge membrane. Regulation of actin capping may also occur in order to spatially regulate where actin filaments are allowed to elongate. According the capping protein 'funneling' hypothesis, nearly all filament barbed ends are capped quickly and tightly by capping protein with the exception of a relatively small number of ends most proximal to the cell edge. This effectively funnels actin monomer addition to the barbed ends closest to the cell edge membrane, making force production more efficient (Carlier and Pantaloni, 1997).

Several negative regulators of capping protein activity have been identified. Phosphatidylinositol (4,5)-bisphosphate (PIP2), a component of the plasma membrane, has been found to bind directly to capping protein and inhibit its ability to cap barbed ends (Schafer et al., 1996). Based on their crystal structure of capping protein, Yamashita et al. speculate that PIP2 may bind to nitrates proximal to the actin binding sites, and may thus sterically hinder barbed end binding (Yamashita et al., 2003). Actin elongation resulting from PIP2-dependent uncapping has been observed in platelets, and may also play a role at the leading edge (Allen, 2003; Hartwig et al., 1995). However, the high affinity of capping protein for the barbed end relative to the concentrations of PIP2 necessary to uncap make it appear unlikely that this mode of uncapping is a major mechanism by which to create free barbed ends at the leading edge (DiNubile and Huang, 1997).

Carmil was first isolated from Dictyostelium where it was found to immunoprecipitate in a complex that included Arp2/3, capping protein and a type I myosin (Jung et al., 2001). Carmil was subsequently found to be a high-affinity (Kd = 1 nM) inhibitor of capping protein that drastically reduces the affinity of capping protein for barbed ends (Uruno et al., 2006; Yang et al., 2005). Carmil localizes to the lamellipod of human glioblastoma cells, and depletion of Carmil causes decreased F-actin and lamellipodial protrusion in these cells (Yang et al., 2005). Uruno et al. found that full-length Carmil was much less effective at inhibiting capping protein than a proteolytically cleaved fragment, suggesting that Carmil may be auto-inhibited in vivo (Uruno et al., 2006).

Another mode of capping protein regulation comes in the form of barbed end competition. In recent years, several classes of proteins have surfaced as barbed end cappers and appear to have antagonistic relationships with capping protein in vivo and in vitro (Harris et al., 2004; Schirenbeck et al., 2005; Zigmond et al., 2003). As mentioned earlier, formins are known to nucleate actin filaments and move processively with the fast-growing end. As barbed end binders, formins compete with capping protein for filament binding and thereby protect growing barbed ends from being capped (Zigmond et al., 2003). Similarly, members of the Ena/VASP family appear to associate with filament barbed ends and compete with capping protein (Bear et al., 2002).

5. Cofilin

The cofilin and actin depolymerizing factor (ADF) family of proteins are small, essential, abundant, and conserved across eukaryotic phyla. In vertebrates, two isoforms of cofilin and one of ADF exist; however, all isoforms are often expressed in the same cell and appear to have overlapping functions (Lappalainen et al., 1998). Lower eukaryotes, including yeast and fruit flies, appear to have only one copy of cofilin/ADF.

Cofilin acts to increase the rate of actin turnover in cells by both enhancing actin monomer dissociation from filaments and by severing actin filaments. Enhanced actin turnover by cofilin is due in large part to its preference for binding ADP actin, with a greater preference for monomeric ADP actin over filamentous ADP actin (Carlier et al., 1997; McGough et al., 1997). Its mechanism of action can be broken down into several key biochemical steps (Carlier et al., 1999): (1) cofilin binds to filamentous ADP actin in a cooperative manner, and enhances phosphate release from filamentous ADP-Pi actin (Blanchoin and Pollard, 1999), (2) binding of cofilin induces depolymerization of the filament due to filament twisting (discussed further below) and cofilin's preference for monomeric ADP actin over filamentous ADP actin (Carlier et al., 1997; McGough et al., 1997), and (3), rapid exchange of monomeric ADP-ADF-actin for ATP-profilin-actin in the cytosol (Blanchoin and Pollard, 1998). In this manner, cofilin acts to increase both the rates of actin depolymerization and of monomeric ATP actin production in the cell.

Cryo-electron microscopy of cofilin-bound actin filaments revealed a stunning result: cofilin changes actin filament twist, resulting in a 75% shorter crossover length (the distance between where one actin proto-filament crosses over the other) (McGough et al., 1997). This finding provides an elegant mechanistic explanation of how cofilin works at a molecular level. Cofilin binds to ADP filamentous actin and induces a small local change in twist, which grows larger and is propagated as more cofilin binds in a cooperative manner. Actin monomers at the pointed end of an actin filament have fewer contacts to stabilize their interaction with other actin monomers in the filament, and quickly dissociate as actin-cofilin dimers. Distal from the pointed end, twisting of the filament decreases lateral contacts between the actin proto-filaments, causing filament breakage and severing (McGough and Chiu, 1999).

The primary means of regulating cofilin activity appears to be by phosphorylation at Ser3. This phosphorylation, which is conserved across most species (Bamburg, 1999), renders the protein inactive and unable to bind actin (Agnew et al., 1995; Nagaoka et al., 1996). Two related groups

of kinases have been identified as phosphorylating cofilin in vivo and in vitro: LIM kinases (LIMK) (Arber et al., 1998; Yang et al., 1998) and TES kinases (TESK) (Toshima et al., 2001). Both kinase families appear to be specific for cofilin; no other substrates for LIMK or TESK have been reported. Cofilin-specific activating phosphatases have also been recently identified, and include slingshot and chronophin (Ambach et al., 2000; Gohla et al., 2005; Huang et al., 2006; Niwa et al., 2002). Phosphorylation and dephosphorylation of cofilin appear to play distinct roles in cell motility; Nishita et al. observed through depletion experiments that LIMK is necessary for the establishment of the leading edge, while slingshot was required for maintaining a single 'front' (Nishita et al., 2005). Depletion of cofilin or its regulatory phosphatases, or overexpression of regulatory kinases can all lead to accumulation of filamentous actin in vivo (Arber et al., 1998; Hotulainen et al., 2005; Niwa et al., 2002; Rogers et al., 2003).

Cofilin activity and localization are also affected by other cellular factors. As seen with Arp2/3, tropomyosin is implicated in the spatial regulation of cofilin. Tropomyosin-decorated filaments are protected against depolymerization and severing by cofilin both in vitro and in vivo (DesMarais et al., 2002; Ono and Ono, 2002). PIP2, a component of the plasma membrane, also serves as a negative regulator of cofilin activity (Yonezawa et al., 1990). This inhibition may also serve to spatially confine cofilin activity to older actin networks distal from the cell edge.

Actin dynamics at the leading edge

The rearward flow of the actin cytoskeleton at the leading edge of spreading and motile cells has been a source of fascination for generations of cell biologists. Early in the 1970s, it was noted that particles (typically, fluorescently conjugated antibodies or lectins) placed at the front edge of an immobile immune cell could adhere to the plasma membrane and be carried rearwards towards the cell body. This curious activity was termed 'capping' since the particles tended to aggregate at the cell center, forming a 'cap' over the perinuclear region. Capping was thought to be either the direct result of membrane flow (Bretscher, 1976) or flow of the underlying cortical

cytoskeleton (Bourguignon and Singer, 1977). The former hypothesis was eventually eliminated, and actin was identified as the source of centripetal motion (Heath, 1983).

To avoid confusion, it should be noted that actin polymerization at the leading edge may not necessarily be coupled to cell movement. In non-moving cells, such as Drosophila S2 cells, as well as the immune cells that were the subject of early capping experiments described above, actin polymerization causes the actin network to move rearward relative to the substrate while the cell edge remains immobile (Chapter 2). In small, highly motile cells such as fish keratocytes, the actin network remains immobile relative to the substrate, but moves rearward relative to the cell edge as the cell moves forward (Theriot and Mitchison, 1991).

The ability to label actin directly with fluorophores has greatly advanced our understanding of actin network dynamics in vivo. Microinjection of rhodamine-labeled actin into fibroblast cells coupled with FRAP (fluorescence recovery after photobleaching) revealed that the actin network at the cell edge moves towards the cell center with a constant velocity (Wang, 1985; Wang and Taylor, 1980). With improvements in microscopic resolution and fluorescence detection, it became possible to use lower quantities of labeled protein and still visualize the cytoskeleton. This led to the development of a technique called fluorescent speckle microscopy (FSM) by Waterman-Storer and Salmon, which has subsequently been used to study the dynamics of microtubule and actin networks in vivo (Waterman-Storer and Salmon, 1997). Waterman-Storer and Salmon found that microinjection of small quantities of fluorescently labeled tubulin (<2% of the cellular concentration) into cells resulted in random incorporation of labeled monomer into the microtubule network (Waterman-Storer et al., 1998). Brighter and dimmer areas were visible along a single microtubule, and this pattern could be used as fiduciary marks that could be used to study the dynamics of the microtubule network (Waterman-Storer and Danuser, 2002). The use of relatively low concentrations of fluorophore in FSM reduced background cytoplasmic fluorescence substantially, and also allowed for clear visualization of proteins that were

associated with, and thus immobilized by, large macromolecular assemblies such as the microtubule or actin cytoskeleton.

Speckle microscopy of actin allowed for the direct measurement of treadmilling velocities through manual measurement of speckles or through the creation of kymographs. Kymographs follow the movement of particles along their axis of movement in a graph-like format, with one axis representing each frame of a movie, and the other axis representing distance traveled. The slope of the line created by the speckle indicates its velocity. In this manner, it is possible to quickly quantify the movement of multiple speckles that appear in the same area and move in the same direction for the duration of a movie. Salmon et al. employed kymographs of fluorescent actin in newt epithelial cells and found that they could visually distinguish four zones of actin dynamics (Salmon et al., 2002). These zones were called (in order from the most cell-edge proximal compartment to the most distal) the lamellipodium, lamellum, convergence zone, and cell body. Lamellipodial actin speckles moved the fastest, at 1.6 μm/min, while lamellar actin moved more slowly (0.3 μm/min). Actin speckles in the cell body moved in the anterograde direction at 0.4 μm/min, and speckles in the convergence zone showed no movement (Salmon et al., 2002).

A potential issue with conventional speckle imaging is that a typical speckle is thought to arise from the fluorescence of at least two fluorophores within close enough proximity to be resolved as a single spot. Tracking this spot could lead to misinterpretations if the fluorophores are located on different filaments that move at different rates or directions. To resolve this problem, Watanabe and Mitchison employed total internal reflection fluorescence (TIRF) microscopy to study actin filament dynamics in live cells (Watanabe and Mitchison, 2002). TIRF allows for the clear resolution of a single fluorophore, such as a single GFP-actin molecule . Using this method, Watanabe and Mitchison found that a majority of actin speckles appearing at the cell edge disappeared within 8 seconds, suggesting that actin filaments are assembled and disassembled on a rapid time scale. In addition, they observed two distinct zones of actin polymerization based on the rate of speckle appearance: a 1 μm wide zone proximal to the cell edge with high levels of

polymerization, and the rest of the leading edge, which exhibited notably lower levels of polymerization.

One major drawback of the speckle analyses discussed thus far (kymograph analyses and manual tracking) is the limited amount of data that can be collected; only a tiny fraction of all the speckles that appear in a given cell can be analyzed using these methods. Recently, automated speckle tracking has been developed to cull large amounts of information on actin dynamics from movies of labeled actin monomers in a single cell. Using algorithms to identify and track single fluorescent particles, Danuser et al. have followed the movement of 10^5 - 10^6 speckles per cell in a given movie. These methods, termed quantitative FSM (qFSM) allowed them to make an important discovery about the structure of actin networks in motile cells and formulate the two-network model of the leading edge (Danuser, 2005; Ponti et al., 2004).

Using qFSM, Ponti et al. created 'kinematic' maps of actin turnover where the appearance of a speckle indicated actin assembly and its disappearance correlated to filament disassembly (Ponti et al., 2004). They found that the leading edge appears to be composed of two distinct networks, the lamellipodium and the lamellum, that overlap spatially. Lamellipodial actin exhibited fast speckle velocities and surprising kinetics: nearly all actin assembly took place at the very cell edge and was almost completely disassembled within 1-3 microns. In the lamellum, actin polymerization and depolymerization appeared random and patchy, and actin speckles were typically slow and long-lived. This lamellar actin kinetic signature was found to exist throughout the leading edge, suggesting that the two actin networks overlap proximal to the cell edge. Ponti et al. examined the role of the lamellipod and the lamellum by perturbing one compartment or the other using cytoskeletal drugs. They observed that, even in the absence of lamellipodial actin dynamics, the cells were still able to spread and move. This led to the controversial hypothesis that the lamellum, not the lamellipod, is the main driving force for leading edge protrusion. A subsequent study using microinjected tropomyosin supported this hypothesis. Gupton et al. reported that the microinjection of skeletal muscle tropomyosin into epithelial cells inhibited the

formation of the lamellipod, based on the loss of normal lamellipodial actin dynamics and Arp2/3 and cofilin localization (Gupton et al., 2005). However, these cells are still able to undergo leading edge membrane protrusion and migration despite the loss of the lamellipod, suggesting once again that the lamellipod is not necessary for these activities.

Through speckle microscopy of actin in vivo, we have gained a greater understanding of how cells regulate the leading edge actin networks. My graduate work has focused on refining further our understanding of how the dendritic nucleation model operates and is regulated in vivo using microscopic and biochemical tools.

We have found that it is possible to utilize FSM not only for actin, but for actin binding proteins as well. In Chapter 2, I describe the dynamics of several actin regulatory proteins, including Arp2/3, capping protein and tropomyosin, examined using FSM in live Drosophila S2 cells. I found that expression of these proteins at low levels allowed for the clear visualization and analysis of speckles. Depletion of actin regulatory proteins, including capping protein and cofilin, gave us insights into the roles of these proteins in vivo, and led us to the conclusion that filament capping and disassembly have opposing roles in the cell. Capping protein is needed to establish the lamellipodial actin network, while disassembly factors including cofilin and twinfilin, function to limit the size of the lamellipod.

Previous projects have focused on the regulation of the Arp2/3 complex in vivo. In Chapter 3, I describe the Squiggy project in which I tested for a functional relationship between 14-3-3 proteins and the Arp2/3 complex in vitro and in vivo. Finally, in the Appendix, I show preliminary results of the localization and function of different Carmil isoforms in S2 cells.

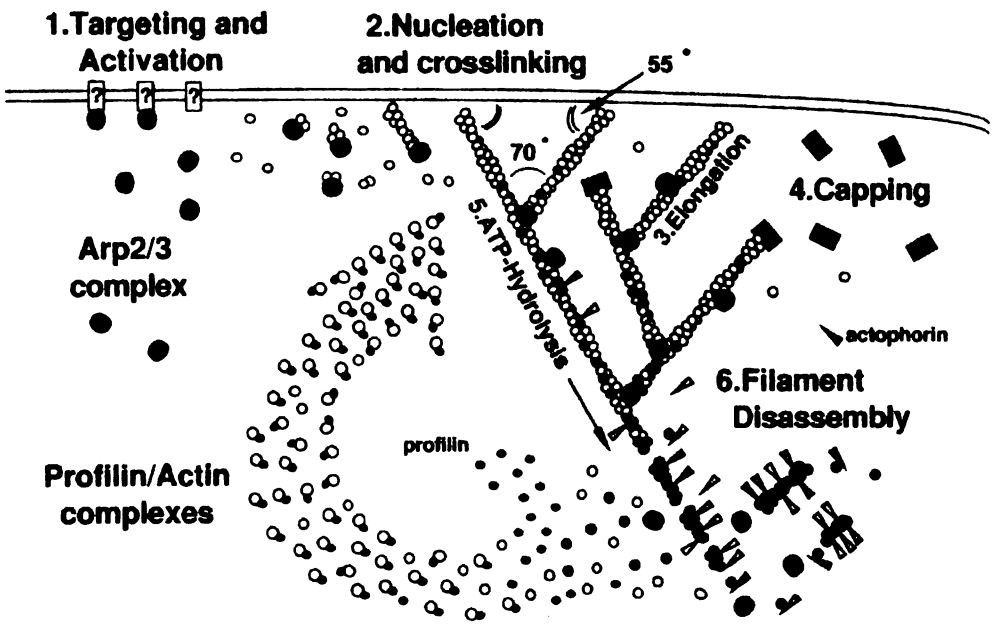

Figure 1-1. Actin networks at the leading edge, the übermodel. (1) Arp2/3 complex is targeted and activated by binding to nucleation promotion factors at the leading edge membrane. (2) Activated Arp2/3 binds to the sides of mother filaments and nucleates a new daughter filament, forming a Y-shaped branch. (3) The barbed end of actin filaments elongate until they are (4) capped by capping protein. (5) As the actin network flows towards the cell body and ages, ATP is hydrolyzed by monomers in F-actin. (6) ADF/cofilin family proteins disassemble ADP filamentous actin by severing filaments and catalyzing filament depolymerization from filament ends. Reprinted with permission from R. Dyche Mullins.

Chapter Two

Architecture of Lamellipodial Actin Networks: Spatial and Temporal Relationships between Filament Nucleation, Capping, Debranching, and Depolymerization

Janet Iwasa and R. Dyche Mullins

Submitted to Current Biology, June 2006

Background. The leading actin network in many motile cells is composed of two compartments, called the lamellipod and the lamellum, defined by filament geometry, velocity of retrograde flow, and kinetics of filament assembly and disassembly. Construction of the lamellipod requires a set of conserved proteins that form a biochemical cycle, centered around filament nucleation and branching by the Arp2/3 complex. The timing of this cycle and the roles of its components in determining network architecture *in vivo*, however, are not well understood.

Results. We performed fluorescent speckle microscopy on spreading *Drosophila* S2 cells using labeled derivatives of actin, the Arp2/3 complex, capping protein, and tropomyosin. We find that the leading edge of S2 cells is composed of a 1.4 μm wide, membrane-proximal lamellipod and a 4 μm wide, cell body-proximal lamellum and that capping protein and the Arp2/3 complex interact with distinct subcompartments of the lamellipodial network. Both incorporate into the network at the cell edge but capping protein dissociates after 15 seconds, and covers less than half the width of the lamellipod (0.58±0.01μm). The Arp2/3 complex dissociates 7 seconds after capping protein and covers two thirds of the lamellipod (0.83±0.01μm). The lamellipodial actin network persists for 14 additional seconds following the loss of the Arp2/3 complex. Depletion of capping protein by RNAi results in displacement of the Arp2/3 complex from the leading edge and disappearance of the lamellipodial actin network, with little effect on lamellar actin dynamics. In contrast, depletion of factors that control stability of actin filaments, including cofilin, slingshot, twinfilin, or tropomyosin produces dramatic expansion of the lamellipodial compartment at the expense of the lamellum.

Conclusions. Speckle microscopy enables us to reconstruct the timing of biochemical events that control assembly of the lamellipodial actin network. The Arp2/3 complex incorporates into the lamellipodial network at the cell edge but does not remain associated throughout the entire width of the lamellipod, indicating that Arp2/3-mediated branches fall apart well before the lamellipodial network itself disassembles. Capping protein is required at the cell edge for Arp2/3 complex activity and for formation of a lamellipodial network but it dissociates from the network at the moment when filament disassembly is first detected. Cofilin, twinfilin, and tropomyosin appear to play no role in assembling the lamellipodial network itself but function together to limit its size.

Introduction

Amoeboid cell motility requires construction of dynamic networks of actin filaments at the cell's leading edge. These networks form characteristic compartments, defined by: (i) proximity to the membrane, (ii) rates of filament assembly and disassembly, and (iii) velocity of filament movement (Salmon et al., 2002; Vallotton et al., 2004; Watanabe and Mitchison, 2002). Salmon et al. identified four distinct compartments in the actin cytoskeleton of migrating newt lung epithelial cells (Salmon et al., 2002). At the very front of a migrating cell, in a compartment called the lamellipod, actin filaments are nucleated, crosslinked, and treadmill rapidly rearward toward the cell body as they elongate from their membrane-proximal barbed ends. Filaments in this compartment are relatively short-lived and depolymerize not far from the cell edge. Behind the lamellipod is a slower-moving actin network called the lamellum. The origin of actin filaments in the lamellum is more mysterious but their retrograde movement requires activity of the non-muscle myosin II motor protein. Myosin II localizes near the rear of the lamellum, where it contacts the cell body. Retrograde flow of actin causes filaments to accumulate at the boundary between the lamellum and the cell body. This region is, therefore, referred to as the convergence zone. Most lamellar actin filaments appear to be disassembled in the convergence zone (Salmon et al., 2002). A fourth population of filaments in the cell body undergoes anterograde flow and merges with the lamellar actin in the convergence zone.

We previously proposed a biochemical cycle for assembly and disassembly of actin filaments in motile actin networks, based on dendritic nucleation by the Arp2/3 complex (Pollard et al., 2000). In our model, the Arp2/3 complex is activated at the membrane of the leading edge by interaction with nucleation promoting factors and preexisting actin filaments and nucleates new daughter filaments that form an interconnected, branching network (Welch and Mullins, 2002). The new filaments elongate from their free barbed ends and the free energy of polymerization is converted into work, pushing the cell membrane forward. Each filament elongates until capping protein binds to its barbed end and terminates its growth (Carlier and Pantaloni, 1997). Actin

disassembly is catalyzed in part by cofilin, which, together with profilin, promotes recycling of actin monomers (Bamburg, 1999). This mechanism is thought to drive actin dynamics primarily in the lamellipod, in part because tropomyosin prevents binding of both cofilin and the Arp2/3 complex to actin filaments in the lamellum (Blanchoin et al., 2001; DesMarais et al., 2002). This view is consistent with the morphologies of the actin networks of motile cells revealed by electron microscopy. Svitkina et al. found the lamellipodial network to be composed primarily of very short (100 nm) and densely-branched actin filaments which contain significant amounts of the Arp2/3 complex. These authors also reported that lamellar regions of the cell contain much longer actin filaments with few or no side branches and much less Arp2/3 complex (Svitkina and Borisy, 1999).

In vitro the Arp2/3 complex requires no additional crosslinking factors to generate actin networks, produce force, and drive sustained motility. *In vivo*, however, other crosslinkers, including ABP-280, play important roles in organizing actin networks at the leading edge (Flanagan et al., 2001). Understanding the contributions of the Arp2/3 complex and other factors to actin network organization and stability *in vivo* requires understanding the timing of their interactions with the network. Cofilin and capping protein also play essential roles in promoting sustained, Arp2/3-dependent motility *in vitro* but their contributions to construction of motile actin networks *in vivo* are less clear. Capping protein terminates filament elongation and cofilin disassembles filaments so that, generally speaking, both proteins should decrease filament content *in vivo*. The kinetics of the two reactions, however, are quite different. Capping protein can terminate elongation of any free filament barbed end while cofilin interacts preferentially with filaments that have hydrolyzed their bound ATP and released the inorganic phosphate.

In this study, we use fluorescent speckle microscopy of actin, Arp2/3, capping protein, and tropomyosin to correlate the spatial and temporal dynamics of the actin network at the leading edge of *Drosophila* S2 cells with those of the proteins that construct the network. We find that the lamellipodial compartment is more complex than previously appreciated and contains at least

three subcompartments: (i) a distal zone near the cell edge in which the Arp2/3 complex and capping protein associate with the network, (ii) a middle zone lacking capping protein but containing the Arp2/3 complex, and (iii) a region near the boundary with the lamellum lacking both proteins. We also find that assembly of the lamellipod depends critically on the presence of both the Arp2/3 complex and capping protein. Loss of cofilin, the cofilin phosphatase slingshot, or tropomyosin leads to the expansion of the lamellipod at the expense of the lamellum. Our data reveal the precise timing of molecular events at the leading edge and indicate that cofilin and capping protein play profoundly different roles in determining the architecture of motile actin networks *in vivo*.

Results

Actin speckle dynamics reveal multiple cytoskeletal networks at the leading edge of *Drosophila* S2 cells.

Rogers et al. previously used *Drosophila* S2 cells to study the function of actin regulatory proteins (Rogers et al., 2003). In the present study we use fluorescent speckle microscopy to study the organization and dynamics of the S2 cytoskeleton in finer detail. When plated on concanavilin A, S2 cells spread symmetrically and eventually adopt a circular morphology with the nucleus and cell body at the center surrounded by a 4-5 micron wide, actin-rich cortex. The height of the peripheral, actin-rich region is less than 200 nm, making it well-suited for speckle microscopy. We expressed *Drosophila* actin, fused at the C-terminus to Enhanced Green Fluorescent Protein (EGFP), under control of a copper-inducible promoter. Upon addition of copper, the cells produce high levels of fluorescent actin, which incorporates mainly into the peripheral cortex (unpublished observations). In the absence of added copper, the leakiness of the promoter produces low, but stable, levels of GFP-actin expression and results in the appearance of fluorescent speckles.

Consistent with the localization of endogenous actin by phalloidin staining, GFP-actin speckles appear primarily in the peripheral regions of S2 cells. We observed the highest density of actin speckles within one micron of the cell edge and the lowest density in the cell body (Figure 1, 2a). To characterize cytoskeletal dynamics we analyzed trajectories of more than 600 individual speckles from 42 kymographs obtained from 11 representative cells (Figure 1b, top panel). For each trajectory we plotted the distance from the cell edge at which the speckle first appears versus its average velocity (Figure 2c, top panel). This analysis reveals three distinct classes of speckles: (i) fast-moving speckles within one micron of the cell edge, (ii) slower moving speckles between the cell edge and the cell body, and (iii) immobile speckles in the cell body. Speckles appearing within 5% of the cell radius (typically <1 micron) from the cell edge move toward the cell body at an average speed of 2.46±0.04 μm/min and travel an average distance of 1.40±0.03

μm (Figure 2b, black line). Speckles born between 5% and 35% of the cell radius (1 - 6 microns) from the cell edge move significantly slower, averaging 1.31±0.04 μm/min over an average distance of 0.77±0.03 μm (Table 1). Speckles born more than 35% of the cell radius (more than 6 microns) from the cell edge are largely immobile with an average velocity of 0.15±0.02 μm/min. The distinction between the three populations is apparent from the distribution of speckle velocities, even when location is not taken into account. We fit the cumulative distribution of all speckle velocities to several models and found that a three-population model fit the data significantly better than models based on either one or two populations (Figure 2d). The mean values of the three populations match the average velocities calculated by binning trajectories based on distance from the cell edge (Figures 2c-d). Thus, based on both location and velocity we can distinguish three compartments in the actin cytoskeleton of S2 cells: two mobile compartments at the cell periphery and one immobile compartment in the cell body. These compartments are remarkably similar to those previously described by Ponti et al. in newt lung epithelial cells and Ptk1 cells (Ponti et al., 2004). These authors referred to the membrane proximal actin network as the lamellipod and the slow-moving network immediately behind it as the lamellum. We follow the same convention here.

The activities of actin regulatory proteins define unique subcompartments of the peripheral cytoskeleton.

We next used fluorescent speckle microscopy to examine the localization and dynamics of key actin regulatory factors. We used leaky expression from the same copper inducible promoter to generate low levels of EGFP fused to either the p16 (ArpC5) or Arp3 subunit of the Arp2/3 complex, the alpha subunit of capping protein (CPA), or cytoskeletal tropomyosin (cTm) in S2 cells. Previous studies demonstrated that these proteins can be fluorescently tagged without disrupting *in vivo* function (Aizawa et al., 1997; Helfman et al., 1999; Schafer et al., 1998).

The distribution of fluorescently-tagged Arp2/3 complex is similar to previously published immuno-localization studies in S2 cells (Rogers et al., 2003). The localization and dynamics of both GFP-Arp3 and GFP-p16 speckles were identical but our GFP-p16 construct generated less background fluorescence and slightly higher contrast than GFP-Arp3. For this reason we used GFP-p16 in many experiments in preference to GFP-Arp3. Based on appearance of either GFP-p16 or GFP-Arp3 speckles the complex associates almost exclusively with the lamellipodial actin network within one micron of the cell edge (Figure 1). From movies of 10 different cells expressing either GFP-p16 or GFP-Arp3, we created 81 kymographs and analyzed over 650 speckle trajectories (Table 1). When we plot distance from the cell edge versus velocity we observe the same three populations of speckles as with labeled actin. The relative numbers in each population, however, are quite different, with the large majority of Arp2/3 complex speckles being born in the lamellipodial region (within 0.5 μm of the cell edge). Near the cell edge Arp2/3 complex speckles undergo retrograde flow at the same velocity as lamellipodial actin speckles (2.44±0.03 μm/min versus 2.46±0.04 μm/min) but have a significantly shorter average lifetime (21.6±0.6 sec versus 35.4±0.6 sec) and do not travel as far from the cell edge (0.83±0.01 μm versus 1.40±0.03 μm; Table 1). We confirmed that the Arp2/3 complex associates only with the most membrane-proximal 2/3 of the lamellipodial network by expressing both GFP-actin and RFP-p16 simultaneously in the same cells (data not shown).

Ponti et al. (Ponti et al., 2004) used quantitative image analysis to map the kinetics of appearance and disappearance of actin speckles and found that the lamellipod contains a narrow (1μm) band of rapid speckle appearance near the cell edge followed by a band of rapid speckle disappearance. These authors interpreted speckle appearance and disappearance as localized filament assembly and disassembly and considered the polarized pattern they observed a signature feature of the lamellipod. We created similar maps of both actin and Arp2/3 complex speckle kinetics using software designed by the Danuser group (Figure 3a-b). Similar to the previous study, our actin map contains sharp, polarized bands of assembly and disassembly within 1.5 microns of the cell edge. We observe a similarly polarized pattern in our Arp2/3 speckle

kinetics map. Consistent with our kymograph analysis we find that rapid appearance of Arp2/3 complex speckles occurs near the cell edge and coincides with the peak of actin filament assembly while Arp2/3 speckle disappearance precedes peak actin disassembly by 0.6 μm (Figure 3c). This analysis is based on automated tracking of every observable speckle in the cell and does not suffer from the same potential for bias as kymograph analysis. From these data we conclude that the interaction of the Arp2/3 complex with the actin network defines a previously undescribed subcompartment of the actin cytoskeleton comprising the most membrane-proximal two thirds of the lamellipodial network.

A small number of mobile Arp2/3 complex speckles appear outside the lamellipodial zone. Most of these speckles arise from hot spots within the lamellum. These hot spots are fixed points from which multiple GFP-p16 speckles appear and then undergo retrograde flow at the lamellar velocity. The distribution of all Arp2/3 speckle velocities, however, is well-fit by a double Gaussian with peaks corresponding to the lamellipodial and cell body velocities of actin speckles (Figure 2d), indicating the relative scarcity of Arp2/3 complex speckles in the lamellum.

Capping protein speckles are restricted to an even narrower zone within the lamellipod than Arp2/3 complex speckles, often appearing as a thin, bright ring of fluorescence at the very cell edge (Figure 1a). From 12 cells expressing GFP-CPA, we created 127 kymographs and analyzed over 500 individual speckle trajectories (Table 1). This analysis reveals that capping protein speckles in the lamellipod are restricted to a narrow zone, within 0.58±0.01 μm of the cell edge and have an average lifespan of 15.0±0.6 sec. Capping protein speckles move at an average velocity of 2.57±0.05 μm/min, similar to actin and the Arp2/3 complex in the lamellipod (Figure 2b-c). The distribution of CPA speckle velocities fits a double Gaussian with means matching the average velocities of actin in the lamellipod and cell body (Figure 2d). Capping protein association thus defines an additional subcompartment of the lamellipod, one significantly smaller than that defined by the Arp2/3 complex. Unlike the Arp2/3 complex, capping protein speckles do not move from hot spots within the lamellum but do occasionally form bright, stable,

unmoving spots distal to the cell edge. Together our results indicate that actin, the Arp2/3 complex, and capping protein occupy unique but nested zones within the lamellipodial actin network. This fact is most easily appreciated in average intensity line scans created from speckle movies of each factor (Figure 2a).

Finally, we analyzed the localization and dynamics of cytoplasmic tropomyosin (cTm) speckles. We generated and analyzed 103 kymographs and over 550 speckle trajectories from 10 representative cells. GFP-cTm speckles are born at least one micron from the cell edge and are almost completely absent from the lamellipodial region (Figure 2). In general, the velocity of GFP-cTm speckles in the lamellum and cell body regions matched those of GFP-actin speckles, with a lamellar velocity of 0.91±0.03 μm/min and a cell body velocity of 0.29±0.03 μm/min (Table 1). A double Gaussian with peaks corresponding to actin speckle velocities in the lamellum and cell body fits the distribution of cTm speckle velocities well (Figure 2c). We note that the zones of tropomyosin and Arp2/3 complex localization and movement are almost completely mutually exclusive.

Depletion of Tropomyosin, Slingshot or Twinfilin causes expansion of the lamellipod at the expense of the lamellum.

Having characterized the dynamic organization of the actin networks at the leading edge, we next sought to understand the molecular mechanisms by which they are constructed. We incubated cells with double stranded (ds) RNAs designed to deplete various actin regulatory proteins and then observed the effect of depletion on cell morphology and on dynamics of actin, capping protein, tropomyosin, and the Arp2/3 complex by speckle microscopy.

Depletion of cTm with dsRNA produces specific and reproducible aberrations in the actin networks at the leading edge. In a typical RNAi-treated sample, 50% of cells appeared wild type, 35% had discontinuous, ragged leading edges, and 15% were stellate, with long actin-rich

projections, or were otherwise not well spread. Consistent with these ratios, immuno-blotting indicated approximately 50% depletion of endogenous cTm after 7 days of RNAi treatment (supplemental figure S1a). To test whether the range of phenotypes observed represents cell-to-cell variation in the degree of cTm knockdown, we used an S2 cell line that stably expresses GFP-cTm. After 7 days of cTm RNAi treatment, we fixed the cells and stained them with phalloidin. The efficiency of cTm depletion varied from cell to cell, and the intensity of GFP-cTm fluorescence was inversely proportional to the severity of the morphological phenotype. Cells expressing the highest levels of GFP-cTm appeared wild type, while cells expressing little or no GFP-cTm were ragged-edged or stellate (supplemental figure S1b). For the rest of our analysis we focused on cells exhibiting the ragged-edged phenotype, which probably represents partial knockdown of cTm. We did not attempt to analyze stellate cells because they do not form stable leading edges.

The leading edges of cTm-depleted cells are more dynamic and undergo much more rapid and extensive local protrusion and retraction than untreated cells (Figure 4f). By confocal time-lapse imaging we observe only two classes of actin speckles in cTm-depleted cells: (i) fast-moving speckles distributed uniformly around the cell periphery and (ii) immobile speckles in the cell body. From kymograph analysis the velocity of the fast-moving speckles is intermediate between the lamellipodial and lamellar speckle velocities measured in untreated cells. The distribution of actin speckle velocities in cTm depleted cells is best described by a double Gaussian rather than a triple Gaussian, with a mean velocity of 2.08±0.03 μm/min for the fast-moving population (Figure 4d). In addition, the lifetime of the fast-moving speckles is 25% longer than that of lamellipodial actin speckles in untreated cells (Table 1). The overall effect of the perturbation is that the peripheral actin cytoskeleton now appears to be formed from a single, homogeneous network (Figure 4c-e).

To determine whether this network represents a fast-moving lamellum or a greatly expanded lamellipod, we examined the rates of actin filament turnover and the dynamics of proteins

characteristic of lamellipodial networks. In cTm-depleted cells we observed broad, polarized bands of actin assembly and disassembly that, together, span the width of the peripheral cortex (Figure 3c). Such polarized assembly and disassembly is more characteristic of lamellipodial than lamellar networks. In addition, the spatial distributions of Arp2/3 complex and capping protein speckles are greatly expanded and completely coincident, no longer restricted to nested subcompartments (Figure 4c). Individual GFP-p16 and GFP-CPA speckles travel farther and have a longer lifespan than in mock-treated RNAi controls, with some speckles reaching the boundary of the cell body. The GFP-p16 and GFP-CPA speckles appearing distal to the cell edge also show relatively fast velocities and long lifespans. In cTm RNAi-treated cells, hotspots of actin and GFP-p16 fluorescence frequently appear distal from the cell edge (Figure 4a-b) and at the boundary with the cell body large spots of fluorescence that are bright and immobile are often observed for both GFP-p16 and GFP-CPA (Figure 4a-b).

Interestingly, depletion of the cofilin phosphatase slingshot or the actin sequestering and severing protein twinfilin results in a phenotype almost identical to that of cTm RNAi (Table 1, supplemental figures S2, S3). Based on examinations of fixed cells, neither slingshot nor twinfilin RNAi affects the ability of cells to spread and the general morphologies of RNAi-treated cells are indistinguishable from untreated controls. Speckle microscopy of labeled actin, capping protein and the Arp2/3 complex, however, reveals that the peripheral actin cytoskeleton in slingshot or twinfilin depleted cells appears to be a single, homogeneous, lamellipodial network. As in cTm-depleted cells, however, the velocities of speckles in the peripheral network of slingshot or twinfilin depleted cells are slightly slower than lamellipodial retrograde flow velocities in untreated cells (Table 1). These results suggest that, like cytoskeletal tropomyosin, loss of slingshot or twinfilin leads to dramatic expansion of the lamellipodial network.

Depletion of cofilin results in decreased retrograde velocities of actin networks at the leading edge and expansion of the lamellipod.

Cofilin severs and depolymerizes actin filaments and plays a critical role in regulating turnover of filament networks *in vivo* (Bamburg et al., 1999; McGough et al., 1997). We depleted cofilin in S2 cells using dsRNA against Drosophila cofilin/ADF (twinstar) and fixed and stained cells with fluorescent phalloidin. Consistent with a previous report (Rogers et al., 2003), we found that cofilin RNAi caused most S2 cells (76%) to remain rounded and non-adherent on the concanavilin A substrate. 4% of depleted cells exhibit a wide zone of dense actin similar to the slingshot depletion phenotype, 6% had stellate morphologies with thick, ropelike bundles of actin, and 14% appeared WT.

Although a majority of cofilin-depleted cells remain non-adherent, 20-30% of the population eventually spread if given sufficient time (1.5 - 2 hours, approximately double the normal time allowed). After spreading, the gross morphology of these cells appears normal. Phalloidin staining of fixed RNAi treated cells revealed long coils of actin filaments in cells that were unable to spread on concanavilin A-coated coverslips, and slightly elevated levels of F-actin in cells that were well spread, similar to cTm-depleted cells (data not shown). By confocal microscopy of live cells expressing GFP actin, the leading edge networks of cofilin-depleted cells move considerably slower than controls (Figure 5a,c-d). On average, GFP-actin speckles flowed towards the cell body with a velocity of 0.88±0.05μm/min in the lamellipodial region (compared to 2.46±0.04μm/min in untreated cells) and 0.48±0.03μm/min in the lamellar region (compared to 1.31±0.04μm/min micron per minute in untreated cells). Similarly, GFP-p16 and GFP-CPA also traversed the lamellipod at slower rates, with velocities of 1.11±0.04μm/min and 1.25±0.08μm/min, respectively (Table 1).

Cofilin-depleted cells, like cells depleted of cTm, slingshot and twinfilin, exhibit expanded zones of capping protein and Arp2/3 complex speckle flow as well as increased speckle lifespans (Table 1, Figure 5a-c). Because of the slow speed of the speckles relative to the length of the time-lapse sequences, many trajectories were truncated in the kymographs (Figure 5a). As a result, lifespan and distance measurements are somewhat underestimated. Nonetheless, it is clear that, as

judged by the association of the Arp2/3 complex and capping protein, the lamellipodial actin network is expanded in cofilin-depleted cells. In addition the lamellipodial actin, Arp2/3 complex, and capping protein zones are now completely coincident.

Depletion of capping protein abolishes the lamellipodial compartment but has little effect on the lamellum.

We depleted the alpha subunit of capping protein from GFP-actin or GFP-p16 expressing S2 cells using RNAi and observed its effects on the leading edge actin network. After a 7-day RNAi treatment, over 95% of cells showed intense membrane ruffling but were still able to spread efficiently on concanavilin A-coated coverslips. RNAi using dsRNA against the beta subunit or using dsRNA against both subunits resulted in identical phenotypes and similar efficacies (data not shown).

We examined the effect of CPA RNAi on actin network architecture more closely by phalloidin staining fixed cells. Actin filaments in CPA RNAi treated cells were long and bundled, curving around the margins of the cell and often forming bright clumps or tangles (Figure 6e). In most capping protein-depleted cells, no transition between lamellipod and lamellum could be distinguished.

Confocal microscopy of capping protein-depleted cells revealed that the membrane ruffles are dynamic and move continuously. GFP-actin speckles near the cell edge move, on average 25% slower than lamellipodial actin speckles in untreated cells. Actin speckles at the cell edge also undergo retrograde motion for a significantly shorter distance, averaging 0.70±0.02 microns from the leading edge. Farther from the cell edge actin speckles moved at velocities characteristic of lamellar actin speckles in untreated cells, with a mean velocity of 0.94±0.04μm/min. The distribution of actin speckle velocities fit well to a three-population model with means that match those in untreated cells. However, the peak corresponding to the intermediate, lamellar, flow

velocity is disproportionately large compared to untreated cells (Figure 6c). Scatter plots of distance versus velocity also indicate that, even near the cell edge, the majority of speckles move at speeds characteristic of lamellar actin networks in untreated cells (Figure 6b).

Arp2/3 complex speckles in capping protein-depleted cells were largely immobile and appeared to be aggregated in bright puncta, often in areas distal from the cell edge. Kymograph analyses showed that velocities of GFP-p16 speckles in all areas of the cell averaged less than 0.5 microns per minute (Figure 6c).

Discussion

Speckle microscopy has been used previously to characterize dynamics of actin networks in migrating cells. Here, we use it to study the dynamics of proteins that assemble these networks. Under our experimental conditions, fluorescent speckles appear only when diffusion of a labeled protein is restricted by association with a large cellular structure such as the cytoskeleton (Waterman-Storer et al., 1998). We correlated the position and velocity of speckles generated by three actin-associated proteins with those generated by actin itself to confirm their association with the actin network. Using this technique we determined when and where the Arp2/3 complex, capping protein, and tropomyosin associate with the peripheral cytoskeleton of *Drosophila* S2 cells. Because these proteins are active only when bound to filamentous actin, imaging their association with the network provides a dynamic map of when and where they exert their influence on cytoskeletal architecture. We coupled this dynamic mapping approach with dsRNA-induced knockdown of protein expression to determine the specific effects of filament capping and disassembly on the structure of leading edge networks.

Ponti et al. (Ponti et al., 2004) identified two distinct actin networks at the leading edge of motile cells, which they referred to as the *lamellipod* and the *lamellum*. The lamellipod is a membrane-proximal zone characterized by rapid appearance and disappearance of actin filaments and rapid retrograde flow of the actin network from the cell edge toward the cell body. The lamellum extends farther toward the cell body from the cell edge; has lower rates of filament appearance and loss; and undergoes slower retrograde flow. In addition, filament assembly and disassembly in the lamellipod is polarized, with the highest rate of assembly at the cell edge and the highest rate of disassembly at the boundary with the lamellum. Assembly and disassembly in the lamellum are more uniformly distributed and occur at much lower rates than in the lamellipod. In our study of fluorescent actin speckles we observe the same arrangement at the leading edge of *Drosophila* S2 cells, which have two actin networks, easily distinguished by velocity of retrograde flow and proximity to the cell edge. Following the convention of Ponti et al. (Ponti et al., 2004) we

refer to the membrane-proximal network as the lamellipod and the cell body-proximal network as the lamellum.

Association of capping protein and the Arp2/3 complex with the lamellipodial actin network.

Based on its localization to actin branches near the cell edge (Svitkina and Borisy, 1999) and its ability to construct force-generating networks *in vitro* (Carlier et al., 2003), the Arp2/3 complex has been proposed to play a central role in assembling the lamellipodial actin network (Pollard et al., 2000). Gupton et al. (Gupton et al., 2005) considered its presence a signature of the lamellipod itself. This idea is strongly supported by our speckle microscopy studies, which indicate that the Arp2/3 complex associates primarily with the membrane-proximal, lamellipodial actin network. The majority of actin filaments in the lamellipod are nucleated at the cell edge and disassembled 35 seconds later, approximately one and a half microns from where they were born ((Ponti et al., 2004) and this study). Most Arp2/3 speckles also appear at the very cell edge and undergo retrograde flow at the same rate as lamellipodial actin. On average, these speckles have a lifetime of 22 seconds and disappear within a narrow zone approximately 0.8 μm from the cell edge. This zone is clearly distinct from the region where lamellipodial actin speckles begin rapidly disappearing. This result has several important implications: (1) The lamellipodial actin network is not held together solely by the Arp2/3 complex and can retain its structure for a time in the absence of the complex. Further studies will be required to determine which crosslinkers make the most important contributions to maintaining integrity of the lamellipod in the absence of the Arp2/3 complex. One excellent candidate is ABP-280, which has been shown to support leading edge protrusion and motility in several cell types (Flanagan et al., 2001; Sokol and Cooley, 2003). (2) *In vivo,* filament debranching is not driven by filament depolymerization and is a separate process. This is very different from *in vitro* reconstitution studies in which the Arp2/3 complex dissociates from motile actin networks only when the filaments to which it is attached are

disassembled (Samarin et al., 2003). The processes of debranching and Arp2/3 dissociation *in vivo* clearly require further study.

A small number of Arp2/3 complex speckles (17.8%) appear within the lamellar actin network and undergo retrograde flow at the lamellar velocity. These speckles appear randomly throughout the lamellum, with no apparent bias toward the cell edge. This pattern corresponds to the pattern of actin speckle appearance we observe within the lamellum of S2 cells and that other groups have observed in lamellar regions of newt lung epithelial cells, Ptk1 cells (Ponti et al., 2004), and *Xenopus* keratinocytes (Watanabe and Mitchison, 2002). Our results suggest that some of this lamellar actin polymerization is due to a low level of Arp2/3 complex activity.

Capping protein is even more tightly localized within the lamellipod than the Arp2/3 complex. Almost all capping protein speckles appear at the cell edge and move toward the cell body at the lamellipodial actin velocity but they disappear much more quickly than Arp2/3 speckles – within 15 seconds, or 0.6 μm from the cell edge. The Arp2/3 complex is localized in part by its interaction with membrane-associated WASP/Scar family proteins while capping protein localization probably reflects the fact that the lamellipod has the highest sustained rate of new filament formation of any region in the cell (Chan et al., 2000). If the Arp2/3 complex is nucleating actin filaments at the cell edge and capping protein is binding their barbed ends, why do the two proteins dissociate from the network with different kinetics? Formally, there are three possibilities: (1) Filaments are specifically uncapped by a factor within the lamellipod (Allen, 2003). (2) Filaments bound to capping protein are preferentially targeted for early disassembly. (3) The mechanism of filament disassembly in the lamellipod releases capping protein from the network before the Arp2/3 complex. Because knockdown of the actin disassembly factor cofilin results in expansion of both the Arp2/3 and capping protein zones as well as their complete overlap (Figure 5), we favor the third idea. When overlaid on our maps of actin speckle dynamics the place where capping protein speckles disappear corresponds to the earliest time/position at which actin disassembly is observed. Since the pointed ends of filaments in the lamellipod are anchored to

the network by the Arp2/3 complex, any cofilin-mediated filament severing will increase the mobility of the barbed end more than that of the pointed end (Figure 7). More generally, severing one filament from which multiple daughter filaments branch will release one more molecule of capping protein than Arp2/3 complex.

One of the most striking results from our study is that knockdown of capping protein expression results in loss of the lamellipodial actin network and almost complete loss of Arp2/3 complex associated with actin at the leading edge. The fact that actin speckles still appear at the leading edge of capping protein-depleted S2 cells and undergo slow retrograde movement indicates that the underlying lamellar actin network is intact and that the effect of capping protein knockdown is specific to the lamellipod. Mejillano et al. recently found that depletion of capping protein in a mouse melanoma cell line caused explosive filopodium formation and displacement of the Arp2/3 complex from the leading edge (Mejillano et al., 2004). These authors speculated that, in the absence of capping protein, filopodium-forming factors such as Ena/VASP family proteins might displace the Arp2/3 complex from the leading edge. We find, however, that loss of capping protein mislocalizes the Arp2/3 complex even in the absence of filopodium formation. The most likely explanation for the difference in our results is that S2 cells express lower amounts of the filopodial machinery than those used by Mejillano et al. (Unperturbed S2 cells, for example, never spontaneously form filopodia ((Mejillano et al., 2004; Rogers et al., 2003) and this study)). Thus, displacement by filopodium forming factors cannot account for the effect of capping protein knockdown on Arp2/3 complex localization. Another possible explanation is that removal of capping protein perturbs the global cellular balance between filamentous and monomeric actin. In the absence of capping protein, individual filaments polymerize longer and use up more monomeric actin. Under these conditions the monomer concentration may fall low enough to globally inhibit Arp2/3 complex activity. This interpretation, however, is not consistent with the fact that loss of cofilin, slingshot, or twinfilin also shifts the balance between filamentous and monomeric actin but produces the opposite effect on Arp2/3 distribution. Our results argue

strongly that limiting filament growth at the cell edge plays a specific role in determining lamellipodial architecture and promoting efficient Arp2/3 complex activity.

The observation that capping protein is required for efficient Arp2/3 activity and lamellipod formation *in vivo* is consistent with studies of actin-based motility systems reconstituted *in vitro* from purified components. Both the Arp2/3 complex and capping protein, for example, are required to reconstitute actin-dependent motility of the intracellular pathogen *Listeria monocytogenes* (Carlier et al., 2003) and to generate motility of micron-sized particles coated with Arp2/3 activators. In the absence of capping protein the Arp2/3 complex generates disorganized clouds of filamentous actin around *Listeria* (Welch et al., 1998a) or polystyrene microspheres coated with the Arp2/3-activating domains of ActA or N-WASP (Noireaux et al., 2000). Addition of capping protein induces these actin clouds to break symmetry and form organized, polarized, and motile networks ((van der Gucht et al., 2005) and our unpublished observations). Taken together, these results suggest a kinetic synergy between the Arp2/3 complex and capping protein and that self-sustaining lamellipod formation requires a precise balance between the rates of filament nucleation and capping. This is consistent with theoretical and experimental studies indicating that efficiency of protrusion driven by growth of dendritically-branched networks is highly sensitive to the average filament length (Bear et al., 2002; Mogilner and Oster, 1996).

Cofilin-mediated actin disassembly limits the size of the lamellipod

In most cell types cofilin localizes to a zone near the lamellipod/lamellum junction (Svitkina and Borisy, 1999) but the precise role of cofilin activity in determining dynamic network architecture, however, has not been established. *In vitro*, cofilin severs and depolymerizes actin filaments that have hydrolyzed their bound ATP and released the inorganic phosphate (Carlier et al., 1997; McGough and Chiu, 1999; McGough et al., 1997). Consistent with this *in vitro* activity, several groups have reported that loss of cofilin function *in vivo*, either through depletion or by

overexpression of the inhibitory LIM kinase, causes accumulation of filamentous actin (Arber et al., 1998; Hotulainen et al., 2005; Rogers et al., 2003). Other studies have reported that filament severing by cofilin at the cell edge promotes actin assembly and is required for rapid membrane protrusion (Chan et al., 2000; Ghosh et al., 2004).

Rogers et al. reported that severe depletion of cofilin in S2 cells inhibits adhesion and promotes accumulation of thick actin bundles ((Rogers et al., 2003) and our unpublished observations). Depletion of the cofilin-activating phosphatase slingshot produces a milder but related phenotype in which cells accumulate an unusually wide and dense peripheral actin network. Rogers et al. hypothesized that this slingshot phenotype represents a partial loss of cofilin activity (Rogers et al., 2003). Consistent with Rogers et al., we find that the most severely cofilin-depleted S2 cells are completely non-adherent. Less severely depleted cells are capable of attaching to a substrate and spreading if given sufficient time. Speckle microscopy of actin, Arp2/3 complex, and capping protein in these cells reveals that, as in the case of slingshot depletion, cofilin depletion specifically expands the lamellipodial actin network at the expense of the lamellar network. Observation of this dynamic phenotype required speckle microscopy studies of all three proteins: actin, Arp2/3 complex, and capping protein. Speckling of actin alone revealed a single population of slow-moving filaments in slingshot-depleted cells but could not resolve whether this was a lamellar or lamellipodial network. The fact that Arp2/3 complex and capping protein speckles traverse the entire width of this zone revealed it to be a broad, slow-moving lamellipod. This result is dramatically different from the effect of knocking down capping protein and demonstrates that, even though depolymerizing filaments and terminating their elongation have the same global effect on monomer and polymer concentrations they play fundamentally different roles in determining actin network architecture.

In addition to cofilin and slingshot, depletion of twinfilin or tropomyosin also produces expansion of the lamellipod at the expense of the lamellum. In both cases, speckles produced by labeled actin, Arp2/3, or capping protein travel at a constant velocity from the cell edge all the way into

the cell body. In addition, the actin networks in these cells exhibit the polarized assembly dynamics characteristic of the lamellipod rather than the lamellum (Figure 3a,c, Supplemental Figure S3). Twinfilin, a protein composed of two ADF/cofilin-like domains, has been described historically as an actin monomer-sequestering protein (Palmgren et al., 2002). Recently, however, yeast twinfilin has been shown to sever actin filaments in vitro (Moseley et al., 2006). Our results suggest that twinfilin and cofilin work synergistically to disassemble lamellipodial actin networks, and that loss of either enables the expansion of the lamellipod and loss of the two-network system.

Tropomyosin, an actin side-binding protein, inhibits both Arp2/3 binding and actin severing by cofilin (Blanchoin et al., 2001; Nishida et al., 1984). In this study, we find that cTm binds to actin networks at the lamellipod/lamellum junction just behind the Arp2/3 complex zone and remains stably bound well into the cell body. Several studies have supported the role of tropomyosin as a spatial regulator of the Arp2/3 complex. By immunostaining, DesMarais et al. found that tropomyosin is excluded from areas with dense actin networks containing the Arp2/3 complex (DesMarais et al., 2002). Gupton et al. demonstrated that microinjection of skeletal muscle tropomyosin inhibits the formation of lamellipodia in PtK1 cells, as judged by the depletion of Arp2/3 and cofilin from the leading edge and loss of the signature lamellipodial actin dynamics (Gupton et al., 2005). In the absence of tropomyosin, we expect that both Arp2/3 and cofilin are free to bind to actin filaments distal from the cell edge. Localization of the Arp2/3 complex, however, is also determined by association with nucleation promoting factors at the cell membrane whereas cofilin appears to bind ADP actin wherever it appears in the cell. This fact, coupled with the similarity in phenotype between cells depleted of tropomyosin and cofilin, suggests that loss of cofilin from the lamellipod boundary is the primary cause for the lamellipodial expansion seen in cTm depleted cells.

Conclusions

Using fluorescent speckle microscopy we have reconstructed the timing of critical events in the construction of actin filament networks at the leading edge of motile cells. Filaments are nucleated and crosslinked by the Arp2/3 complex and subsequently capped by capping protein at the cell edge. Both proteins remain associated with the network but dissociate at distinctly different times and locations. Capping protein is lost from the network after 14 seconds, the Arp2/3 complex dissociates after 21 seconds and the lamellipodial actin network itself is disassembled after 35 seconds. The loss of the Arp2/3 complex from the actin network before network disassembly indicates that debranching is not driven by filament disassembly but is a separate process. Dissociation of capping protein from the network coincides with the earliest detectable actin disassembly events. Also, capping protein activity is required for interaction of the Arp2/3 complex with the actin network and for construction of the lamellipod. This effect appears to be independent of any effect of capping activity on the global balance between monomeric and filamentous actin and is specific for the lamellipodial network. Loss of capping activity has little or no effect on dynamics of the lamellar actin network. We also find that cofilin, twinfilin, slingshot, and tropomyosin appear to play no role in the constructing the lamellipodial network but function mainly to limit its size.

Experimental Procedures

Cell culture and RNAi treatment

Drosophila Schneider S2 cells were cultured and treated with dsRNA as previously described (Rogers et al., 2003). Cells were plated on concanavilin A for at least 30 minutes prior to fixation or live cell microscopy. RNAi against capping protein was done with dsRNA specific to the alpha subunit, though RNAi treatment against the beta subunit or against both alpha and beta subunits resulted in identical phenotypes. Cells were depleted of cTm by treatment with dsRNA specific to type II tropomyosin isoforms. Cofilin RNAi was performed using dsRNA against the entire coding sequence.

Plasmid construction and transfection

Gateway cloning technology (Invitrogen) was used to create vectors for fluorescent protein expression in S2 cells. Drosophila genes for p16 (ArpC5), Arp3, cTm, capping protein alpha and beta, and cofilin (twinstar) were cloned from a S2 cDNA library, sequenced, and inserted into p-Entr-D-TOPO plasmids. Genes were then cloned into destination vectors that included either a GFP or RFP tag under the control of a copper promoter. Actin, Arp3, p16, cofilin and capping protein alpha subunit were tagged with a N-terminal fluorescent tag, while tropomyosin was labeled at its C-terminus. S2 cells were transfected using Cellfectin (Invitrogen), 1-2 micrograms of destination plasmid, and 0.5 micrograms of pCoHygro plasmid (Invitrogen) (for stable cell line construction only). After two days, fluorescent protein was observed in transient cell lines, or hygromycin was added to select for stably transfected cells.

Speckle microscopy

S2 cells transiently or stably expressing low quantities of fluorescent protein were plated on concanavilin A-coated glass-bottom dishes (MatTek) and observed between 30 minutes and 1.5 hours after plating. Images were taken with an Orca ER II camera (Hamamatsu) mounted to an Axiovert microscope (Zeiss) using Metamorph software (Molecular Devices) at 1- or 3-second

intervals with integration times between 300 and 800 milliseconds. A majority of images were collected at 2x binning with the exception of a subset of GFP-capping protein images, which were taken at 1x binning. To best capture retrograde motion, images were taken from a confocal section proximal to the coverslip.

Immunofluorescence and fixation

Cells were fixed in 3% paraformaldehyde for at least 10 minutes in HL3 buffer and permeabilized by a 2 or 5 minute incubation in 0.1% Triton X-100 in PBS (Rogers et al., 2003). Actin filaments were visualized with 200nM Alexa-488 or Alexa-568 phalloidin (Molecular Probes/Invitrogen) and chromosomes stained with 0.5 micrograms/mL DAPI. Images were acquired using an Orca II cooled CCD camera (Hamamatsu) equipped on a Nikon TE300 inverted microscope using Simple PCI software (Compix).

Kymograph analysis

Kymograph analyses were done using ImageJ (http://rsb.info.nih.gov/ij) using a plugin written by J. Rietdorf and A. Seitz (http://www.embl.de/eamnet/html/body_kymograph.html). For sparsely speckled cells, 1-micron thick lines were used to create kymographs. For densely speckled cells, such as GFP-actin, kymographs were constructed using a 4-micron thick line. In the latter case, kymographs were constructed using the montage feature in ImageJ. Individual speckle trajectories and the outline of the leading edge were drawn by hand in ImageJ and were analyzed using Matlab (Mathworks). For a given cell, between 4 and 12 kymographs were created, and between 6 and 12 cells were used for every RNAi and control condition.

Actin speckle tracking and assembly maps

FsmCenter, a software package designed by the Danuser group (Scripps, La Jolla, CA) was used to track GFP-actin speckles in S2 cells and to create actin assembly maps. CytoProbe, written by Matthias Machacek, was used to create graphs showing activity from the cell edge.

Acknowledgements

We thank members of the Mullins laboratory for their insights, support and helpful discussions. We are grateful to Ron Vale and his laboratory members for the use of microscopic equipment, reagents and technical assistance. Special thanks are due to Gaudenz Danuser and Matthias Machacek for training and use of fsmCenter and cytoProbe, and for helpful discussions. Finally, we thank Tapio Heino, Katherine Miller and Tadashi Uemura for generously providing antibodies. This work was supported by grants to RDM from the NIH (RO1 grant GM61010) and the Sandler Family Supporting Foundation, funding from the UCSF/UCB Nanomedicine Development Center, and a National Science Foundation Graduate Research Fellowship to JHI.

protein tagged	RNAi treatment	cellular compartment	no. of trajectories	velocity (μm/min)	distance travelled (μm)	lifetime (min)
actin	none	LP	244	2.46±0.04	1.40±0.03	0.59±0.01
		LM	251	1.31±0.04	0.77±0.03	0.63±0.02
		CB	193	0.15±0.02	0.11±0.02	0.85±0.03
	CPA	LP	281	1.76±0.06	0.70±0.02	0.48±0.01
		LM	306	0.94±0.04	0.50±0.02	0.62±0.02
		CB	164	0.24±0.03	0.16±0.02	0.88±0.04
	cofilin	LP	147	0.88±0.05	1.00±0.05	1.45±0.07
		LM	239	0.48±0.03	0.67±0.03	1.83±0.06
		CB	187	0.14±0.01	0.24±0.02	1.90±0.06
	cTm	LP	502	2.08±0.03	1.82±0.03	0.92±0.02
		LM	260	1.70±0.04	1.46±0.05	0.89±0.02
		CB	241	0.51±0.03	0.46±0.03	1.14±0.03
	slingshot	LP	136	1.39±0.04	1.71±0.08	1.32±0.07
		LM	123	1.09±0.04	1.50±0.08	1.45±0.07
		CB	51	0.29±0.04	0.36±0.06	1.57±0.11
	twinfilin	LP	270	1.75±0.04	2.13±0.06	1.33±0.04
		LM	148	0.98±0.05	1.25±0.06	1.47±0.05
		CB	164	0.33±0.03	0.45±0.04	1.76±0.05
p16/Arp3	none	LP	468	2.44±0.03	0.83±0.01	0.36±0.01
		LM	116	1.13±0.07	0.44±0.03	0.49±0.03
		CB	67	0.18±0.04	0.09±0.02	0.77±0.06
	CPA	LP	102	0.45±0.04	0.31±0.02	0.89±0.05
		LM	268	0.20±0.02	0.14±0.01	0.97±0.04
		CB	293	0.08±0.01	0.06±0.01	1.06±0.04
	cofilin	LP	184	1.11±0.04	0.91±0.04	0.91±0.03
		LM	113	0.60±0.05	0.58±0.05	1.30±0.07
		CB	117	0.07±0.02	0.08±0.02	1.99±0.08
	cTm	LP	387	1.76±0.03	1.01±0.03	0.68±0.02
		LM	374	1.33±0.04	0.86±0.02	0.83±0.03
		CB	216	0.59±0.05	0.31±0.02	1.33±0.06
	slingshot	LP	245	1.76±0.04	1.22±0.04	0.71±0.02
		LM	186	1.70±0.05	1.05±0.04	0.66±0.02
		CB	90	0.76±0.08	0.53±0.06	1.19±0.09
	twinfilin	LP	160	1.06±0.04	0.98±0.04	1.03±0.04
		LM	204	0.85±0.03	0.77±0.03	1.12±0.04
		CB	208	0.42±0.03	0.36±0.03	1.38±0.05
CPA	none	LP	319	2.57±0.05	0.58±0.01	0.25±0.01
		LM	101	0.05±0.02	0.03±0.01	0.87±0.04
		CB	204	0.01±0.01	0.01±0.01	1.05±0.03
	cofilin	LP	120	1.25±0.08	0.81±0.04	0.85±0.04
		LM	120	0.67±0.07	0.49±0.04	1.04±0.04
		CB	260	0.11±0.02	0.10±0.02	1.43±0.03
	cTm	LP	125	1.86±0.07	0.97±0.05	0.59±0.03
		LM	132	1.92±0.08	0.94±0.04	0.59±0.03
		CB	135	0.60±0.07	0.34±0.04	1.26±0.07
	slingshot	LP	90	1.73±0.06	1.25±0.07	0.76±0.05
		LM	119	1.51±0.05	1.06±0.05	0.75±0.03
		CB	108	0.81±0.07	0.51±0.04	1.08±0 08
	twinfilin	LP	215	1.50±0.03	1.24±0.04	0.84±0.02
		LM	177	1.13±0.04	0.94±0.04	0.92±0.04
		CB	154	0.51±0.05	0.39±0.03	1.28±0.06
cTm	none	LP	6	1.69±0.28	1.52±0.22	0.98±0.18
		LM	334	0.91±0.03	1.07±0.03	1.32±0.03
		CB	227	0.29±0.03	0.35±0.03	1.75±0.04

Table 2-1. Summary of values for speckle trajectories based on kymograph analysis. Error was calculated as standard deviation divided by the square root of the total number of observations (standard error).

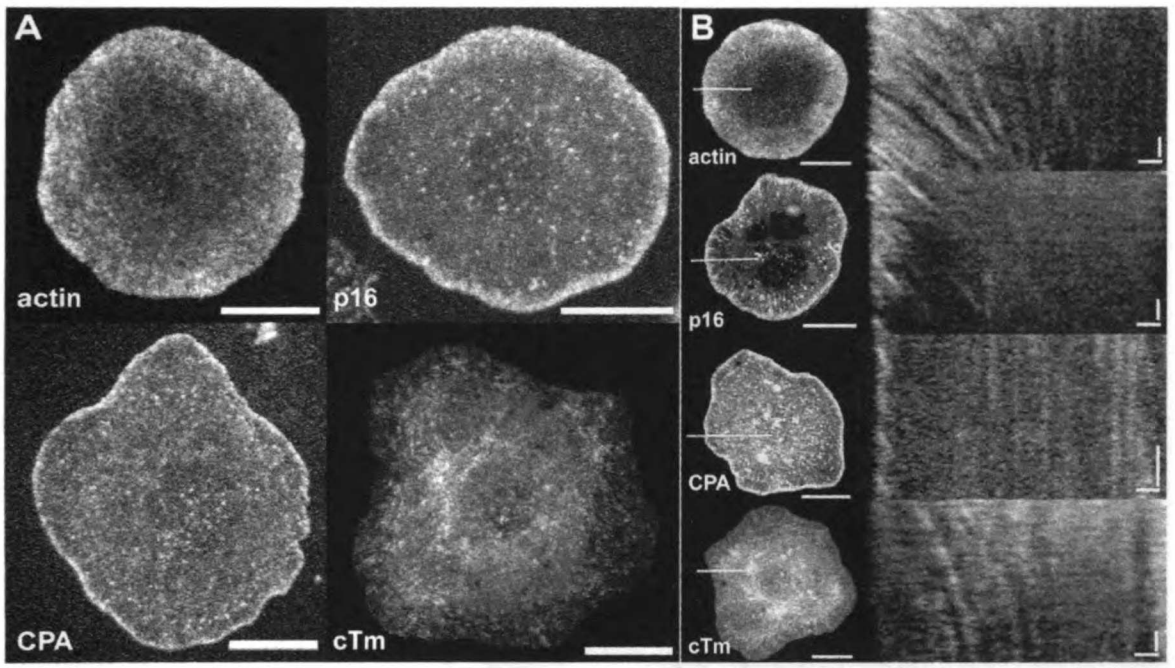

Figure 2-1. GFP-tagged actin and actin regulatory proteins occupy unique compartments at the S2 cell leading edge. (A) Live S2 cells expressing GFP-actin, GFP-p16 (Arp2/3 subunit), GFP-capping protein alpha (CPA), and GFP-cytoskeletal tropomyosin (cTm) were imaged using confocal microscopy. Images are a single frame from time-lapse movies of live S2 cells plated on concanavilin A for approximately 1 hour. Scale bar, 10 microns. (B) Kymographs of GFP speckles reveal dynamic compartmentalization of actin and actin-binding proteins. Left panel, maximum intensity projections of time-lapse movies of S2 cells expressing GFP-actin (top panel), GFP-p16, GFP-CPA, and GFP-cTm. Scale bar, 10 microns. White line at 9 o'clock position indicates area of cell from which kymographs (right panel) were constructed. Right panel, X-axis scale bar, 1 micron; Y-axis scale bar, 30 seconds.

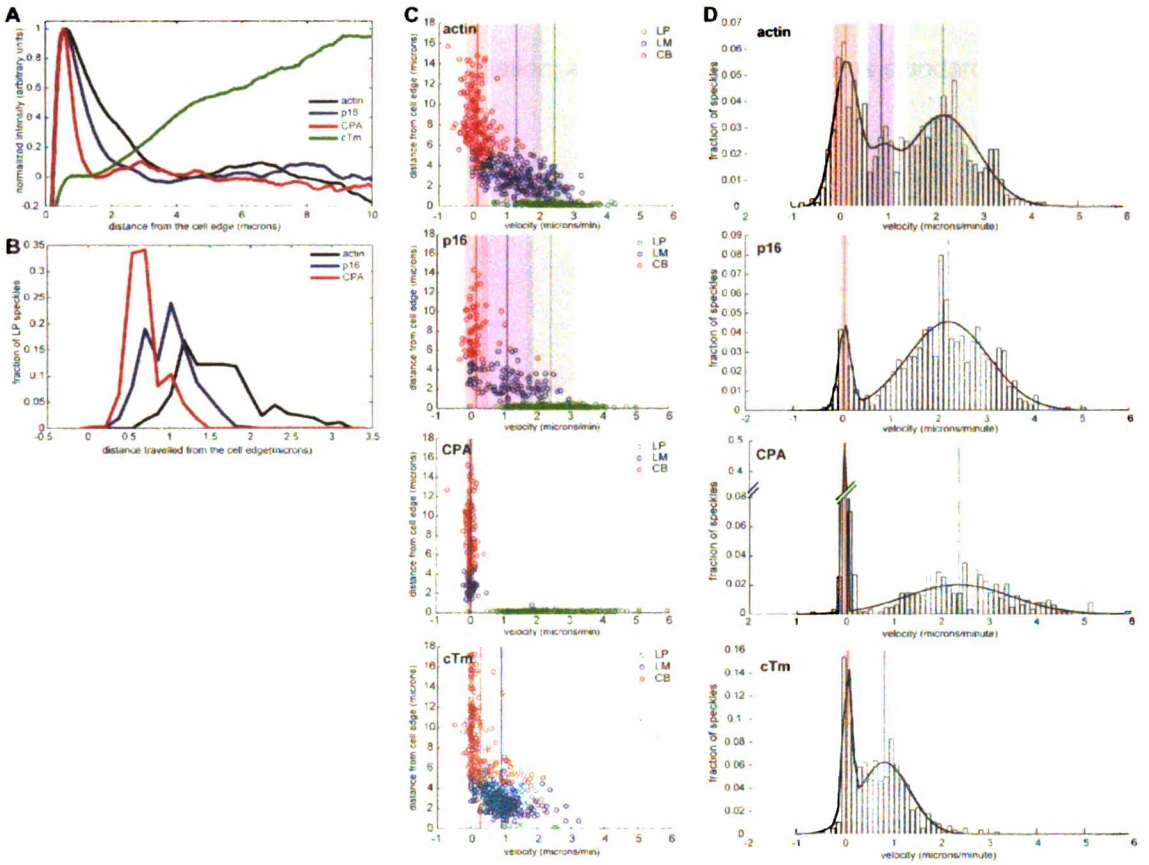

Figure 2-2. Quantitative analysis of GFP-actin, GFP-p16, GFP-CPA and GFP cTm speckle localization and dynamics. (A) Normalized average fluorescence intensity line scan of GFP fluorescence taken from a representative movie of an S2 cell expressing GFP-actin, GFP-p16, GFP-CPA or GFP-cTm displayed as a function of distance from the cell edge. (B-D) Individual speckle trajectories were analyzed using kymograph analyses. At least 10 cells expressing each GFP construct were analyzed. (B) Line histogram showing distance traveled by GFP-actin, GFP-p16 and GFP-CPA speckles originating in the LP. Speckles used in this histogram are shown as green circles in each of the scatter plots in (D). (C) Probability density function (PDF) of the velocities of all GFP speckles of (top to bottom) actin, cTm, p16 and CPA. PDF is overlayed with best fit derived from cumulative density function curve fitting (black line). Vertical lines indicate means, and shaded areas indicate standard deviation for each population. (D) Scatter plots of distance from the cell edge versus velocity; top to bottom: actin, cTm, p16 and CPA. Speckle trajectories were labeled as originating in the lamellipod (LP, green circles), lamella (LM, blue

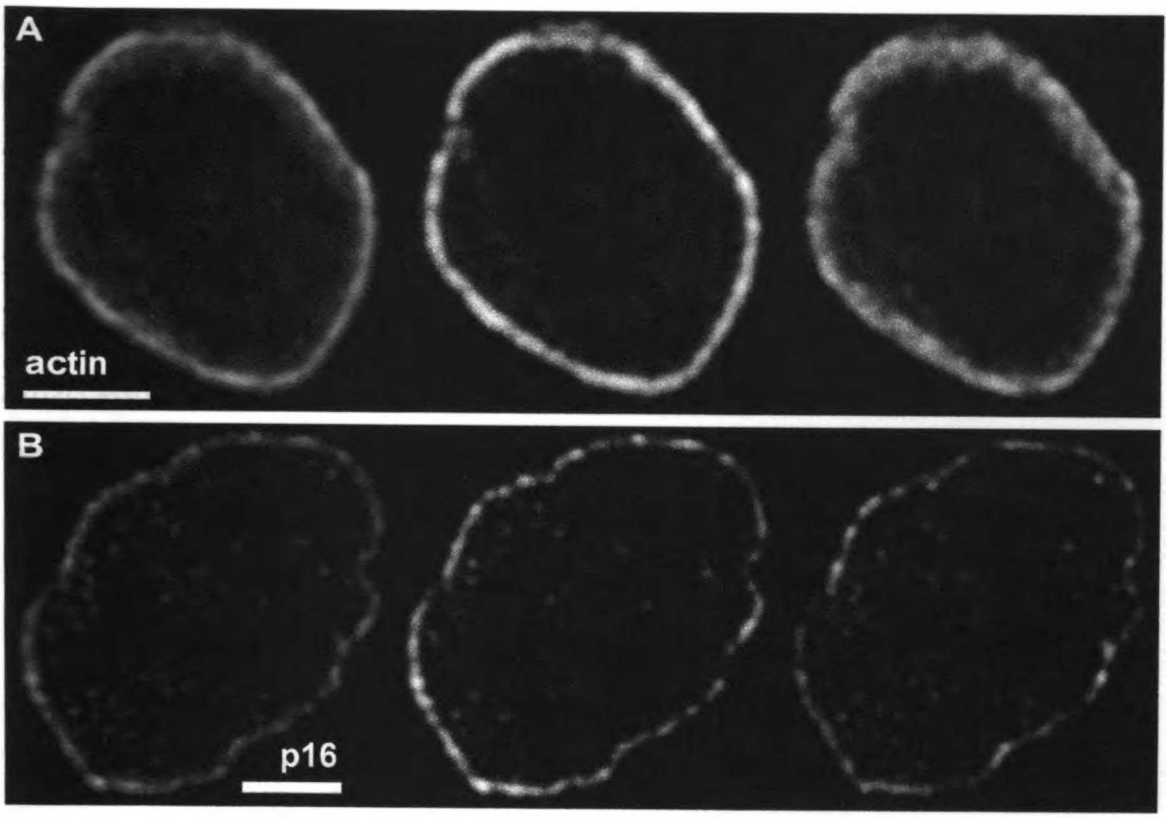
A
actin
B
p16

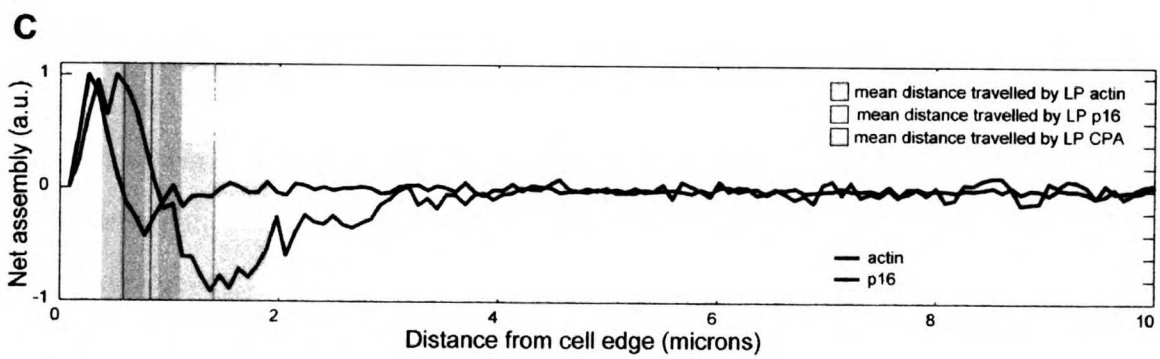
C
Net assembly (a.u.)
1
0
-1
0
2
4
6
8
10
Distance from cell edge (microns)
mean distance travelled by LP actin
mean distance travelled by LP p16
mean distance travelled by LP CPA
actin
p16

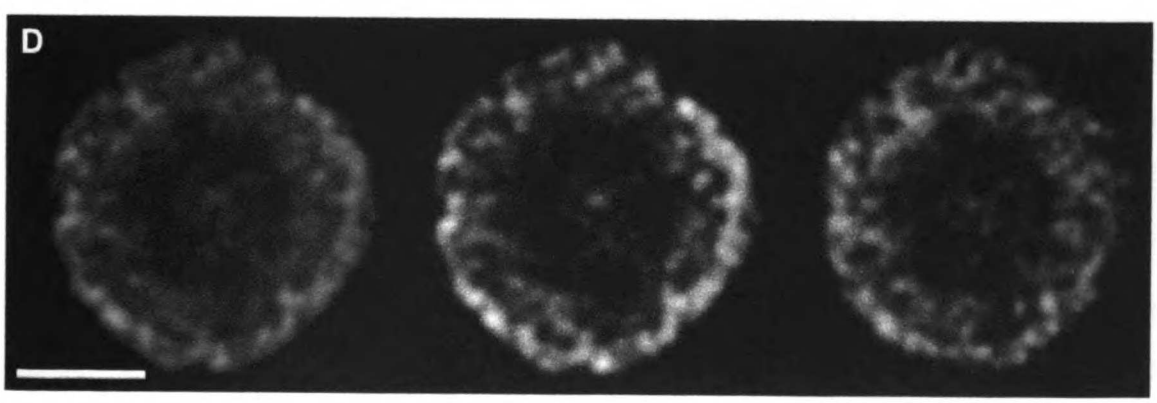
D

Figure 3. Visualization of network assembly in S2 cells. (A-B) Time averaged turnover map of F-actin (A) and p16 (B) calculated from speckle tracking analysis of a S2 cell expressing GFP-actin or GFP-p16. Analysis of speckles was done using fsmCenter software created by the Danuser group (Scripps) using algorithms that have previously been described [14]. Actin assembly (A) or Arp2/3 association (B) is shown in red (center), and actin disassembly (A) or p16 dissociation (B) is shown in green (right). Scale bar, 10 microns. (C) Net actin turnover and Arp2/3 association rate profiles as a function of distance from the cell edge. Thick green line indicates actin net assembly calculated from cell shown in (A). Thick blue line indicates net Arp2/3 association/dissociation to the actin network, calculated from the cell shown in (B). Shaded regions show mean (line) and standard deviation (shaded area) of the average distance traveled by capping protein (red), Arp2/3 (blue) and actin (green) calculated from kymograph analyses. Figure was created using cytoProbe software from the Danuser group (Scripps). (D) Turnover map of F-actin calculated from speckle tracking analysis of a S2 cell depleted of cTm and expressing GFP-actin. Actin assembly is shown in red (center), and actin disassembly is shown in green (right). Scale bar, 10 microns.

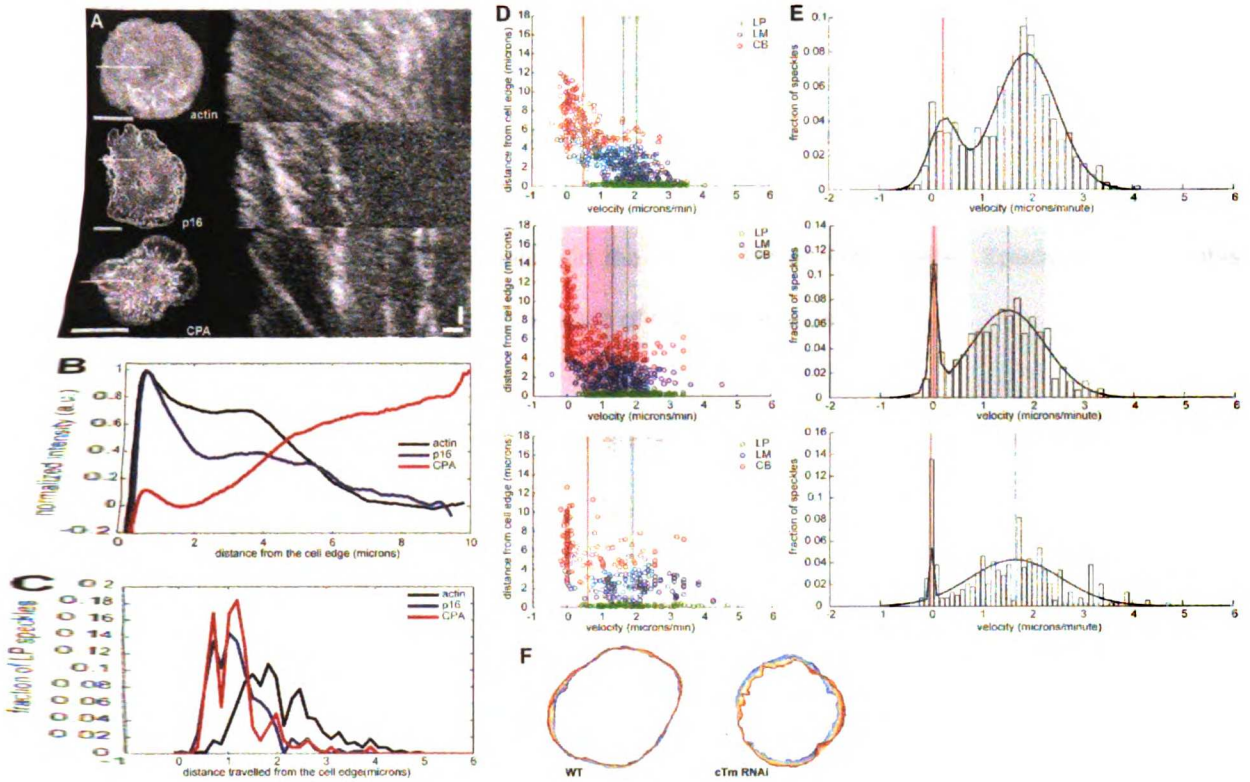

Figure 2-4. Tropomyosin RNAi causes expansion of the lamellipod and the expense of the lamella. (A) Left panel, maximum intensity projections of time-lapse movies of S2 cells treated with cTm dsRNA and expressing (from top to bottom) GFP-actin, GFP-p16, GFP-CPA, and GFP-cTm. Scale bar, 10 microns. White line at 9 o'clock position indicates area of cell from which kymographs (right panel) were constructed. Right panel, X-axis scale bar, 1 micron; Y-axis scale bar, 30 seconds. (B) Cell outlines from each frame of a movie of (left) untreated cell and (right) cTm depleted cell. Blue outline indicates first and red outline the last frame of each movie. (C) Probability density function (PDF) of the velocities of all GFP speckles of (top to bottom) actin, p16 and CPA in cTm depleted cells. PDF is overlayed with best fit derived from cumulative density function curve fitting (black line). Vertical lines indicate means, and shaded areas indicate standard deviation for each population. (D) Normalized average fluorescence intensity line scan of GFP fluorescence taken from a representative movie of a cTm depleted S2 cell expressing GFP-actin, GFP-p16 or GFP-CPA displayed as a function of distance from the cell edge. (E) Scatter plots of distance from the cell edge versus velocity; top to bottom: actin, cTm,

p16 and CPA. Speckle trajectories were labeled as originating in the lamellipod (LP, green circles), lamella (LM, blue circles) or cell body (CB, red circles) based on their starting distance from the cell edge. Vertical lines indicate mean velocity for each population, and shaded area indicates standard deviation. (F) Line histogram showing distance traveled by GFP-actin, GFP-p16 and GFP-CPA speckles originating in the LP in cTm depleted cells. Speckles used in this histogram are shown as green circles in each of the scatter plots in (E).

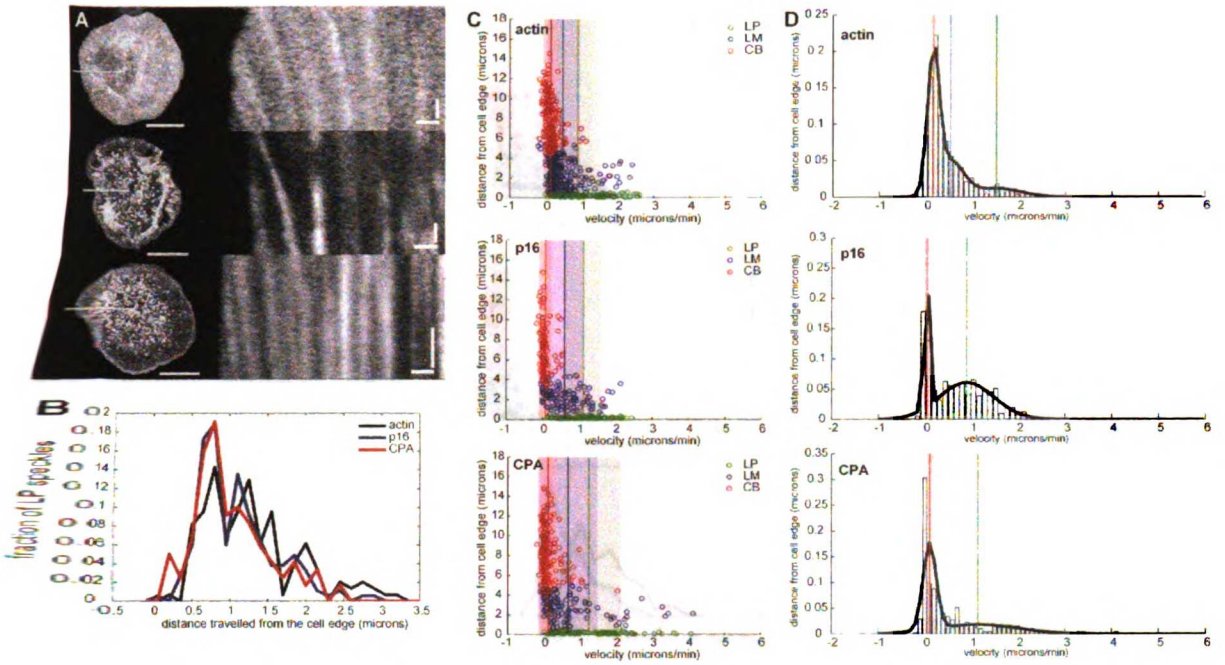

Figure 2-5. Cofilin RNAi causes decreased velocities and lamellipodial expansion. (A) Left panel, maximum intensity projections of time-lapse movies of S2 cells depleted of cofilin and expressing (top to bottom) GFP-actin, GFP-p16 and GFP-CPA. Scale bar, 10 microns. White line at 9 o'clock position indicates area of cell from which kymographs (right panel) were constructed. (B) Line histogram showing distance traveled by GFP-actin, GFP-p16 and GFP-CPA speckles originating in the LP in cofilin depleted cells. Speckles used in this histogram are shown as green circles in each of the scatter plots in (D). (C) Probability density function (PDF) of the velocities of all GFP speckles of (top to bottom): actin, p16 and CPA in cofilin depleted cells. PDF is overlayed with best fit derived from cumulative density function curve fitting (black line). Vertical lines indicate means, and shaded areas indicate standard deviation for each population. (D) Scatter plots of distance from the cell edge versus velocity in cells expressing (top to bottom) GFP-actin, GFP-p16 or GFP-CPA. Speckle trajectories were labeled as originating in the lamellipod (LP, green circles), lamella (LM, blue circles) or cell body (CB, red circles) based on their starting distance from the cell edge. Vertical lines indicate mean velocity for each population, and shaded area indicates standard deviation.

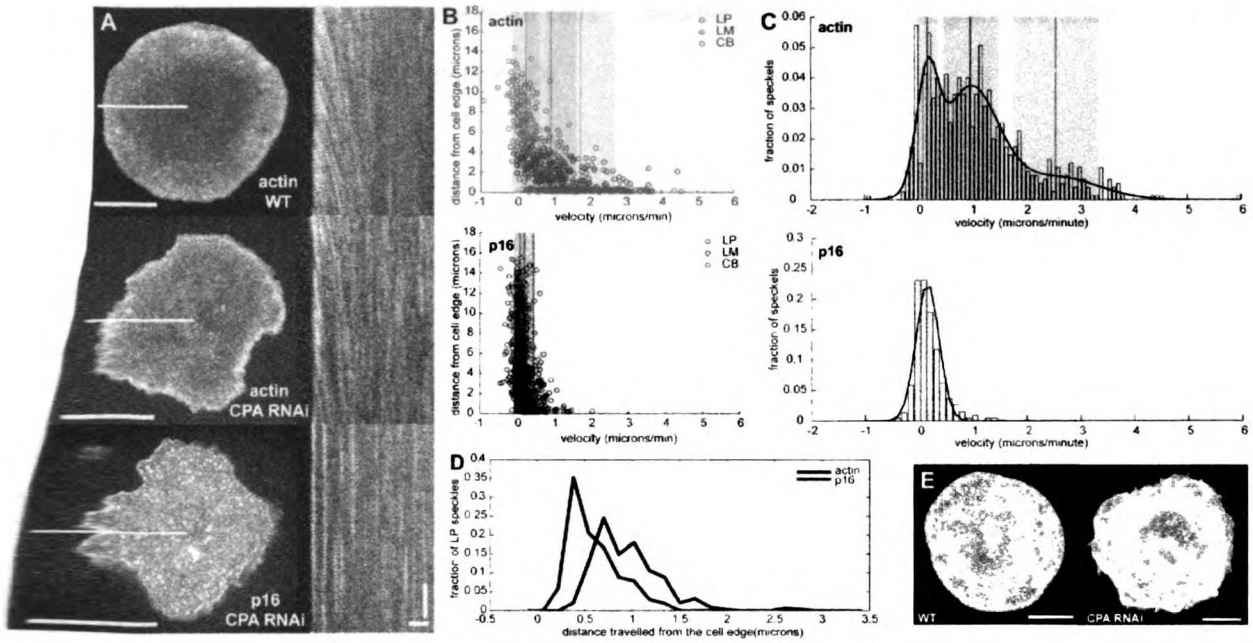

Figure 2-6. Depletion of capping protein abolishes the lamellipod but has little effect on lamellar dynamics. (A) Left panel, maximum intensity projections of time-lapse movies of (top to bottom) untreated S2 cell expressing GFP-actin, and CPA depleted cells expressing GFP-actin and GFP-p16. Scale bar, 10 microns. White line at 9 o'clock position indicates area of cell from which kymographs (right panel) were constructed. Right panel, X-axis scale bar, 1 micron; Y-axis scale bar, 30 seconds. (B) S2 cells were fixed and F-actin was visualized with Alexa488 phalloidin. Left: untreated cell; right: CPA-depleted cell. (C) Probability density function (PDF) of the velocities of all GFP speckles of actin (top) and p16 in CPA depleted cells. PDF is overlayed with best fit derived from cumulative density function curve fitting (black line). Vertical lines indicate means, and shaded areas indicate standard deviation for each population. (D) Scatter plots of distance from the cell edge versus velocity in cells expressing GFP-actin (top) or GFP-p16. Speckle trajectories were labeled as originating in the lamellipod (LP, green circles), lamella (LM, blue circles) or cell body (CB, red circles) based on their starting distance from the cell edge. Vertical lines indicate mean velocity for each population, and shaded area indicates standard deviation. (E) Line histogram showing distance traveled by GFP-actin and GFP-p16 speckles

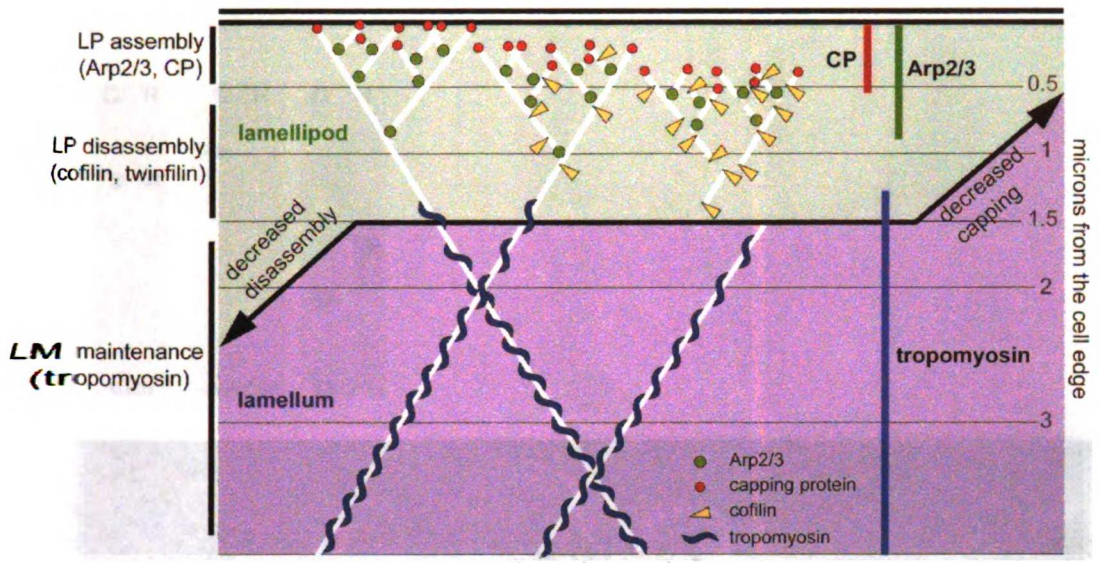

Figure 2-7. Schematic model of of actin and actin regulatory proteins at the leading edge. Arp2/3 (green circles), capping protein (red circles), cofilin (yellow triangles) and actin (white lines) build lamellipodial actin networks (green area), while tropomyosin (blue 'S' shapes) is associated with lamellar actin networks (blue area). Decreased capping due to depletion of capping protein leads to collapse of the lamellipod and expansion of the lamellum. Decreased disassembly due to cofilin, slingshot, twinfilin or tropomyosin depletion leads to the expansion of the lamellipod at the expense of the lamellum.

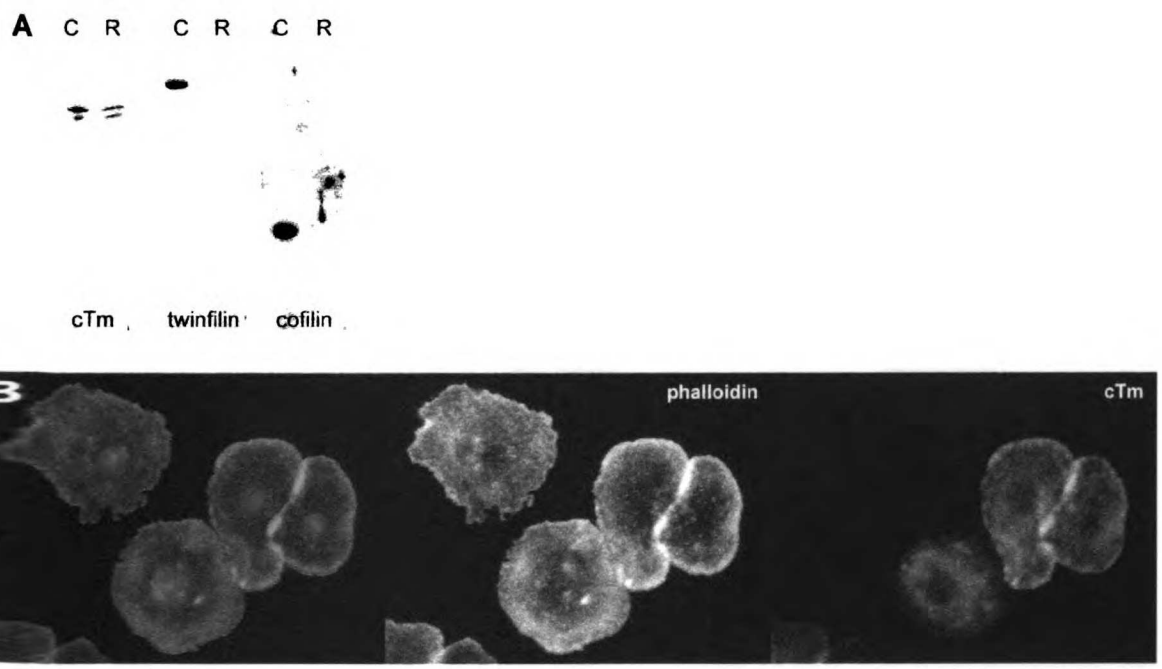

Figure 2-S1. Depletion of target proteins in S2 cells. (A) Western blot against showing depletion of tropomyosin (cTm, left), twinfilin (center) and cofilin (right) in S2 cell extracts. In each case, left lane is control untreated extracts (C), and right lane is extracts from cells treated with dsRNA for 7 days (R). (B) cTm RNAi knockdown correlates with leading edge morphological abnormalities. Epifluorescent microscopic images of stably transfected GFP-tropomyosin cell line depleted of cTm. Left: overlay. Middle: Alexa 568 phalloiding staining. Right: GFP fluorescence.

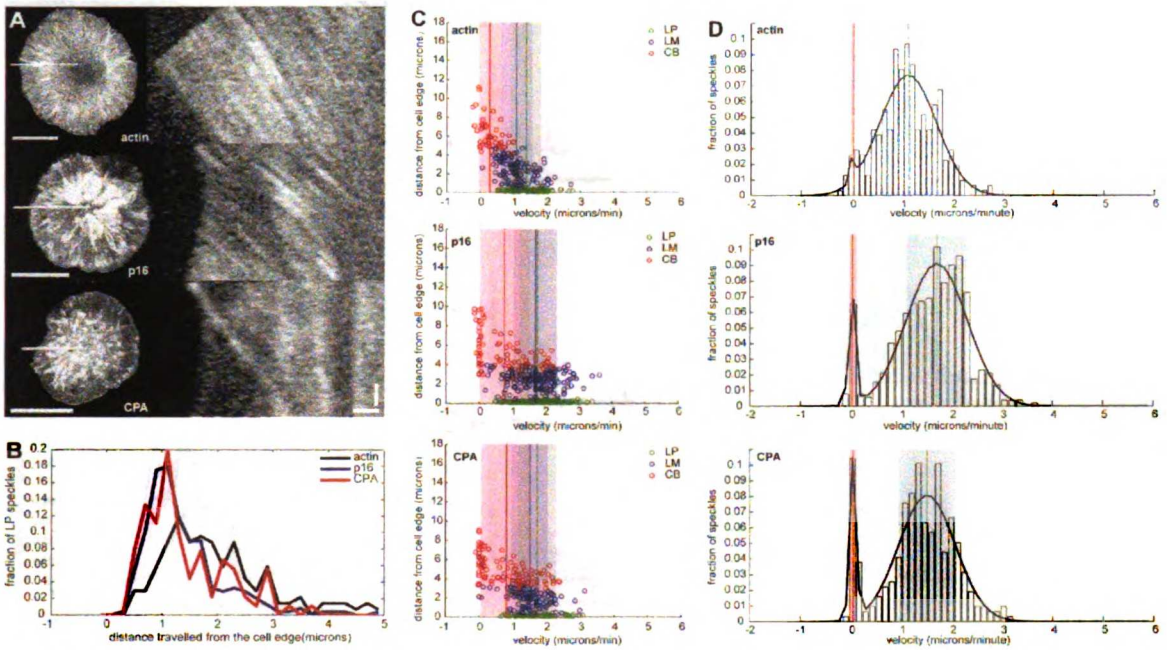

Figure 2-S2. Slingshot RNAi causes expansion of the lamellipod and the expense of the lamella. (A) Left panel, maximum intensity projections of time-lapse movies of S2 cells treated with slingshot dsRNA and expressing (from top to bottom) GFP-actin, GFP-p16 and GFP-CPA. Scale bar, 10 microns. White line at 9 o'clock position indicates area of cell from which kymographs (right panel) were constructed. Right panel, X-axis scale bar, 1 micron; Y-axis scale bar, 30 seconds. (B) Line histogram showing distance traveled by GFP-actin, GFP-p16 and GFP-CPA speckles originating in the LP in slingshot depleted cells. Speckles used in this histogram are shown as green circles in each of the scatter plots in (C). (C) Scatter plots of distance from the cell edge versus velocity; top to bottom: actin, p16 and CPA. Speckle trajectories were labeled as originating in the lamellipod (LP, green circles), lamella (LM, blue circles) or cell body (CB, red circles) based on their starting distance from the cell edge. Vertical lines indicate mean velocity for each population, and shaded area indicates standard deviation. (D) Probability density function of the velocities of all GFP speckles of (top to bottom) actin, p16 and CPA in slingshot depleted cells. PDF is overlayed with best fit derived from cumulative density function curve fitting (black line). Vertical lines indicate means, and shaded areas indicate standard deviation for each population.

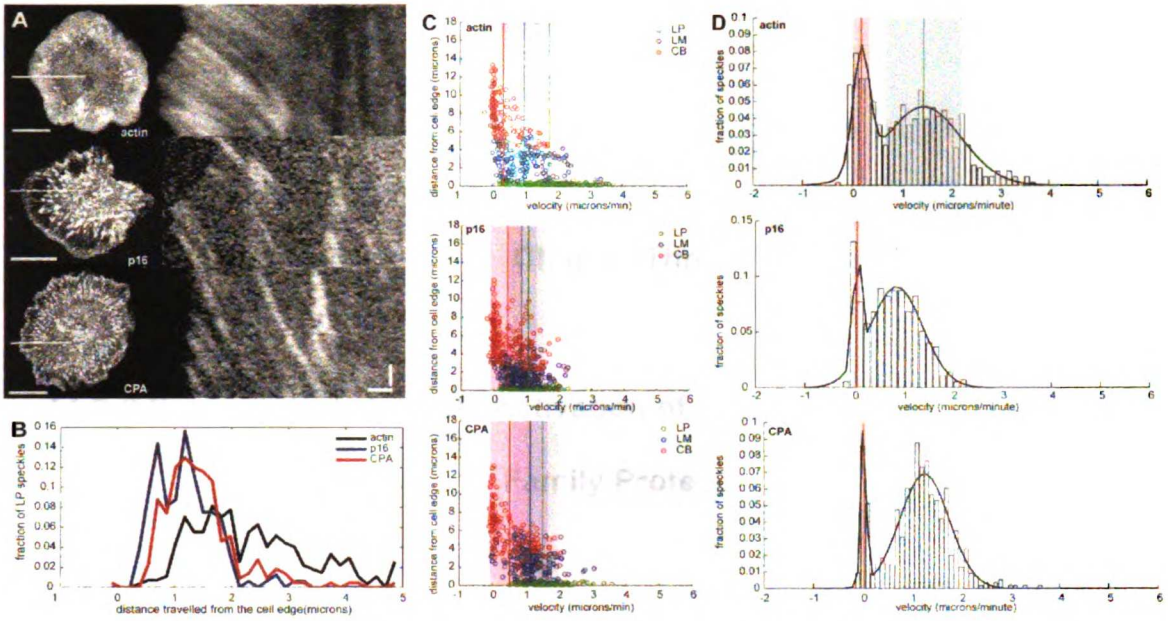

Figure 2-S3. Twinfilin RNAi causes expansion of the lamellipod and the expense of the lamella. (A) Left panel, maximum intensity projections of time-lapse movies of S2 cells treated with twinfilin dsRNA and expressing (from top to bottom) GFP-actin, GFP-p16 and GFP-CPA. Scale bar, 10 microns. White line at 9 o'clock position indicates area of cell from which kymographs (right panel) were constructed. Right panel, X-axis scale bar, 1 micron; Y-axis scale bar, 30 seconds. (B) Line histogram showing distance traveled by GFP-actin, GFP-p16 and GFP-CPA speckles originating in the LP in twinfilin depleted cells. Speckles used in this histogram are shown as green circles in each of the scatter plots in (C). (C) Scatter plots of distance from the cell edge versus velocity; top to bottom: actin, p16 and CPA. Speckle trajectories were labeled as originating in the lamellipod (LP, green circles), lamella (LM, blue circles) or cell body (CB, red circles) based on their starting distance from the cell edge. Vertical lines indicate mean velocity for each population, and shaded area indicates standard deviation. (D) Probability density function of the velocities of all GFP speckles of (top to bottom) actin, p16 and CPA in slingshot depleted cells. PDF is overlayed with best fit derived from cumulative density function curve fitting (black line). Vertical lines indicate means, and shaded areas indicate standard deviation for each population.

Chapter Three

14-3-3 Competitively Inhibits Activation of Phosphorylated Arp2/3 by WASp Family Proteins

Foreword

This study investigates a potential regulatory interaction between the Arp2/3 complex and 14-3-3 proteins. The so-called Squiggy project was born from the observation made by Jonathan Zalevsky that a specific amoeboid 14-3-3 isoform was consistently purified in abundance from an Arp2/3 complex affinity column. I followed up on this observation and tested first for the direct binding and biochemical function of the interaction, and later examined this interaction in vivo. I found that BMH2, a yeast 14-3-3 protein, and amoeboid Arp2/3 can interact directly in vitro, and that this interaction is exclusive of Arp2/3 binding to nucleation promoting factors (NPFs). The interaction between BMH2 and Arp2/3 is weak, however, and BMH2 can only weakly inhibit Arp2/3 activation in the presence of NPFs in polymerization assays. The 14-3-3 protein family is known for binding phosphorylated substrates, and I showed that phosphorylation of Arp2/3 appears to be necessary for its interaction with BMH2. I chose to study the in vivo role of the 14-3-3/Arp2/3 interaction in the yeast *Saccharomyces cerevisiae* because of previous experience with this model system and because I had done all my previous biochemistry work with BMH2, a yeast protein. Although I collected promising evidence that 14-3-3 and Arp2/3 may operate in the same pathway in yeast based on synthetic lethality/growth rate assays, I was unable to show that Arp2/3 and 14-3-3 proteins bind to any appreciable degree in vivo despite numerous and varied attempts. In addition, finding the occurrence of Arp2/3 phosphorylation whatsoever in yeast extracts proved difficult. Although the in vitro biochemistry data is compelling, the lack of evidence showing that this interaction functions in vivo led me to eventually abandon this project.

Recently, Lawrence LeClaire in the Mullins lab has found that phosphorylation of Arp2/3 renders the complex inactive, even in the presence of NPFs (personal communication). This mode of Arp2/3 regulation appears to be conserved across species and must be taken into consideration for any model involving 14-3-3 proteins and the Arp2/3 complex in the future.

Abstract

The activity of the Arp2/3 complex is regulated by its binding to nucleation promoting factors, such as N-WASp and SCAR. Here we report on a novel class of Arp2/3 binding proteins which act as inhibitors of Arp2/3 activation by WASp family proteins. We initially isolated a 14-3-3 epsilon homologue from *Acanthamoeba castellanii* as a predominant species eluted from an Arp2/3 affinity column. We subsequently found that 14-3-3 protein binds to the Arp2/3 complex directly within its conserved amphipathic binding cleft and competes with nucleation promotion factors for Arp2/3 complex binding. In *in vitro* actin polymerization assays, 14-3-3 protein weakly inhibits polymerization by activated Arp2/3. The interaction between 14-3-3 and the Arp2/3 complex is regulated by the phosphorylation of the Arp2/3 complex, as shown by chemical crosslinking. In the yeast *Saccharomyces cervisiae*, we find that Arp2/3 and 14-3-3 proteins have a synthetic growth phenotype, suggesting that these complexes function in the same pathway. Together, these findings suggest a role for 14-3-3 proteins as Arp2/3 complex inhibitors that act by blocking the binding of nucleation promoting factors.

Introduction

The spatial and temporal regulation of actin polymerization is crucial for the viability of a eukaryotic cell. Most new actin filaments are formed by nucleation by the Arp2/3 complex, a highly conserved seven-subunit complex that has been found in all eukaryotes in which it has been studied (for review, see (Welch and Mullins, 2002). The Arp2/3 complex, which has low nucleation activity alone, becomes competent to nucleate filaments upon binding to a nucleation promotion factor (NPF) such as a member of WASp family proteins (Machesky et al., 1999; Welch et al., 1998b). Nucleotide hydrolysis by Arp2/3 is regulated by binding to a NPF and filamentous actin, and is required for nucleation of new actin filaments. Phosphate release is thought to allow dissociation of a NPF from Arp2/3 (Dayel et al., 2001). It appears that Arp2/3 complex activity is thus regulated spatially by the localization of NPFs and F-actin, and temporally by its hydrolysis of nucleotide.

Regulation of Arp2/3 activity by post-translational modifications of the Arp2/3 complex has not yet been reported, though specific subunits are phosphorylated in certain cell types. Singh, et al. report that the A isoform of the p16-Arc (ARPC5) subunit of neutrophil Arp2/3 is phosphorylated *in vivo* by MAPK-activated protein kinase-2 (MAPKAPK2) (Singh et al., 2003a). MAPKAPK2 is activated downstream of the MAPK p38, whose activity is necessary for neutrophil chemotaxis and exocytosis. The functional effect of p16-Arc phosphorylation on Arp2/3 activity is currently unclear.

14-3-3 proteins are acidic, abundant proteins found in all eukaryotes. In higher eukaryotes, up to seven isoforms have been isolated; these various isoforms share a highly conserved homo- or heterodimeric structure and ability to bind target proteins in a large amphipathic pocket (Ichimura et al., 1995; Liu et al., 1995). In general, 14-3-3 ligands are proteins containing a conserved phosphoserine motif (Yaffe et al., 1997), though nonphosphorylated binding proteins have also been found (Masters et al., 1999). 14-3-3 proteins have been implicated as having key roles in a

number of signalling cascades such as the Ras/Raf pathway in mammalian cells (for review see (Kolch, 2000)) and the pseudohyphal growth MAPK cascade in yeast (Roberts et al., 1997). There is also a growing body of evidence showing that 14-3-3 is required for the regulation of large complexes such as ion channels (Bunney et al., 2002; Kagan et al., 2002; Zhou et al., 1999).

In recent years, 14-3-3 proteins have also been shown to be involved in the maintenance of the cytoskeleton. Gohla and Bokoch showed that the 14-3-3 zeta isoform binds and stabilizes phosphorylated cofilin, which causes an increase in the cellular pool of inactive phosphocofilin (Gohla and Bokoch, 2002). There are also reports indicating that 14-3-3 isoforms interact with intermediate filaments (van Hemert et al., 2003) and kinesins (Dorner et al., 1999; Ichimura et al., 2002).

We have isolated a 14-3-3 epsilon isoform, named Squiggy, as a binding partner of the Arp2/3 complex in *Acanthamoeba castellanii*. Using a close homologue of Squiggy, the yeast 14-3-3 protein BMH2, we found that the interaction between Arp2/3 and 14-3-3 is direct and is dependent on Arp2/3 phosphorylation. 14-3-3 is able to compete with NPFs for binding of phosphorylated Arp2/3, and is thus able to inhibit Arp2/3 activation in *in vitro* pyrene actin polymerization assays. In yeast, 14-3-3 and Arp2/3 have a synthetic relationship and appear to operate in the same or parallel pathways.

Results

The Arp2/3 complex binds directly to 14-3-3 proteins within their conserved amphipathic groove

We first identified 14-3-3 as a binding partner of the Arp2/3 complex by way of an affinity column in which amoeboid Arp2/3 was covalently conjugated to an Affigel matrix. Amoeba extract was poured over this Arp2/3 column and, after extensive 150 mM KCl washes, we washed the column with 0.5 M KCl and 1 M KCl and collected wash fractions. By SDS-PAGE, several protein bands were visible, including a prominant species of approximately 30 kD (Figure 3-1a). By mass spectrometry, we identified the 30 kD species as an amoeboid 14-3-3 protein which we named Squiggy. By BLAST search, Squiggy is closest in homology to the epsilon isoform of 14-3-3. We created degenerate primers based on distal protein sequences and isolated a 249 bp fragment of Squiggy which encodes the N-terminal one-third of the protein. Other proteins that eluted at 500 mM KCl included actin and elongation factor 2 (EF2). These proteins did not elute from an Affigel matrix conjugated to BSA.

To determine whether the Arp2/3 complex binds directly to 14-3-3 proteins or indirectly through intermediate proteins, we performed polarization anisotropy. For these experiments, we chose to use recombinant yeast 14-3-3 protein as a more tractable alternative to cloning and purifying amoeboid 14-3-3 proteins. The budding yeast *Saccharomyces cerevisiae* expresses two 14-3-3 homologues named BMH1 and BMH2. We used BMH2 in these studies since there is preexisting evidence that BMH2, more than BMH1, plays a role in the maintenance of the actin cytoskeleton in yeast. BMH2 was cloned into a pProEX vector, expressed with a 6x His tag and purified on Ni-NTA resin as described. Since all 14-3-3 proteins appear to form hetero- and homodimers *in vitro* and *in vivo*, we tested the oligomerization of our recombinant BMH2 via analytical ultracentrifugation. As expected, BMH2 formed homodimers with virtually none of the protein exisiting in monomeric form. We performed polarization anisotropy using rhodamine-labelled His-tagged BMH2 in the presence of increasing concentrations of amoeboid Arp2/3 complex. The

labelling reaction took advantage of the single cysteine in BMH2 which is located on an exposed surface distal to the binding pocket. Arp2/3 bound the 14-3-3 protein with a K_d of approximately 2 μM.

Members of the 14-3-3 protein family share the ability to bind target proteins within a highly conserved amphipathic binding cleft. Previous experiments have shown that small engineered peptides, such as R18, can bind many members of the 14-3-3 family with nanomolar affinity and displace naturally occurring binding partners. The R18 peptide, though it does not contain a phosphorylated serine, has been shown to bind within the amphipathic groove(Wang et al., 1999). We tested whether R18 peptide could displace Arp2/3 using polarization anisotropy. In this experiment, Arp2/3 was mixed with rhodamine-labelled BMH2, and increasing concentrations of unlabelled R18 peptide was added. We found that the R18 peptide efficiently displaced Arp2/3 from the binding groove of BMH2. Arp2/3 thus binds directly to the amphipathic binding cleft of 14-3-3 proteins.

14-3-3 proteins partially compete with activators for Arp2/3 complex binding but does not activate

Nearly all Arp2/3 binding proteins to date have been found to act as nucleation promoting factors. We tested whether BMH2 could also activate the Arp2/3 complex in a pyrene-actin polymerization assay. Even at high (millimolar) concentrations of BMH2, no nucleation promoting activity was detected (data not shown). Next, we tested whether BMH2 competes with known nucleation promoting factors for binding of Arp2/3, or whether a trimeric complex of Arp2/3, 14-3-3 and activators could be formed. Rhodamine labelled BMH2 was prebound to Arp2/3 complex, increasing concentrations of unlabelled N-WASp WA was added and anisotropy measurements were taken. We found that rhodamine-BMH2 could be completely displaced by the addition of excess N-WASp WA, indicating that 14-3-3 and NPFs compete for the same binding site(s) on the Arp2/3 complex. Note that the anisotropy value of the rhodamine-BMH2 in the presence of

Arp2/3 and an excess of N-WASp WA and the anisotropy value of rhodamine-BMH2 alone are the same. Conversely, we prebound rhodamine-labelled SCAR WA to Arp2/3 and added increasing concentrations of unlabelled BMH2. We observed that BMH2 could compete with SCAR WA for Arp2/3 complex binding. Despite the addition of a vast excess of BMH2, however, approximately two-thirds of the labelled SCAR WA remained bound to Arp2/3 and could not be displaced by 14-3-3 protein. Note here that the anisotropy value of rhodamine-SCAR WA in the presence of Arp2/3 and an excess of BMH2 does not match the anisotropy value of rhodamine-SCAR WA alone. From these experiments we concluded that only a subpopulation of amoeboid Arp2/3 is able to bind 14-3-3 proteins,

14-3-3 protein decreases the rate of polymerization by Arp2/3

We next tested whether 14-3-3 could compete with the binding of activators of Arp2/3 in *in vitro* actin polymerization assays. Addition of recombinant BMH2 to the polymerization reaction (2 μM 8% pyrene labelled actin, 2 nM Arp2/3 and 10 nM ActA) caused a decrease in the polymerization, quantified by calculating the rate of free ends formation of a polymerization reaction with and without the addition of 14-3-3 protein. At the highest concentration (9 μM), BMH2 was not able to completely inhibit Arp2/3 mediated nucleation, but caused a decrease in free end formation by more than 20 fold.

14-3-3 binding to Arp2/3 is dependent on phosphorylation

Given that 14-3-3 proteins are known to bind phophoserine peptides, we wondered whether BMH2 binding to Arp2/3 is dependent upon phosphorylation and which subunit(s) of the Arp2/3 complex mediate the interaction with 14-3-3 proteins. We used the zero-length crosslinker EDC to crosslink recombinant BMH2 to amoeboid Arp2/3. When Arp2/3 and BMH2 were mixed and crosslinker was added, we detected several higher molecular weight protein species that did not appear when crosslinker was added to either BMH2 alone or to the Arp2/3 complex alone. We

identified the proteins present in these higher molecular weight species by immunoblot using antibodies specific to BMH2 or to one of the Arp2/3 subunits. By Western, we observed that BMH2 appears to form crosslinks to the smallest Arp2/3 subunits, p14 (ARPC5) and p18 (ARPC3). In both cases, a new species of approximately 50 kD, which is consistent with a BMH2 monomer (31 kD) crosslinked to either p14 or p18. Treatment of the Arp2/3 complex with lambda phosphatase prior to the crosslinking reaction inhibited the formation of BMH2-p14 and BMH2-p18 crosslinks. Likewise, addition of the R18 peptide, which binds within the conserved cleft of 14-3-3 proteins. resulted in drastically reduced crosslinking efficiency of BMH2 to p14 and p18.

Synthetic relationship between BMH2 and Arp2/3 in yeast

We were next interested in finding whether Arp2/3 and 14-3-3 proteins interact in vivo. Deletions of either BMH1 or BMH2 in haploid yeast yielded no discernable phenotype, though a double BMH1ΔBMH2Δ deletion proved to be lethal (data not shown). The p18 subunit of the Arp2/3 complex has been shown to be non-lethal in yeast (Winter et al., 1999) and we found that haploid p18Δ cells are very slow growing compared to WT cell or BMH2Δ cells (Figure 5). We created diploid p18ΔBMH2Δ mutants and performed tetrad dissections to isolate haploid cells with the double deletion genotype. We found that haploid p18ΔBMH2Δ cells show a small growth advantage compared to p18Δ cells (Table 1). Conversely, overexpression of BMH2 using a galactose expression system exacerbates the growth defect of p18Δ colonies (Figure 5b). These experiments suggest that 14-3-3 and Arp2/3 complexes may function in the same or parallel pathways in yeast, and both are required for cell growth and viability.

Discussion

Arp2/3 complex activity is regulated through the binding of NPFs such as the WA portion of N-WASp or SCAR. NPF binding triggers hydrolysis of ATP by Arp2/3 (Dayel et al., 2001) coupled with a predicted conformational change (Robinson et al., 2001; Zalevsky et al., 2001b), allowing Arp2/3 to become nucleation competent. In order to efficiently nucleate new actin filaments, Arp2/3 also requires F-actin. Current models of Arp2/3 activation suggest that Arp2/3 binds to the side of preexisiting actin filament, is activated by a NPF, and subsequently nucleates a new daughter filament from the side of the mother filament. With this model in mind, we can imagine a few different ways to negatively regulate the activity of the Arp2/3 complex: (a) inhibition of NPFs such that they are unable bind Arp2/3, (b) inhibition of Arp2/3 filament side binding activity, (c) inhibition of actin monomer binding or conformational change, and (d) inhibition of Arp2/3 binding to a NPF. In higher eukaryotes, the ability of NPFs to bind to Arp2/3 appears to be carefully regulated in the cell. Full length N-WASp and WASp are autoinhibited and unable to bind to Arp2/3 in the absence of cdc42 and/or PIP2 (Kim et al., 2000). SCAR (WAVE1) is constitutively active but forms a complex *in vivo* in which it remains inactive until the complex is dissociated by interaction with Rac (Eden et al., 2002).

There are few examples of negative regulation of Arp2/3 mediated polymerization by proteins that bind Arp2/3 directly. Recently, Rodal, et al. reported that yeast coronin binds directly to Arp2/3 and inhibits Arp2/3-mediated actin polymerization; they do not believe this activity is caused by blocking side binding or NPF binding (Humphries et al., 2002). The mechanism by which coronin inhibits Arp2/3 activity remains to be elucidated.

Protein phosphorylation is critical in countless signalling cascades as a means to create new binding sites or to alter the activity of a protein. Arp2/3 has been shown to be phosphorylated on at least the smallest subunit, p16 (ARPC5) in neutrophils (Singh et al., 2003a). It is not clear how phosphorylation of p16 affects Arp2/3 activity or binding partners, but it is intriguing that

phosphorylation occurs downstream of p38, a MAPK which has been shown to be involved in actin cytoskeletal remodeling.

We have found that 14-3-3 protein binds directly to Arp2/3 with micromolar affinity, similar to that of NPFs (Marchand et al., 2001). In purifying Arp2/3 from *Acanthamoeba*, it appears that we are able to isolate a mixed population of phosphorylated and nonphosphorylated complexes. This became clear after performing polarization anisotropy experiments where we observed that 14-3-3 could not completely compete with fluorescently labelled NPF for binding of Arp2/3, even at millimolar concentrations.

The 14-3-3 and Arp2/3 interaction was discovered by affinity chromatography of *Acanthamoeba* extracts, suggesting that this association in vivo. We found that in the yeast *Saccharomyces cerevisiae*, there is a synthetic relationship between 14-3-3 proteins and the Arp2/3 complex, further supporting that this association may be conserved across species and plays an important role in the regulation of actin networks.

Materials & Methods

Identification of Arp2/3 binding proteins

Arp2/3 complex was purified from *Acanthamoeba* as previously described (Dayel et al., 2001; Zalevsky et al., 2001a). Arp2/3 or BSA was coupled to Affigel-15 resin (Bio-Rad, Hercules, CA) in MOPS buffer for 4 hours at 4°C, washed with 0.25 M TrisCl, pH 8.0, 50 mM NaCl. 8 g of amoeba were pelleted, washed in extract buffer, and dounce homogenized with 20 strokes in a Wheaton homogenizer (Wheaton, Millville, NJ). The extract was cleared with a 10 minute spin at 3,000 rpm followed with a high-speed spin in a Beckman ultracentrifuge at 38,000 rpm for two hours at 4°C. 10 mL of cleared extract was passed over Arp2/3, BSA or Affigel-15 (no coupled protein) resins, and washed with 100 column volumes of extract buffer. Fractions were collected after washing with extract buffer supplemented with 150 mM, 500 mM and 1 M KCl. Fractions were analyzed by SDS-PAGE, and abundant species were sequenced by mass spectrophotometry. Homologous proteins were found by a protein BLAST search (http://www.ncbi.nlm.nih.gov:80/BLAST/), aligned using Clustal W (http://www.ebi.ac.uk/clustalw/) and a shaded alignment was created using ESPript (http://prodes.toulouse.inra.fr/ESPript/cgi-bin/ESPript.cgi).

Protein purification

Full length *Saccharomyces cerevisiae* BMH2 was cloned from genomic DNA by standard PCR with a forward primer GGATCCATGTCCCAAACTCGTGAAGATTCTGTT and reverse primer GAATTCTTATTTGGTTGGTTCACCTTGAGTTTG, using proofreading polymerase. BMH2 was subcloned into a pProEX-HTb vector (Invitrogen, Carlsbad, CA), expressed in BL21 cells with a C-terminal 6xHis tag and purified on NiNTA resin (Qiagen, Valencia, CA) in a native preparation. Arp2/3 from *Acanthamoeba* was purified as previously described (Dayel et al., 2001).

Analytical ultracentrifugation

Analytical ultracentrifugation was performed at room temperature in KMEI buffer (50 mM KCl, 1 mM $MgSO_4$, 1 mM EGTA, 10 mM imidazole, pH 7.0) with 1 mM DTT and 1 mM ATP at the following speeds: 10,000 rpm, 14,000 rpm and 20,000 rpm.

Fluorescent labelling of proteins

To fluorescently label BMH2, 6xHis tagged BMH2 was dialyzed overnight into 50 mM KCl, 1 mM EDTA, 2 mM TCEP and 20 mM imidazole, pH 7.0. 100 µL of BMH2 was mixed with 9 µL of 20 mM rhodamine iodoacetimide for 1 hour at room temperature and then overnight at 4°C. The reaction was quenched with DTT. Labelling occurs at the single cysteine in BMH2 (CYS194) with approximately 40% efficiency. Fluorescently labelled ActA was made as previously described (Zalevsky et al., 2001a).

Polarization anisotropy

For binding experiments, rhodamine labelled BMH2 was mixed with unlabelled Arp2/3 at the indicated concentrations. The anisotropies were measured and Kd was calculated as described previously (Zalevsky et al., 2001a). For R18 peptide competition experiments, 5 µM fluorescently labelled BMH2 was premixed with equimolar Arp2/3 and unlabelled R18 peptide (PHCVPRDLSWLDLEANMCLPK, synthesized by SynPep, Dublin, CA; sequence taken from (Wang et al., 1999)) was added at the indicated concentrations. For NPF competition experiments, 2 µM fluorescently labelled BMH2 was premixed with 5 µM Arp2/3 and unlabelled N-WASp WA was added at the indicated concentrations. Conversely, 0.5 µM rhodamine-labelled ActA was premixed with 2 µM Arp2/3 and unlabelled BMH2 was added at the indicated concentrations.

Actin polymerization assays

Actin polymerization assays were done with 2 µM actin, 2 nM Arp2/3, 10 nM ActA and indicated concentration of BMH2. *Acanthamoeba* actin was supplemented with pyrene-labelled

Acanthamoeba actin to 8%. Polymerization was collected on a K2 Multifrequency Fluorometer (ISS, Champagne, IL) and analyzed using Kaleidagraph software (Synergy, Reading PA). Free end formation over time was calculated using the equation [ends] = (d[F-actin]/dt)/([free g-actin]*10 μMs^{-1}).

Chemical crosslinking

3 µM purified amoeba Arp2/3 was mixed with 15 µM 6xHis BMH2 in KMEI buffer. R18 peptide, if used, was added to a final concentration of 15 µM. To crosslink, 6 mM NHS and 3 mM EDC, made freshly and dissolved in DMSO at a stock concentration of 0.1 M, was added. Crosslinking was performed at room temperature for 1 hour and was quenched with 10 mM Tris or 4x SDS-PAGE sample buffer. Crosslinked proteins were analyzed by SDS-PAGE and Western blotting.

Phosphatase treatment of Arp2/3

Purified amoeba Arp2/3 was mixed with 400 units lambda phosphatase (NEB, Beverly, MA), lambda protein phosphatase buffer and $MnCl_2$ at suggested concentrations. As a negative control, Arp2/3 was mixed with buffer and $MnCl_2$ but lambda phosphatase was not added. The phosphatase reaction was performed at 30°C for one hour. If used for crosslinking reactions, the samples were dialyzed overnight in KMEI buffer to remove Tris.

Yeast culture and gene disruption

Strains of WT haploid and diploid yeast was obtained from Ira Herskowitz lab (IH strain) and grown at 30 degrees using standard protocols. p18 or BMH2 knockout strains were generated by replacement of the endogenous copy of the gene of interest with the *HIS3* or *TRYP1* gene by homologous recombination using the Pringle method (Longtine et al., 1998). Correct integration of the marker into the genome was confirmed by PCR. Yeast mating was performed using haploid strains of p13Δ or BMH2Δ. Diploid yeast were sporulated by growth in minimal media and tetrad dissection was performed.

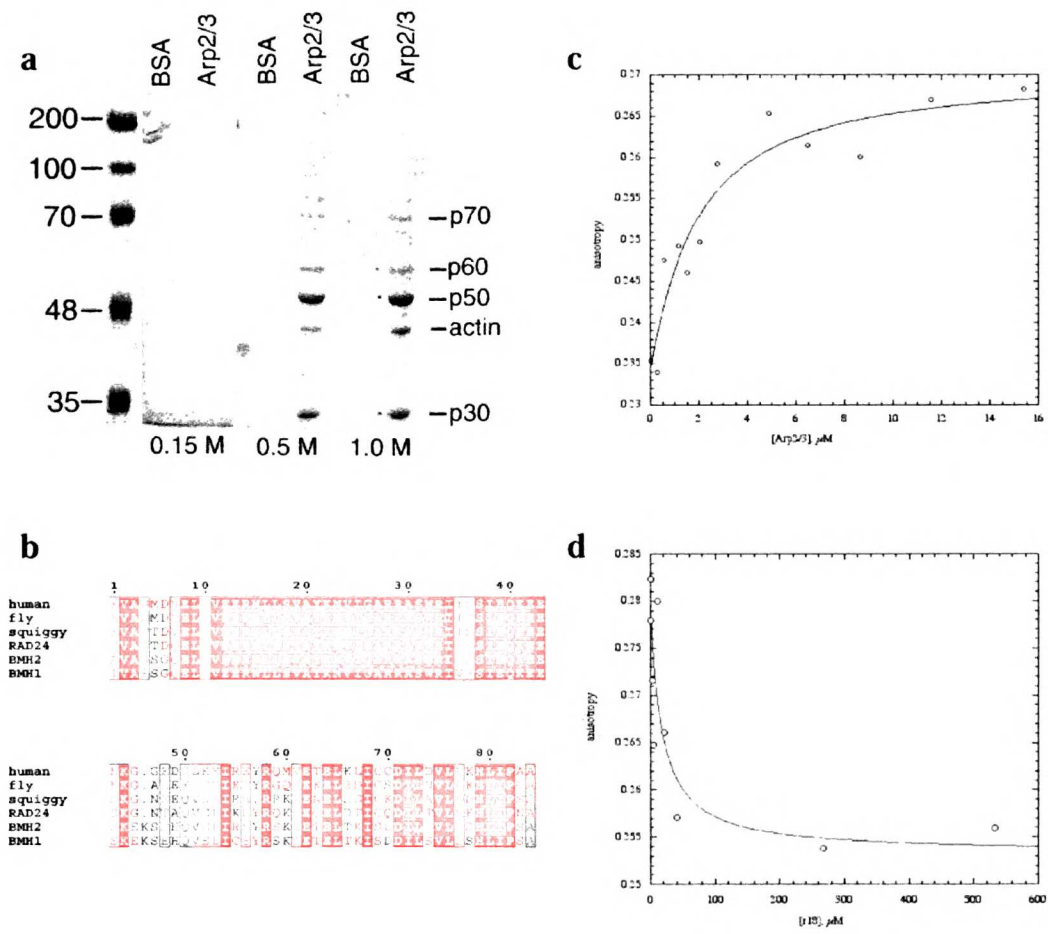

Figure 3-1. Arp2/3 binds to 14-3-3 within its conserved amphipathic groove. (a) Coomassie stained gel of fractions collected from Arp2/3 affinity or control BSA column following 0.15 M, 0.5 M and 1.0 M KCl washes. p30 was identified as a 14-3-3 epsilon homologue by mass spectrophotometry. (b) Sequence alignment of a fragment of amoeba 14-3-3 protein (Squiggy) obtained by PCR, and other 14-3-3 proteins by BLAST search. RAD24 is a 14-3-3 protein from *S. pombe*. BMH1 and BMH2 are the two 14-3-3 proteins found in *S. cerevisiae*. Dark gray letters indicate conservative amino acid changes and lighter gray letters indicate nonconservative changes. (c) Polarization anisotropy of rhodamine-labelled BMH2 protein (0.5 μM) with increasing concentrations of purified amoeba Arp2/3. The calculated Kd is 2 μM. (d) Polarization anisotropy of 5 μM Arp2/3 prebound to 5 μM rhodamine-labelled BMH2 with indicated concentrations of R18 peptide.

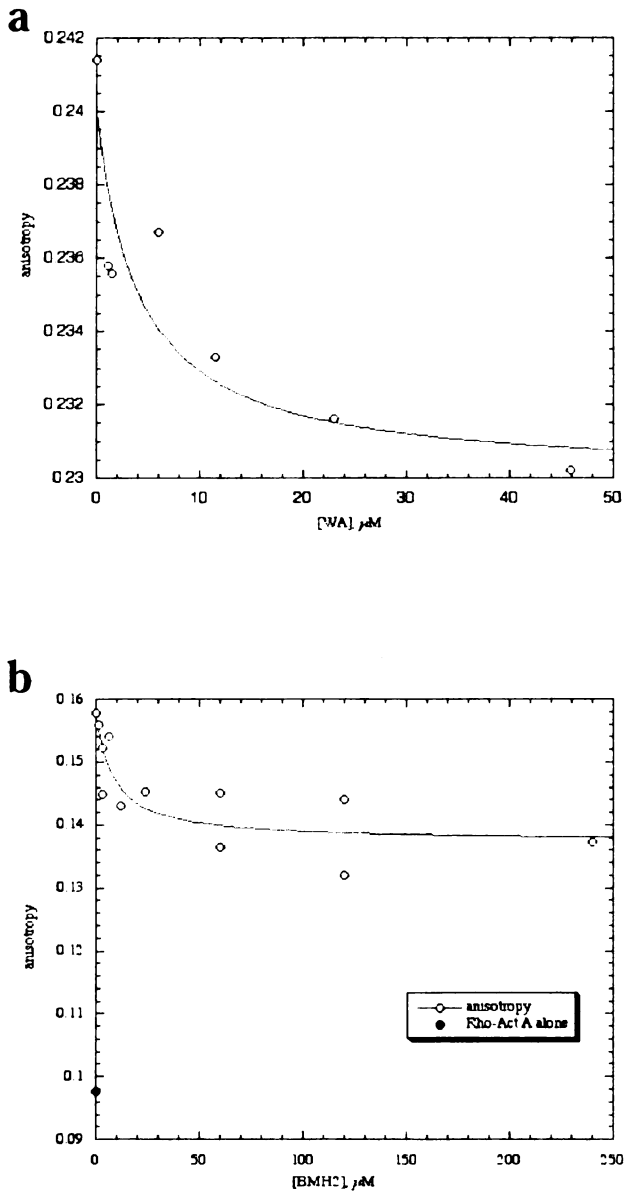

Figure 3-2. 14-3-3 competes with NPFs for the binding of the Arp2/3 complex. (a) Polarization anisotropy of rhodamine-labelled BMH2 (2 μM) prebound to Arp2/3 (5 μM) and indicated concetrations of unlabelled N-WASp WA was added. The drop in anisotropy is consistent with rhodamine-labelled BMH2 alone. (b) Polarization anisotropy of rhodamine-labelled ActA (0.5 μM) premixed with 2 μM Arp2/3 with added concentrations of unlabelled BMH2 protein. Black circle indicates anisotropy measurement of rhodamine-labelled ActA alone.

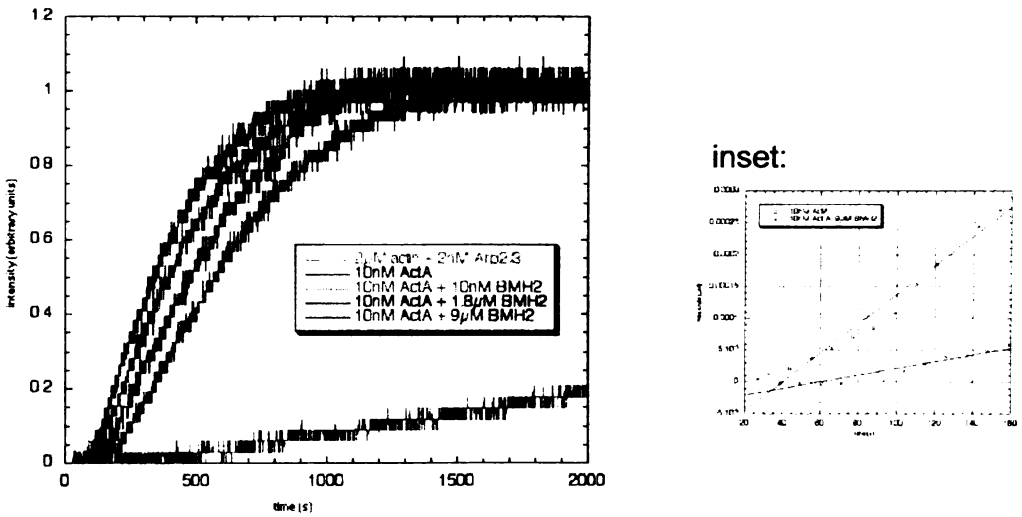

Figure 3-3. 14-3-3 inhibits polymerization by activated Arp2/3. Pyrene-actin polymerization assay showing effect of increasing concentrations of BMH2 protein. Orange line: 2 μM actin (8% pyrene labelled), 2 nM Arp2/3. Green line: 2 μM actin, 2 nM Arp2/3, 10 nM ActA. Pink, blue and brown lines are 2 μM actin, 2 nM Arp2/3, 10 nM ActA with indicated concentrations of BMH2. Inset: rate of free end formation calculated from polymerization data. Line with open circles was calculated from 10 nM Act A polymerization data (green curve); line with crossbars was calculated from 10 nM Act A + 9 μM BMH2 polymerization data (brown curve).

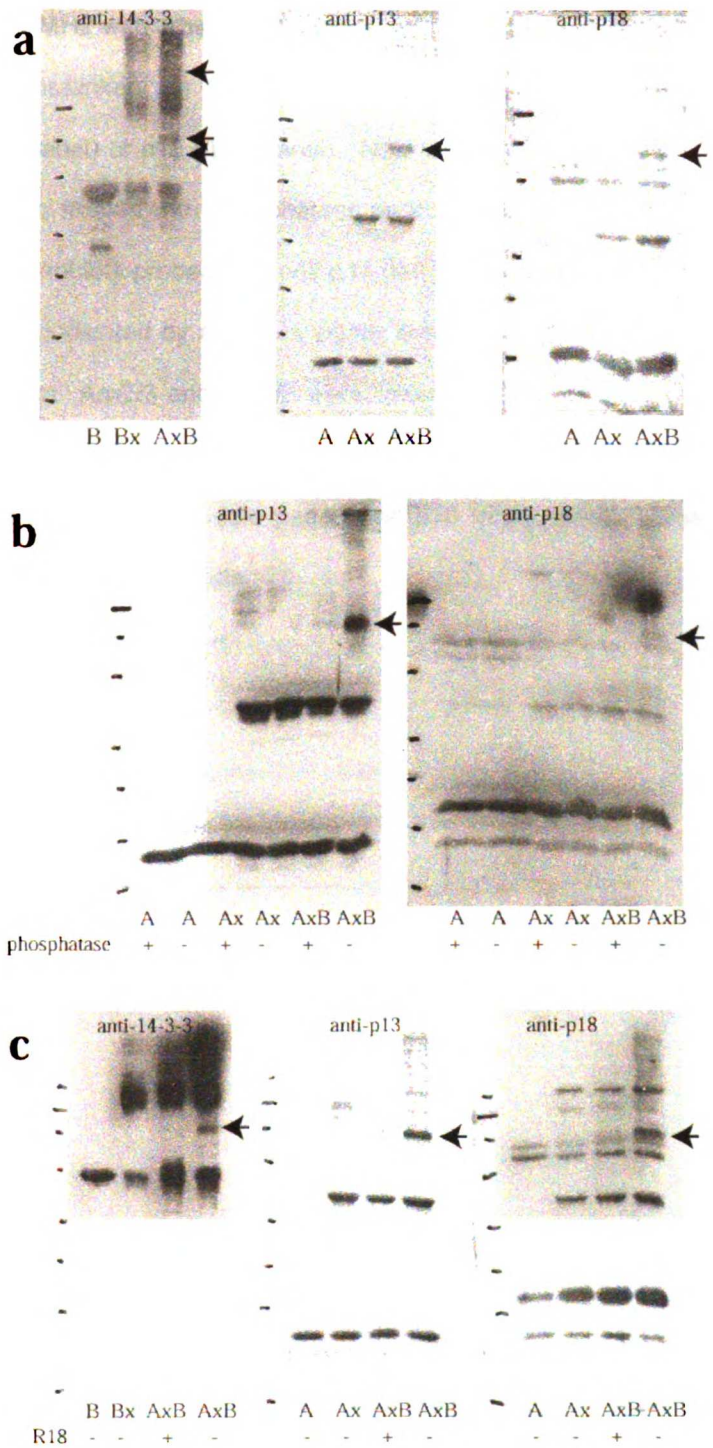

Figure 3-4. Phosphorylation on Arp2/3 is required for 14-3-3 binding. Proteins were crosslinked with EDC, separated by SDS-PAGE, and transferred to a membrane for immunoblotting. "A" and "B" lane samples are Arp2/3 or BMH2 protein alone, "Ax" ad "Bx"

indicates Arp2/3 or BMH2 with crosslinker added, "AxB" samples are BMH2 and Arp2/3 premixed prior to addition of crosslinker. (a) Immunoblots probed with antibodies raised against BMH2 (left panel), p14 (middle panel) or p18 (right panel). New crosslinks are indicated with arrows. (b) A sample of Arp2/3 was treated with phosphatase prior to crosslinking reaction (2^{nd} to last lane in each blot), and immunoblots probed with anti-p14 (left panel) or anti-p18 (right panel) antibodies. Note that crosslinks (indicated by arrow) is significantly reduced when Arp2/3 has been treated with phosphatase. (c) Arp2/3 and BMH2 were mixed with the 14-3-3 antagonist peptide R18 prior to crosslinking (2^{nd} to last lane in each blot) and immunoblots were probed with antibodies against BMH2 (left panel), p14 (middle panel) and p18 (right panel). Crosslinks (arrows) are reduced in the presence of R18 peptide.

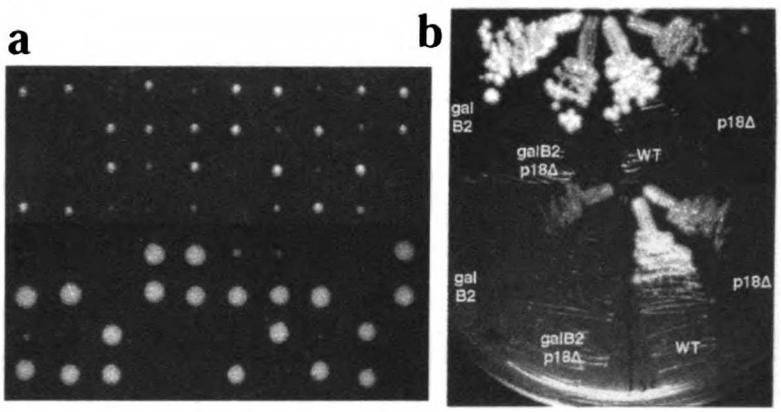

Figure 3-5. Effect of p18Δ BMH2Δ double mutation and overexpression of BMH2 on growth of yeast colonies. (a) p18Δ BMH2Δ diploid cells were sporulated and tetrads were grown at either 25° (top panel) or 30° (bottom panel) for several days. Growth was scored based on the relative size of colonies (see Table 1, below). (b) Haploid cells of WT or p18Δ genotypes were transformed with a gal-BMH2 overexpression plasmid (gal B2) and single colonies were streaked on either a YPD plate (top panel) or galactose plate (bottom panel).

		Dead	+	++	+++
25° growth	WT	0	0	0	18
	p18Δ	3	15	4	0
	BMH2Δ	0	0	0	22
	p18Δ BMH2Δ	1	3	14	0
30° growth	WT	0	0	0	19
	p18Δ	16	1	1	0
	BMH2Δ	0	0	0	16
	p18Δ BMH2Δ	7	6	6	0

Table 3-1. Tetrad growth assay. Diploid p18Δ BMH2Δ cells were sporulated and tetrads were plated on YPD plates and grown at either 30° or 25° as shown in Figure 5. Colonies were evaluated after 3 days of growth and classified as either large (+++), medium (++), small (+), or dead (no growth visible). Colonies were then plated on TRYP- and HIS- plates to assay for the cell genotype.

Appendix

Examination of Carmil function in *Drosophila* S2 Cells

Foreword

Carmil was discovered in Dictyostelium, and was reported to form a complex with capping protein, Arp2/3 and myosin I, giving rise to its name (capping protein, Arp2/3 and myosin I linker) (Jung et al., 2001). Mutants lacking Carmil exhibited macropinocytosis defects, suggesting that Carmil may play a role in directing actin activity to the plasma membrane. Importantly, homologs were identified in a variety of organisms, including mammals, flies, and worms. Subsequently, Remmert et al. reported that Carmil was a "bona fide" interactant with capping protein in Acanthamoeba with a Kd of 0.4 μM (Remmert et al., 2004).

At the time that this project was started, the function of Carmil was unknown, and preliminary results with RNAi yielded promising results. The publication of papers identifying Carmil as a negative regulator of capping protein (Uruno et al., 2006; Yang et al., 2005) dampened my enthusiasm for the project. The study conducted by Yang et al., which included Carmil depletion using RNAi, overlapped considerably with my planned experiments.

This work was done in collaboration with Brad Zuchero, who focused on the purification and biochemical characterization of Carmil isoforms. The methods used to deplete Carmil from S2 cells and to express Carmil isoforms are essentially identical to those described in Chapter 1.

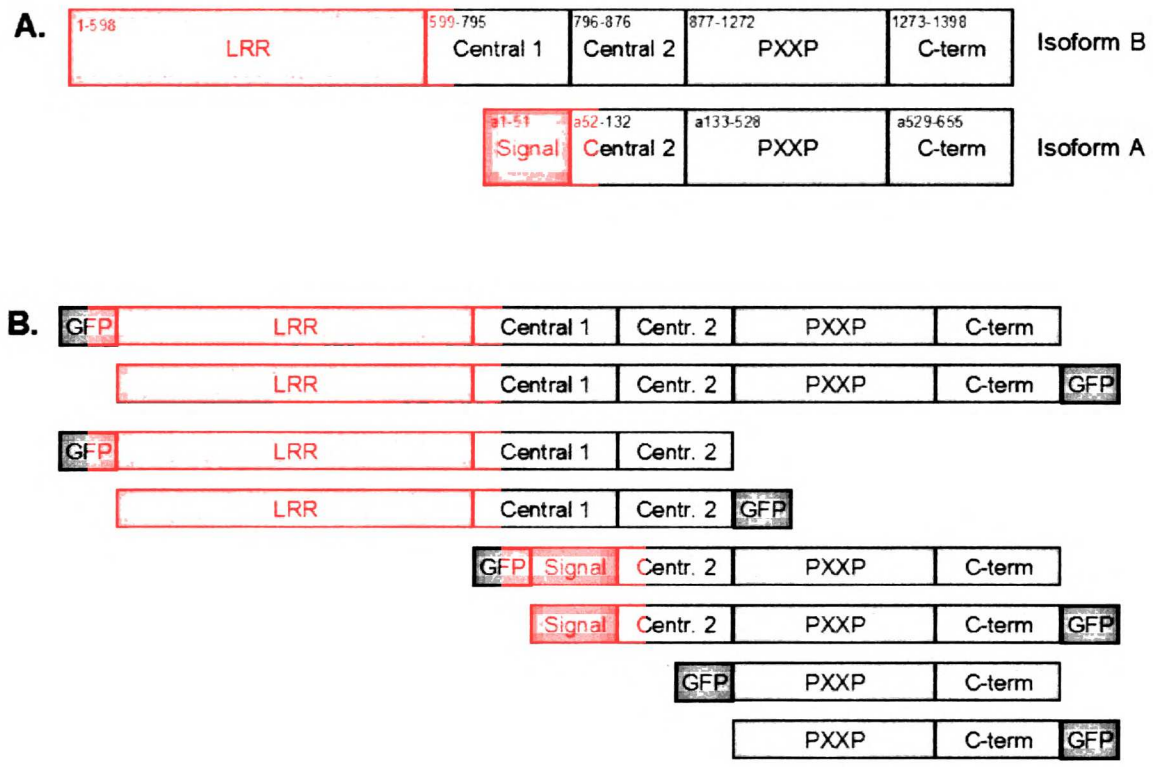

Figure A-1. Drosophila Carmil constructs for *in vivo* study. (A) Two isoforms of Carmil were identified based on genetic database information, cloned from a cDNA library and named isoforms A and B. Isoform A includes a cryptic signal sequence (red). Isoform B includes a leucine-rich repeat (LRR), two central regions, a proline-rich region (PXXP, in pink) which is thought to bind capping protein and Arp2/3, and a C-terminal domain. Numbers in upper left corner of each rectangle indicates the amino acid range for each domain. Domain identification was performed by Brad Zuchero. (B) For expression in S2 cells, N-terminal and C-terminal GFP-tagged constructs were planned for both isoforms. Figure courtesy of Brad "Acan do it" Zuchero.

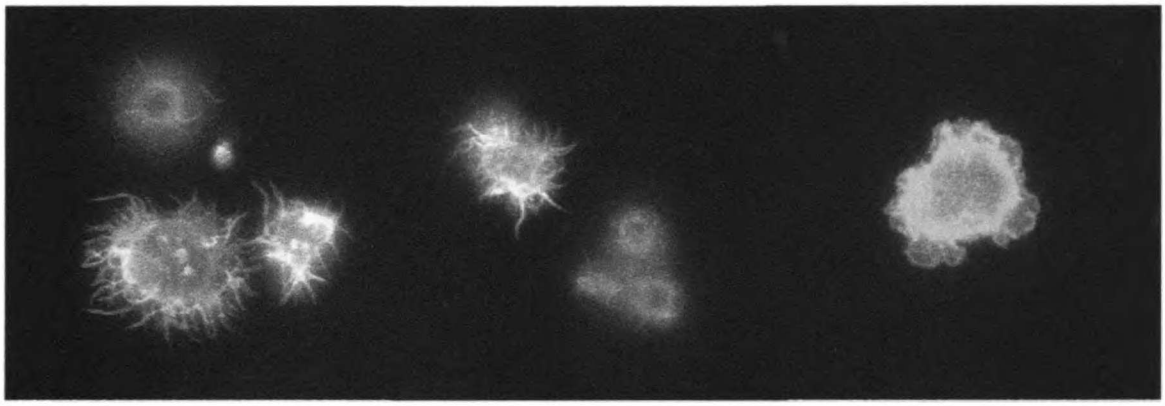

Figure A-2. Depletion of Carmil in S2 cells causes aberrations in lamellar morphology. Three sample images from a 7-day Carmil RNAi trial showing cells with stellate morphology (left, center) and ruffled morphology (right). The footprint of these cells are much smaller than average due to the inability to spread.

	WT	Stellate	Non-spread
Trial 1	25%	21%	54%
Trial 2	5%	66%	29%
Trial 3	29%	28%	30%

Table A-1. Carmil depletion in S2 cells causes aberrations in lamellar morphology. Three Carmil RNAi trials were run independently, and cells were fixed and stained with Alexa488 phalloidin. The lamellar morphology was considered 'WT' if the cell edge was smooth and the cell was well spread. Stellate cells typically showed long actin-rich, spiky protrusions, and non-spread cells typically had a very small footprint without appreciable lamellar spreading.

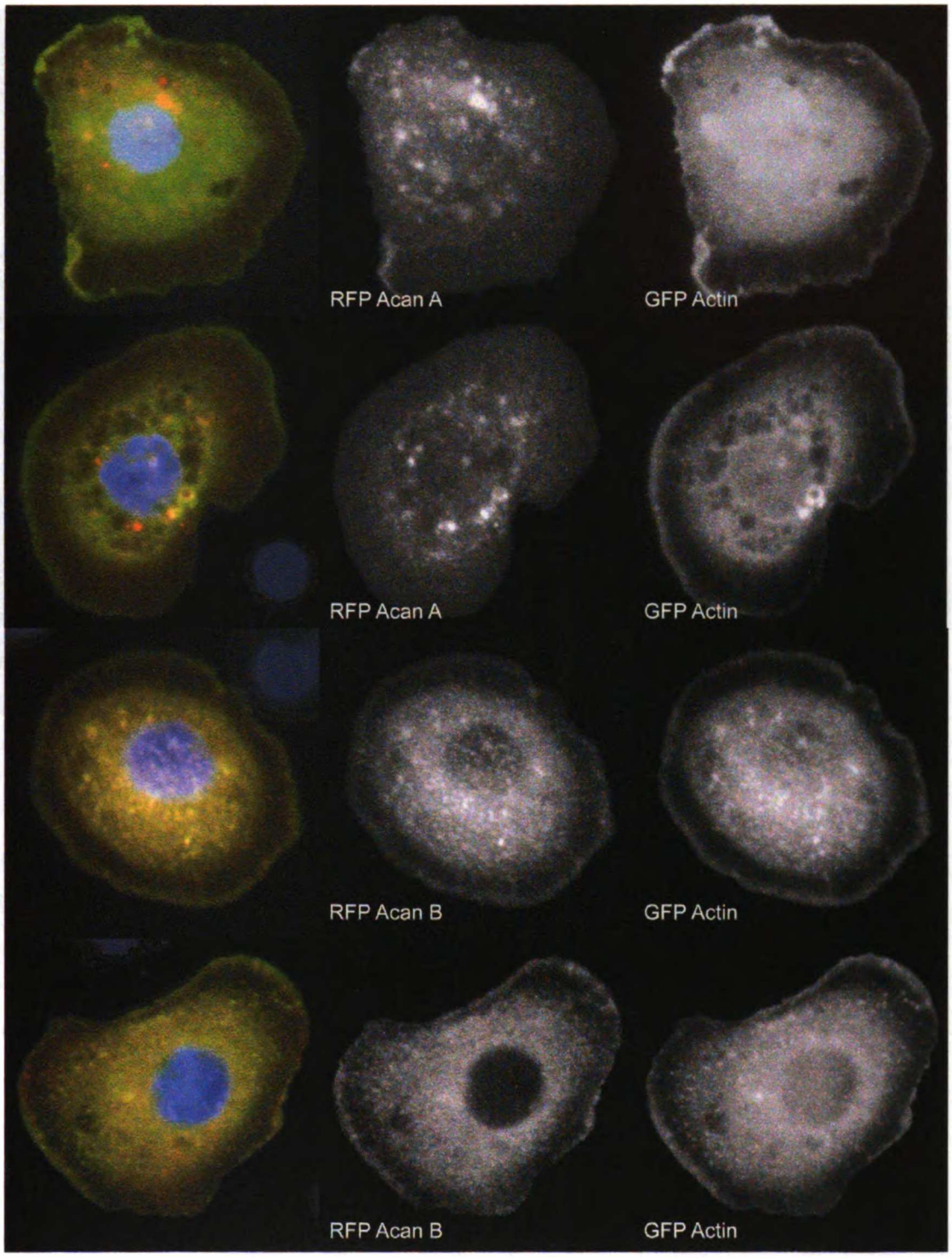

Figure A-3. Carmil isoforms A and B show different expression patterns. RFP-tagged Carmil isoform A (Acan A) coexpressed with GFP-actin shows a punctate, vesicular expression pattern (top two panels). RFP-tagged Carmil isoform B (Acan B) appears to colocalize with GFP actin (bottom two panels).

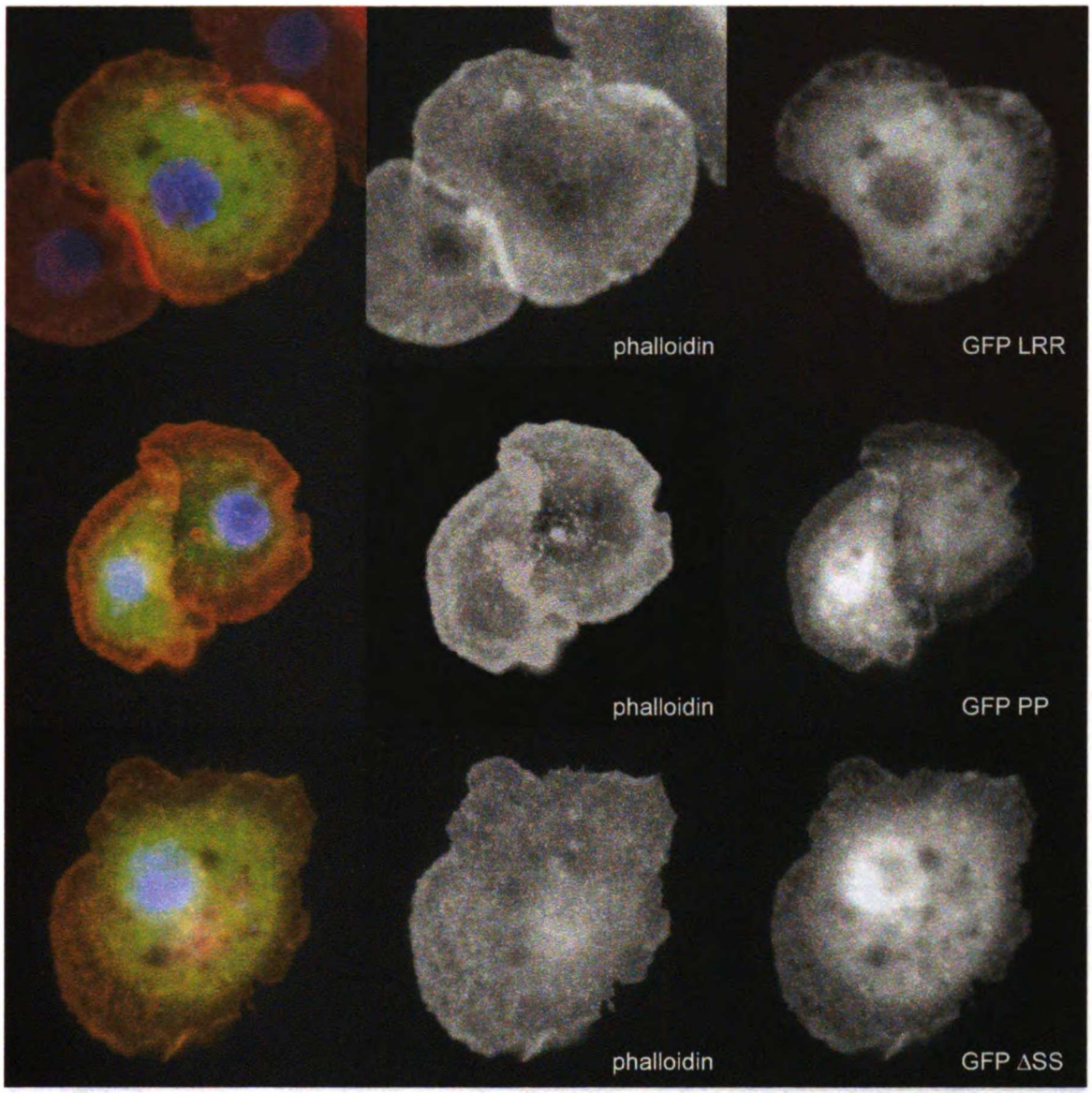

Figure A-4. Expression of Carmil deletion constructs in S2 cells. GFP-Carmil deletion constructs were transiently expressed in S2 cells, fixed, and stained with Alexa 568 phalloidin. GFP LRR indicates LRR+centr1+centr2 construct (see Figure A-1), PP indicates PxxP+C-term construct, and SS indicates centr2+PxxP+C-term construct. All constructs appear to retain some association with the actin cytoskeleton, although LRR exhibits the highest cytoplasmic background fluorescence.

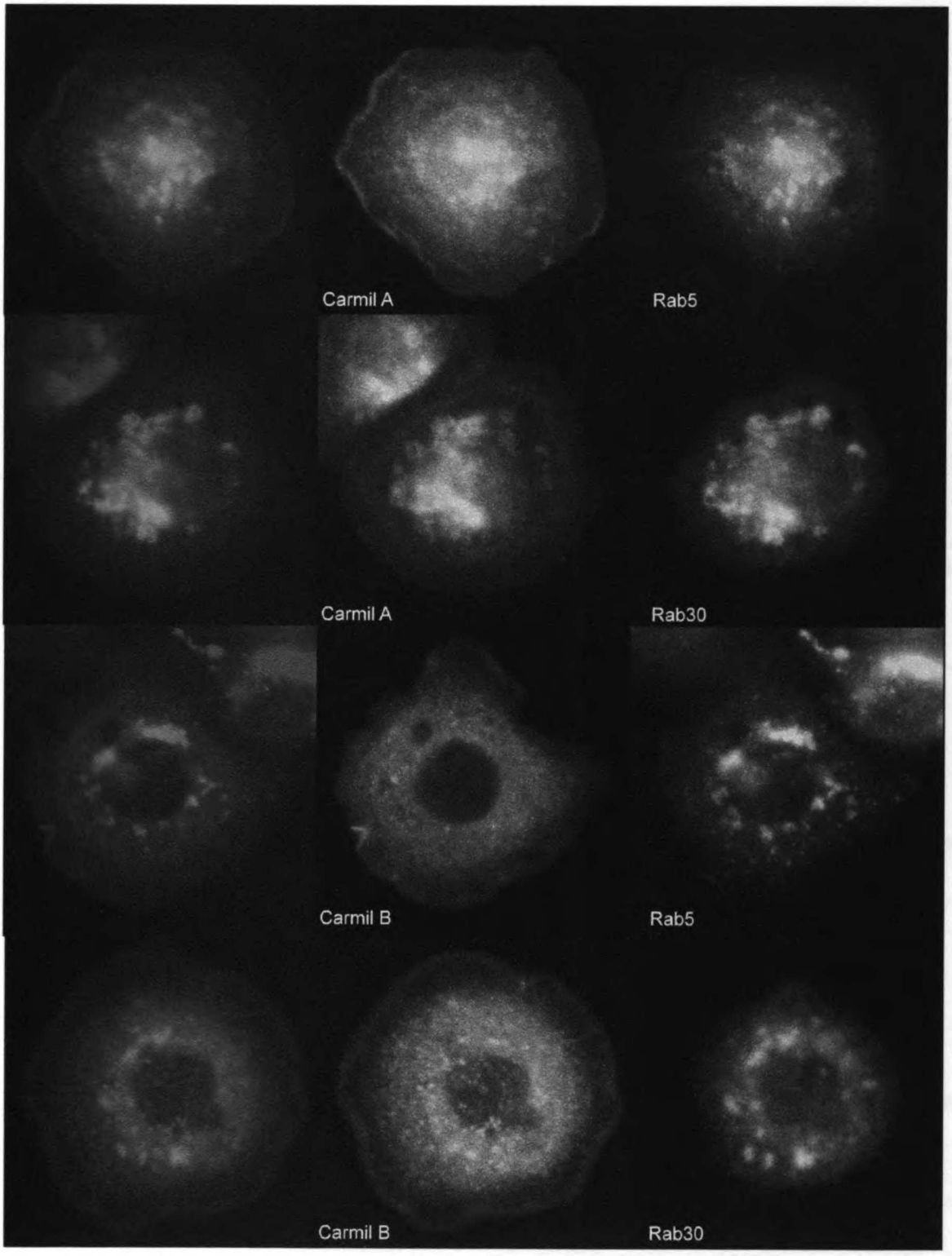

Figure A-5. Carmil isoform A, but not isoform B, colocalizes with Rab5 and Rab30. Top two panels: transient expression of RFP Carmil isoform A in stable GFP-Rab expressing cell lines (top panel, Rab 5, 2nd to top, Rab30). Bottom two panels: transient expression of RFP Carmil

isoform B in stable GFP-Rab expressing cell lines (3rd panel, Rab 5, bottom panel, Rab30). Isoform A colocalizes well with Rab5, a marker for early endosomes, as well as Rab30. Isoform B does not show colocalization with either marker. Rab6, Rab18 and Rab40 were also examined, but showed colocalization with neither isoform. Antonina Roll-Mecak (Vale lab) constructed stable Rab cell lines with constructs made by Jim Wilhelm.

References

Agnew, B.J., L.S. Minamide, and J.R. Bamburg. 1995. Reactivation of phosphorylated actin depolymerizing factor and identification of the regulatory site. *J Biol Chem.* 270:17582-7.

Aizawa, H., Y. Fukui, and I. Yahara. 1997. Live dynamics of Dictyostelium cofilin suggests a role in remodeling actin latticework into bundles. *J Cell Sci.* 110 (Pt 19):2333-44.

Allen, P.G. 2003. Actin filament uncapping localizes to ruffling lamellae and rocketing vesicles. *Nat Cell Biol.* 5:972-9.

Ambach, A., J. Saunus, M. Konstandin, S. Wesselborg, S.C. Meuer, and Y. Samstag. 2000. The serine phosphatases PP1 and PP2A associate with and activate the actin-binding protein cofilin in human T lymphocytes. *Eur J Immunol.* 30:3422-31.

Arber, S., F.A. Barbayannis, H. Hanser, C. Schneider, C.A. Stanyon, O. Bernard, and P. Caroni. 1998. Regulation of actin dynamics through phosphorylation of cofilin by LIM-kinase. *Nature.* 393:805-9.

Aspenstrom, P., U. Lindberg, and A. Hall. 1996. Two GTPases, Cdc42 and Rac, bind directly to a protein implicated in the immunodeficiency disorder Wiskott-Aldrich syndrome. *Curr Biol.* 6:70-5.

Bamburg, J.R. 1999. Proteins of the ADF/cofilin family: essential regulators of actin dynamics. *Annu Rev Cell Dev Biol.* 15:185-230.

Bamburg, J.R., A. McGough, and S. Ono. 1999. Putting a new twist on actin: ADF/cofilins modulate actin dynamics. *Trends Cell Biol.* 9:364-70.

Bear, J.E., T.M. Svitkina, M. Krause, D.A. Schafer, J.J. Loureiro, G.A. Strasser, I.V. Maly, O.Y. Chaga, J.A. Cooper, G.G. Borisy, and F.B. Gertler. 2002. Antagonism between Ena/VASP proteins and actin filament capping regulates fibroblast motility. *Cell.* 109:509-21.

Blanchoin, L., and T.D. Pollard. 1998. Interaction of actin monomers with Acanthamoeba actophorin (ADF/cofilin) and profilin. *J Biol Chem.* 273:25106-11.

Blanchoin, L., and T.D. Pollard. 1999. Mechanism of interaction of Acanthamoeba actophorin (ADF/Cofilin) with actin filaments. *J Biol Chem.* 274:15538-46.

Blanchoin, L., T.D. Pollard, and S.E. Hitchcock-DeGregori. 2001. Inhibition of the Arp2/3 complex-nucleated actin polymerization and branch formation by tropomyosin. *Curr Biol.* 11:1300-4.

Blanchoin, L., T.D. Pollard, and R.D. Mullins. 2000. Interactions of ADF/cofilin, Arp2/3 complex, capping protein and profilin in remodeling of branched actin filament networks. *Curr Biol.* 10:1273-82.

Bourguignon, L.Y., and S.J. Singer. 1977. Transmembrane interactions and the mechanism of capping of surface receptors by their specific ligands. *Proc Natl Acad Sci U S A.* 74:5031-5.

Bretscher, M.S. 1976. Directed lipid flow in cell membranes. *Nature.* 260:21-3.

Bunney, T.D., P.W. van den Wijngaard, and A.H. de Boer. 2002. 14-3-3 protein regulation of proton pumps and ion channels. *Plant Mol Biol.* 50:1041-51.

Carlier, M.F. 1991. Nucleotide hydrolysis in cytoskeletal assembly. *Curr Opin Cell Biol.* 3:12-7.

Carlier, M.F., V. Laurent, J. Santolini, R. Melki, D. Didry, G.X. Xia, Y. Hong, N.H. Chua, and D. Pantaloni. 1997. Actin depolymerizing factor (ADF/cofilin) enhances the rate of filament turnover: implication in actin-based motility. *J Cell Biol.* 136:1307-22.

Carlier, M.F., and D. Pantaloni. 1997. Control of actin dynamics in cell motility. *J Mol Biol.* 269:459-67.

Carlier, M.F., F. Ressad, and D. Pantaloni. 1999. Control of actin dynamics in cell motility. Role of ADF/cofilin. *J Biol Chem.* 274:33827-30.

Carlier, M.F., S. Wiesner, C. Le Clainche, and D. Pantaloni. 2003. Actin-based motility as a self-organized system: mechanism and reconstitution in vitro. *C R Biol.* 326:161-70.

Chan, A.Y., M. Bailly, N. Zebda, J.E. Segall, and J.S. Condeelis. 2000. Role of cofilin in epidermal growth factor-stimulated actin polymerization and lamellipod protrusion. *J Cell Biol.* 148:531-42.

Cooper, J.A., J.D. Blum, and T.D. Pollard. 1984. Acanthamoeba castellanii capping protein: properties, mechanism of action, immunologic cross-reactivity, and localization. *J Cell Biol.* 99:217-25.

Danuser, G. 2005. Coupling the dynamics of two actin networks--new views on the mechanics of cell protrusion. *Biochem Soc Trans.* 33:1250-3.

Dayel, M.J., E.A. Holleran, and R.D. Mullins. 2001. Arp2/3 complex requires hydrolyzable ATP for nucleation of new actin filaments. *Proc Natl Acad Sci U S A.* 98:14871-6.

Dayel, M.J., and R.D. Mullins. 2004. Activation of Arp2/3 complex: addition of the first subunit of the new filament by a WASP protein triggers rapid ATP hydrolysis on Arp2. *PLoS Biol.* 2:E91.

DesMarais, V., I. Ichetovkin, J. Condeelis, and S.E. Hitchcock-DeGregori. 2002. Spatial regulation of actin dynamics: a tropomyosin-free, actin-rich compartment at the leading edge. *J Cell Sci.* 115:4649-60.

DiNubile, M.J., and S. Huang. 1997. High concentrations of phosphatidylinositol-4,5-bisphosphate may promote actin filament growth by three potential mechanisms: inhibiting capping by neutrophil lysates, severing actin filaments and removing capping protein-beta2 from barbed ends. *Biochim Biophys Acta.* 1358:261-78.

Dorner, C., A. Ullrich, H.U. Haring, and R. Lammers. 1999. The kinesin-like motor protein KIF1C occurs in intact cells as a dimer and associates with proteins of the 14-3-3 family. *J Biol Chem.* 274:33654-60.

Eden, S., R. Rohatgi, A.V. Podtelejnikov, M. Mann, and M.W. Kirschner. 2002. Mechanism of regulation of WAVE1-induced actin nucleation by Rac1 and Nck. *Nature.* 418:790-3.

Egile, C., I. Rouiller, X.P. Xu, N. Volkmann, R. Li, and D. Hanein. 2005. Mechanism of filament nucleation and branch stability revealed by the structure of the Arp2/3 complex at actin branch junctions. *PLoS Biol.* 3:e383.

Flanagan, L.A., J. Chou, H. Falet, R. Neujahr, J.H. Hartwig, and T.P. Stossel. 2001. Filamin A, the Arp2/3 complex, and the morphology and function of cortical actin filaments in human melanoma cells. *J Cell Biol.* 155:511-7.

Gautreau, A., H.Y. Ho, J. Li, H. Steen, S.P. Gygi, and M.W. Kirschner. 2004. Purification and architecture of the ubiquitous Wave complex. *Proc Natl Acad Sci U S A.* 101:4379-83.

Ghosh, M., X. Song, G. Mouneimne, M. Sidani, D.S. Lawrence, and J.S. Condeelis. 2004. Cofilin promotes actin polymerization and defines the direction of cell motility. *Science.* 304:743-6.

Gohla, A., J. Birkenfeld, and G.M. Bokoch. 2005. Chronophin, a novel HAD-type serine protein phosphatase, regulates cofilin-dependent actin dynamics. *Nat Cell Biol.* 7:21-9.

Gohla, A., and G.M. Bokoch. 2002. 14-3-3 regulates actin dynamics by stabilizing phosphorylated cofilin. *Curr Biol.* 12:1704-10.

Goldschmidt-Clermont, P.J., M.I. Furman, D. Wachsstock, D. Safer, V.T. Nachmias, and T.D. Pollard. 1992. The control of actin nucleotide exchange by thymosin beta 4 and profilin. A potential regulatory mechanism for actin polymerization in cells. *Mol Biol Cell.* 3:1015-24.

Goley, E.D., S.E. Rodenbusch, A.C. Martin, and M.D. Welch. 2004. Critical conformational changes in the Arp2/3 complex are induced by nucleotide and nucleation promoting factor. *Mol Cell.* 16:269-79.

Gupton, S.L., K.L. Anderson, T.P. Kole, R.S. Fischer, A. Ponti, S.E. Hitchcock-DeGregori, G. Danuser, V.M. Fowler, D. Wirtz, D. Hanein, and C.M. Waterman-Storer. 2005. Cell migration without a lamellipodium: translation of actin dynamics into cell movement mediated by tropomyosin. *J Cell Biol.* 168:619-31.

Harris, E.S., F. Li, and H.N. Higgs. 2004. The mouse formin, FRLalpha, slows actin filament barbed end elongation, competes with capping protein, accelerates polymerization from monomers, and severs filaments. *J Biol Chem.* 279:20076-87.

Hartwig, J.H., G.M. Bokoch, C.L. Carpenter, P.A. Janmey, L.A. Taylor, A. Toker, and T.P. Stossel. 1995. Thrombin receptor ligation and activated Rac uncap actin filament barbed ends through phosphoinositide synthesis in permeabilized human platelets. *Cell.* 82:643-53.

Heath, J.P. 1983. Direct evidence for microfilament-mediated capping of surface receptors on crawling fibroblasts. *Nature.* 302:532-4.

Helfman, D.M., C. Berthier, J. Grossman, M. Leu, E. Ehler, E. Perriard, and J.C. Perriard. 1999. Nonmuscle tropomyosin-4 requires coexpression with other low molecular weight isoforms for binding to thin filaments in cardiomyocytes. *J Cell Sci.* 112 (Pt 3):371-80.

Ho, H.Y., R. Rohatgi, A.M. Lebensohn, M. Le, J. Li, S.P. Gygi, and M.W. Kirschner. 2004. Toca-1 mediates Cdc42-dependent actin nucleation by activating the N-WASP-WIP complex. *Cell.* 118:203-16.

Ho, H.Y., R. Rohatgi, L. Ma, and M.W. Kirschner. 2001. CR16 forms a complex with N-WASP in brain and is a novel member of a conserved proline-rich actin-binding protein family. *Proc Natl Acad Sci U S A.* 98:11306-11.

Hotulainen, P., E. Paunola, M.K. Vartiainen, and P. Lappalainen. 2005. Actin-depolymerizing factor and cofilin-1 play overlapping roles in promoting rapid F-actin depolymerization in mammalian nonmuscle cells. *Mol Biol Cell.* 16:649-64.

Huang, T.Y., C. DerMardirossian, and G.M. Bokoch. 2006. Cofilin phosphatases and regulation of actin dynamics. *Curr Opin Cell Biol.* 18:26-31.

Humphries, C.L., H.I. Balcer, J.L. D'Agostino, B. Winsor, D.G. Drubin, G. Barnes, B.J. Andrews, and B.L. Goode. 2002. Direct regulation of Arp2/3 complex activity and function by the actin binding protein coronin. *J Cell Biol.* 159:993-1004.

Ichimura, T., J. Uchiyama, O. Kunihiro, M. Ito, T. Horigome, S. Omata, F. Shinkai, H. Kaji, and T. Isobe. 1995. Identification of the site of interaction of the 14-3-3 protein with phosphorylated tryptophan hydroxylase. *J Biol Chem.* 270:28515-8.

Ichimura, T., A. Wakamiya-Tsuruta, C. Itagaki, M. Taoka, T. Hayano, T. Natsume, and T. Isobe. 2002. Phosphorylation-dependent interaction of kinesin light chain 2 and the 14-3-3 protein. *Biochemistry.* 41:5566-72.

Innocenti, M., S. Gerboth, K. Rottner, F.P. Lai, M. Hertzog, T.E. Stradal, E. Frittoli, D. Didry, S. Polo, A. Disanza, S. Benesch, P.P. Di Fiore, M.F. Carlier, and G. Scita. 2005. Abi1 regulates the activity of N-WASP and WAVE in distinct actin-based processes. *Nat Cell Biol.* 7:969-76.

Isenberg, G., U. Aebi, and T.D. Pollard. 1980. An actin-binding protein from Acanthamoeba regulates actin filament polymerization and interactions. *Nature.* 288:455-9.

Jung, G., K. Remmert, X. Wu, J.M. Volosky, and J.A. Hammer, 3rd. 2001. The Dictyostelium CARMIL protein links capping protein and the Arp2/3 complex to type I myosins through their SH3 domains. *J Cell Biol.* 153:1479-97.

Kagan, A., Y.F. Melman, A. Krumerman, and T.V. McDonald. 2002. 14-3-3 amplifies and prolongs adrenergic stimulation of HERG K+ channel activity. *Embo J.* 21:1889-98.

Kelly, A.E., H. Kranitz, V. Dotsch, and R.D. Mullins. 2006. Actin binding to the central domain of WASP/Scar proteins plays a critical role in the activation of the Arp2/3 complex. *J Biol Chem.* 281:10589-97.

Kim, A.S., L.T. Kakalis, N. Abdul-Manan, G.A. Liu, and M.K. Rosen. 2000. Autoinhibition and activation mechanisms of the Wiskott-Aldrich syndrome protein. *Nature.* 404:151-8.

Kolch, W. 2000. Meaningful relationships: the regulation of the Ras/Raf/MEK/ERK pathway by protein interactions. *Biochem J.* 351 Pt 2:289-305.

Kovar, D.R. 2006. Molecular details of formin-mediated actin assembly. *Curr Opin Cell Biol.* 18:11-7.

Kozlov, M.M., and A.D. Bershadsky. 2004. Processive capping by formin suggests a force-driven mechanism of actin polymerization. *J Cell Biol.* 167:1011-7.

Lappalainen, P., M.M. Kessels, M.J. Cope, and D.G. Drubin. 1998. The ADF homology (ADF-H) domain: a highly exploited actin-binding module. *Mol Biol Cell.* 9:1951-9.

Liu, D., J. Bienkowska, C. Petosa, R.J. Collier, H. Fu, and R. Liddington. 1995. Crystal structure of the zeta isoform of the 14-3-3 protein. *Nature.* 376:191-4.

Longtine, M.S., A. McKenzie, 3rd, D.J. Demarini, N.G. Shah, A. Wach, A. Brachat, P. Philippsen, and J.R. Pringle. 1998. Additional modules for versatile and economical PCR-based gene deletion and modification in Saccharomyces cerevisiae. *Yeast.* 14:953-61.

Machesky, L.M., S.J. Atkinson, C. Ampe, J. Vandekerckhove, and T.D. Pollard. 1994. Purification of a cortical complex containing two unconventional actins from Acanthamoeba by affinity chromatography on profilin-agarose. *J Cell Biol.* 127:107-15.

Machesky, L.M., R.D. Mullins, H.N. Higgs, D.A. Kaiser, L. Blanchoin, R.C. May, M.E. Hall, and T.D. Pollard. 1999. Scar, a WASp-related protein, activates nucleation of actin filaments by the Arp2/3 complex. *Proc Natl Acad Sci U S A.* 96:3739-44.

Marchand, J.B., D.A. Kaiser, T.D. Pollard, and H.N. Higgs. 2001. Interaction of WASP/Scar proteins with actin and vertebrate Arp2/3 complex. *Nat Cell Biol.* 3:76-82.

Masters, S.C., K.J. Pederson, L. Zhang, J.T. Barbieri, and H. Fu. 1999. Interaction of 14-3-3 with a nonphosphorylated protein ligand, exoenzyme S of Pseudomonas aeruginosa. *Biochemistry.* 38:5216-21.

McGough, A., and W. Chiu. 1999. ADF/cofilin weakens lateral contacts in the actin filament. *J Mol Biol.* 291:513-9.

McGough, A., B. Pope, W. Chiu, and A. Weeds. 1997. Cofilin changes the twist of F-actin: implications for actin filament dynamics and cellular function. *J Cell Biol.* 138:771-81.

Mejillano, M.R., S. Kojima, D.A. Applewhite, F.B. Gertler, T.M. Svitkina, and G.G. Borisy. 2004. Lamellipodial versus filopodial mode of the actin nanomachinery: pivotal role of the filament barbed end. *Cell.* 118:363-73.

Miki, H., S. Suetsugu, and T. Takenawa. 1998. WAVE, a novel WASP-family protein involved in actin reorganization induced by Rac. *Embo J.* 17:6932-41.

Mockrin, S.C., and E.D. Korn. 1980. Acanthamoeba profilin interacts with G-actin to increase the rate of exchange of actin-bound adenosine 5'-triphosphate. *Biochemistry.* 19:5359-62.

Mogilner, A., and G. Oster. 1996. Cell motility driven by actin polymerization. *Biophys J.* 71:3030-45.

Moseley, J.B., K. Okada, H.I. Balcer, D.R. Kovar, T.D. Pollard, and B.L. Goode. 2006. Twinfilin is an actin-filament-severing protein and promotes rapid turnover of actin structures in vivo. *J Cell Sci.* 119:1547-57.

Mullins, R.D., J.A. Heuser, and T.D. Pollard. 1998. The interaction of Arp2/3 complex with actin: nucleation, high affinity pointed end capping, and formation of branching networks of filaments. *Proc Natl Acad Sci U S A.* 95:6181-6.

Mullins, R.D., and T.D. Pollard. 1999. Structure and function of the Arp2/3 complex. *Curr Opin Struct Biol.* 9:244-9.

Nagaoka, R., H. Abe, and T. Obinata. 1996. Site-directed mutagenesis of the phosphorylation site of cofilin: its role in cofilin-actin interaction and cytoplasmic localization. *Cell Motil Cytoskeleton.* 35:200-9.

Nishida, E. 1985. Opposite effects of cofilin and profilin from porcine brain on rate of exchange of actin-bound adenosine 5'-triphosphate. *Biochemistry.* 24:1160-4.

Nishida, E., S. Maekawa, and H. Sakai. 1984. Cofilin, a protein in porcine brain that binds to actin filaments and inhibits their interactions with myosin and tropomyosin. *Biochemistry.* 23:5307-13.

Nishita, M., C. Tomizawa, M. Yamamoto, Y. Horita, K. Ohashi, and K. Mizuno. 2005. Spatial and temporal regulation of cofilin activity by LIM kinase and Slingshot is critical for directional cell migration. *J Cell Biol.* 171:349-59.

Niwa, R., K. Nagata-Ohashi, M. Takeichi, K. Mizuno, and T. Uemura. 2002. Control of actin reorganization by Slingshot, a family of phosphatases that dephosphorylate ADF/cofilin. *Cell.* 108:233-46.

Noireaux, V., R.M. Golsteyn, E. Friederich, J. Prost, C. Antony, D. Louvard, and C. Sykes. 2000. Growing an actin gel on spherical surfaces. *Biophys J.* 78:1643-54.

Ono, S., and K. Ono. 2002. Tropomyosin inhibits ADF/cofilin-dependent actin filament dynamics. *J Cell Biol.* 156:1065-76.

Palmgren, S., M. Vartiainen, and P. Lappalainen. 2002. Twinfilin, a molecular mailman for actin monomers. *J Cell Sci.* 115:881-6.

Pelham, R.J., and F. Chang. 2002. Actin dynamics in the contractile ring during cytokinesis in fission yeast. *Nature.* 419:82-6.

Pollard, T.D., L. Blanchoin, and R.D. Mullins. 2000. Molecular mechanisms controlling actin filament dynamics in nonmuscle cells. *Annu Rev Biophys Biomol Struct.* 29:545-76.

Ponti, A., M. Machacek, S.L. Gupton, C.M. Waterman-Storer, and G. Danuser. 2004. Two distinct actin networks drive the protrusion of migrating cells. *Science.* 305:1782-6.

Prehoda, K.E., J.A. Scott, R.D. Mullins, and W.A. Lim. 2000. Integration of multiple signals through cooperative regulation of the N-WASP-Arp2/3 complex. *Science.* 290:801-6.

Pruyne, D., M. Evangelista, C. Yang, E. Bi, S. Zigmond, A. Bretscher, and C. Boone. 2002. Role of formins in actin assembly: nucleation and barbed-end association. *Science.* 297:612-5.

Quinlan, M.E., J.E. Heuser, E. Kerkhoff, and R.D. Mullins. 2005. Drosophila Spire is an actin nucleation factor. *Nature.* 433:382-8.

Remmert, K., T.E. Olszewski, M.B. Bowers, M. Dimitrova, A. Ginsburg, and J.A. Hammer, 3rd. 2004. CARMIL is a bona fide capping protein interactant. *J Biol Chem.* 279:3068-77.

Roberts, R.L., H.U. Mosch, and G.R. Fink. 1997. 14-3-3 proteins are essential for RAS/MAPK cascade signaling during pseudohyphal development in S. cerevisiae. *Cell.* 89:1055-65.

Robinson, R.C., K. Turbedsky, D.A. Kaiser, J.B. Marchand, H.N. Higgs, S. Choe, and T.D. Pollard. 2001. Crystal structure of Arp2/3 complex. *Science.* 294:1679-84.

Rodal, A.A., O. Sokolova, D.B. Robins, K.M. Daugherty, S. Hippenmeyer, H. Riezman, N. Grigorieff, and B.L. Goode. 2005. Conformational changes in the Arp2/3 complex leading to actin nucleation. *Nat Struct Mol Biol.* 12:26-31.

Rogers, S.L., U. Wiedemann, N. Stuurman, and R.D. Vale. 2003. Molecular requirements for actin-based lamella formation in Drosophila S2 cells. *J Cell Biol.* 162:1079-88.

Romero, S., C. Le Clainche, D. Didry, C. Egile, D. Pantaloni, and M.F. Carlier. 2004. Formin is a processive motor that requires profilin to accelerate actin assembly and associated ATP hydrolysis. *Cell.* 119:419-29.

Safer, D., R. Golla, and V.T. Nachmias. 1990. Isolation of a 5-kilodalton actin-sequestering peptide from human blood platelets. *Proc Natl Acad Sci U S A.* 87:2536-40.

Salmon, W.C., M.C. Adams, and C.M. Waterman-Storer. 2002. Dual-wavelength fluorescent speckle microscopy reveals coupling of microtubule and actin movements in migrating cells. *J Cell Biol.* 158:31-7.

Samarin, S., S. Romero, C. Kocks, D. Didry, D. Pantaloni, and M.F. Carlier. 2003. How VASP enhances actin-based motility. *J Cell Biol.* 163:131-42.

Schafer, D.A., P.B. Jennings, and J.A. Cooper. 1996. Dynamics of capping protein and actin assembly in vitro: uncapping barbed ends by polyphosphoinositides. *J Cell Biol.* 135:169-79.

Schafer, D.A., M.D. Welch, L.M. Machesky, P.C. Bridgman, S.M. Meyer, and J.A. Cooper. 1998. Visualization and molecular analysis of actin assembly in living cells. *J Cell Biol.* 143:1919-30.

Schirenbeck, A., T. Bretschneider, R. Arasada, M. Schleicher, and J. Faix. 2005. The Diaphanous-related formin dDia2 is required for the formation and maintenance of filopodia. *Nat Cell Biol.* 7:619-25.

Severson, A.F., D.L. Baillie, and B. Bowerman. 2002. A Formin Homology protein and a profilin are required for cytokinesis and Arp2/3-independent assembly of cortical microfilaments in C. elegans. *Curr Biol.* 12:2066-75.

Singh, S., D.W. Powell, M.J. Rane, T.H. Millard, J.O. Trent, W.M. Pierce, J.B. Klein, L.M. Machesky, and K.R. McLeish. 2003a. Identification of the p16-Arc subunit of the Arp2/3 complex as a substrate of MAPK-activated protein kinase-2 by proteomic analysis. *J Biol Chem.*

Singh, S., D.W. Powell, M.J. Rane, T.H. Millard, J.O. Trent, W.M. Pierce, J.B. Klein, L.M. Machesky, and K.R. McLeish. 2003b. Identification of the p16-Arc subunit of the Arp 2/3 complex as a substrate of MAPK-activated protein kinase 2 by proteomic analysis. *J Biol Chem.* 278:36410-7.

Sirotkin, V., C.C. Beltzner, J.B. Marchand, and T.D. Pollard. 2005. Interactions of WASp, myosin-I, and verprolin with Arp2/3 complex during actin patch assembly in fission yeast. *J Cell Biol.* 170:637-48.

Skoble, J., D.A. Portnoy, and M.D. Welch. 2000. Three regions within ActA promote Arp2/3 complex-mediated actin nucleation and Listeria monocytogenes motility. *J Cell Biol.* 150:527-38.

Sokol, N.S., and L. Cooley. 2003. Drosophila filamin is required for follicle cell motility during oogenesis. *Dev Biol.* 260:260-72.

Steffen, A., K. Rottner, J. Ehinger, M. Innocenti, G. Scita, J. Wehland, and T.E. Stradal. 2004. Sra-1 and Nap1 link Rac to actin assembly driving lamellipodia formation. *Embo J.* 23:749-59.

Svitkina, T.M., and G.G. Borisy. 1999. Arp2/3 complex and actin depolymerizing factor/cofilin in dendritic organization and treadmilling of actin filament array in lamellipodia. *J Cell Biol.* 145:1009-26.

Theriot, J.A., and T.J. Mitchison. 1991. Actin microfilament dynamics in locomoting cells. *Nature.* 352:126-31.

Tilney, L.G., E.M. Bonder, and D.J. DeRosier. 1981. Actin filaments elongate from their membrane-associated ends. *J Cell Biol.* 90:485-94.

Tobacman, L.S., and E.D. Korn. 1982. The regulation of actin polymerization and the inhibition of monomeric actin ATPase activity by Acanthamoeba profilin. *J Biol Chem.* 257:4166-70.

Toshima, J., J.Y. Toshima, T. Amano, N. Yang, S. Narumiya, and K. Mizuno. 2001. Cofilin phosphorylation by protein kinase testicular protein kinase 1 and its role in integrin-mediated actin reorganization and focal adhesion formation. *Mol Biol Cell.* 12:1131-45.

Uruno, T., K. Remmert, and J.A. Hammer, 3rd. 2006. CARMIL Is a Potent Capping Protein Antagonist: IDENTIFICATION OF A CONSERVED CARMIL DOMAIN THAT INHIBITS THE ACTIVITY OF CAPPING PROTEIN AND UNCAPS CAPPED ACTIN FILAMENTS. *J Biol Chem.* 281:10635-50.

Vallotton, P., S.L. Gupton, C.M. Waterman-Storer, and G. Danuser. 2004. Simultaneous mapping of filamentous actin flow and turnover in migrating cells by quantitative fluorescent speckle microscopy. *Proc Natl Acad Sci U S A.* 101:9660-5.

van der Gucht, J., E. Paluch, J. Plastino, and C. Sykes. 2005. Stress release drives symmetry breaking for actin-based movement. *Proc Natl Acad Sci U S A.* 102:7847-52.

van Hemert, M.J., A.M. Deelder, C. Molenaar, H.Y. Steensma, and G.P. van Heusden. 2003. Self-association of the spindle pole body-related intermediate filament protein Fin1p and its phosphorylation-dependent interaction with 14-3-3 proteins in yeast. *J Biol Chem.* 278:15049-55.

Volkmann, N., K.J. Amann, S. Stoilova-McPhie, C. Egile, D.C. Winter, L. Hazelwood, J.E. Heuser, R. Li, T.D. Pollard, and D. Hanein. 2001. Structure of Arp2/3 complex in its activated state and in actin filament branch junctions. *Science.* 293:2456-9.

Waddle, J.A., T.S. Karpova, R.H. Waterston, and J.A. Cooper. 1996. Movement of cortical actin patches in yeast. *J Cell Biol.* 132:861-70.

Wang, B., H. Yang, Y.C. Liu, T. Jelinek, L. Zhang, E. Ruoslahti, and H. Fu. 1999. Isolation of high-affinity peptide antagonists of 14-3-3 proteins by phage display. *Biochemistry.* 38:12499-504.

Wang, Y.L. 1985. Exchange of actin subunits at the leading edge of living fibroblasts: possible role of treadmilling. *J Cell Biol.* 101:597-602.

Wang, Y.L., and D.L. Taylor. 1980. Preparation and characterization of a new molecular cytochemical probe: 5-iodoacetamidofluorescein-labeled actin. *J Histochem Cytochem.* 28:1198-206.

Watanabe, N., and T.J. Mitchison. 2002. Single-molecule speckle analysis of actin filament turnover in lamellipodia. *Science.* 295:1083-6.

Waterman-Storer, C.M., and G. Danuser. 2002. New directions for fluorescent speckle microscopy. *Curr Biol.* 12:R633-40.

Waterman-Storer, C.M., A. Desai, J.C. Bulinski, and E.D. Salmon. 1998. Fluorescent speckle microscopy, a method to visualize the dynamics of protein assemblies in living cells. *Curr Biol.* 8:1227-30.

Waterman-Storer, C.M., and E.D. Salmon. 1997. Actomyosin-based retrograde flow of microtubules in the lamella of migrating epithelial cells influences microtubule dynamic instability and turnover and is associated with microtubule breakage and treadmilling. *J Cell Biol.* 139:417-34.

Wear, M.A., and J.A. Cooper. 2004. Capping protein: new insights into mechanism and regulation. *Trends Biochem Sci.* 29:418-28.

Welch, M.D., and R.D. Mullins. 2002. Cellular control of actin nucleation. *Annu Rev Cell Dev Biol.* 18:247-88.

Welch, M.D., J. Rosenblatt, J. Skoble, D.A. Portnoy, and T.J. Mitchison. 1998a. Interaction of human Arp2/3 complex and the Listeria monocytogenes ActA protein in actin filament nucleation. *Science.* 281:105-8.

Welch, M.D., J. Rosenblatt, J. Skoble, D.A. Portnoy, and T.J. Mitchison. 1998b. Interaction of human Arp2/3 complex and the Listeria monocytogenes ActA protein in actin filament nucleation. *Science.* 281:105-108.

Winter, D.C., E.Y. Choe, and R. Li. 1999. Genetic dissection of the budding yeast Arp2/3 complex: a comparison of the in vivo and structural roles of individual subunits. *Proc Natl Acad Sci U S A.* 96:7288-93.

Xu, Y., J.B. Moseley, I. Sagot, F. Poy, D. Pellman, B.L. Goode, and M.J. Eck. 2004. Crystal structures of a Formin Homology-2 domain reveal a tethered dimer architecture. *Cell.* 116:711-23.

Yaffe, M.B., K. Rittinger, S. Volinia, P.R. Caron, A. Aitken, H. Leffers, S.J. Gamblin, S.J. Smerdon, and L.C. Cantley. 1997. The structural basis for 14-3-3:phosphopeptide binding specificity. *Cell.* 91:961-71.

Yamashita, A., K. Maeda, and Y. Maeda. 2003. Crystal structure of CapZ: structural basis for actin filament barbed end capping. *Embo J.* 22:1529-38.

Yang, C., M. Pring, M.A. Wear, M. Huang, J.A. Cooper, T.M. Svitkina, and S.H. Zigmond. 2005. Mammalian CARMIL inhibits actin filament capping by capping protein. *Dev Cell.* 9:209-21.

Yang, N., O. Higuchi, K. Ohashi, K. Nagata, A. Wada, K. Kangawa, E. Nishida, and K. Mizuno. 1998. Cofilin phosphorylation by LIM-kinase 1 and its role in Rac-mediated actin reorganization. *Nature.* 393:809-12.

Yonezawa, N., E. Nishida, K. Iida, I. Yahara, and H. Sakai. 1990. Inhibition of the interactions of cofilin, destrin, and deoxyribonuclease I with actin by phosphoinositides. *J Biol Chem.* 265:8382-6.

Zalevsky, J., I. Grigorova, and R.D. Mullins. 2001a. Activation of the Arp2/3 complex by the Listeria acta protein. Acta binds two actin monomers and three subunits of the Arp2/3 complex. *J Biol Chem.* 276:3468-75.

Zalevsky, J., L. Lempert, H. Kranitz, and R.D. Mullins. 2001b. Different WASP family proteins stimulate different Arp2/3 complex-dependent actin-nucleating activities. *Curr Biol.* 11:1903-13.

Zhou, Y., W.M. Schopperle, H. Murrey, A. Jaramillo, D. Dagan, L.C. Griffith, and I.B. Levitan. 1999. A dynamically regulated 14-3-3, Slob, and Slowpoke potassium channel complex in Drosophila presynaptic nerve terminals. *Neuron.* 22:809-18.

Zigmond, S.H., M. Evangelista, C. Boone, C. Yang, A.C. Dar, F. Sicheri, J. Forkey, and M. Pring. 2003. Formin leaky cap allows elongation in the presence of tight capping proteins. *Curr Biol.* 13:1820-3.